

Nanoscale

Accepted Manuscript

This article can be cited before page numbers have been issued, to do this please use: S. Kohli, G. Rathee, I. Jha, L. Phor, H. Sable and V. Chaudhary, *Nanoscale*, 2025, DOI: 10.1039/D5NR02336J.



This is an Accepted Manuscript, which has been through the Royal Society of Chemistry peer review process and has been accepted for publication.

Accepted Manuscripts are published online shortly after acceptance, before technical editing, formatting and proof reading. Using this free service, authors can make their results available to the community, in citable form, before we publish the edited article. We will replace this Accepted Manuscript with the edited and formatted Advance Article as soon as it is available.

You can find more information about Accepted Manuscripts in the [Information for Authors](#).

Please note that technical editing may introduce minor changes to the text and/or graphics, which may alter content. The journal's standard [Terms & Conditions](#) and the [Ethical guidelines](#) still apply. In no event shall the Royal Society of Chemistry be held responsible for any errors or omissions in this Accepted Manuscript or any consequences arising from the use of any information it contains.

Strategically Engineering 2D MXenes-based Advanced Adsorbents for Sustainable Wastewater Remediation of Dyes

View Article Online

DOI: 10.1039/D5NR02336J

Sahil Kohli^{1*‡}, Garima Rathee^{2‡}, Indrani Jha¹, Lakshita Phor³, Harsh Sable⁴, Vishal Chaudhary^{5*}

¹Department of Chemistry, School of Engineering and Technology, Manav Rachna International Institute of Research and Studies, Faridabad, Haryana-121004, India.

²Department of Chemical Engineering, Universitat Politècnica de Catalunya, Barcelona, Spain.

³Department of Physics, University Centre for Research and Development, Chandigarh University, Gharuan, Mohali 140413.

⁴Sharda School of Allied Health Sciences, Sharda University, Greater Noida, U.P. (201306), India.

⁵Centre for Theoretical Physics and Natural Philosophy, Nakhonsawan Studiorum for Advanced Studies, Mahidol University, Nakhonsawan, 60130, Thailand.

*Correspondence:

- sahilkohli41@gmail.com (S.K.), sahil.set@mriu.edu.in
- Chaudhary00vishal@gmail.com (V.C.)

[‡]Equal authorship: SK and GR

Abstract

View Article Online
DOI: 10.1039/D5NR02336J

The exponential growth of the global population in the digital era has accelerated urbanization and industrialization, leading to severe water pollution from the discharge of toxic dyes into aquatic ecosystems. Two dimensional (2D) MXene-based nano-adsorbents have recently emerged as promising candidates for developing sustainable wastewater remediation technologies due to their tunable physicochemical properties, including a high negative zeta potential, a large specific surface area, exceptional adsorption capacity, superior electrical and thermal conductivity, hydrophilicity, and a rich surface chemistry. Strategic optimization approaches for MXenes, encompassing interlayer spacing modification, surface engineering, stoichiometric tuning, morphological control, bandgap engineering, membrane fabrication, hybridization, and functionalization, have significantly enhanced their adsorptive performance and dye removal efficiency for practical wastewater treatment applications. This comprehensive review examines the latest advances in MXene-based nano-adsorbent engineering and their implementation as key components in wastewater treatment strategies for efficient dye removal from industrial effluents, providing fundamental insights into dye-MXene interactions to elucidate underlying removal mechanisms. The review highlights the sustainable characteristics of MXene-based nano-adsorbents, including their dye removal capacity, regeneration potential, recyclability, catalytic efficiency, and enhanced physicochemical properties, while addressing critical challenges, such as toxicity concerns, biocompatibility issues, and scalability limitations, that currently hinder their translation from the laboratory to the market. Innovative solutions are proposed through the integration of digital-age technologies, particularly artificial intelligence and machine learning approaches, with the implementation of these recommendations facilitating the establishment of MXene-based nano-adsorbents as sustainable alternatives to conventional commercial adsorbents. This

aligns with the UN Sustainable Development Goals and contributes to the principles of One Health, promoting global welfare.

Keywords: Nanomaterials; Adsorbents; MXenes; Wastewater remediation; Dyes.

[View Article Online](#)
DOI: 10.1039/D5NR02336J

1. Introduction

View Article Online
DOI: 10.1039/D5NR02336J

As industrialization progresses rapidly to cater to the needs of coming generations, there is improper discharge of toxic pollutants from industry settings, resulting in serious global One Health threats, including water pollution and damage to human health. In accordance with World Health Organization (WHO), environmental contamination impairs the human respiratory, neurological, and immune systems, making people more susceptible to serious diseases, including monkeypox, coronavirus disease (COVID-19), and cancer. As a result, legislators, environmentalists, researchers, and industrialists have expressed concern about the need for environmental rehabilitation. It can be accomplished by monitoring and managing various contaminants (air, water, radiation, and solid) using specific methodologies.^{1–6} Chemical water contaminants are classified as organic and inorganic pollutants. The former comes primarily from human activity, such as sewage plants, agricultural runoff, and industrial effluents. Dye compounds are among the organic pollutants, while radionuclides and heavy metal ions are the most frequent inorganic pollutants found in water. These contaminants are mostly discharged by paper, paint, and textile factories. Most of these industries frequently discharge their effluent into water bodies, which can lead to several issues, including decreased solar penetration into the marine ecosystem, genotoxicity, carcinogenicity, and adverse effects on human wellness, the habitat, and marine life.^{7–9} Harmful molecules of dye in water leads to mutagenicity, and disruption of main human tissues such as liver, kidney, reproductive system, and central nervous system.¹⁰ As a result of industrial and human activity, dyes are regarded as dangerous pollutants since they can be found in surface water.¹¹ To protect the environment, it is crucial to eliminate these harmful toxins from the aquatic environment.¹²

Various technologies have been established in the past few years to effectively remove dye pollutants from the water, including advanced oxidation,^{13–15} catalytic ozonation,¹⁶ flocculation and coagulation,¹⁷ Fenton oxidation and electrocoagulation,¹⁸ ion exchange,¹⁹ membrane

separation,²⁰ and photo-catalysis.^{21,22} These approaches have certain drawbacks (Figure 1), including the production of contaminated sludge, difficulties with disposal and handling, scaling up sophistication problems, high energy consumption, increased colouration of effluents, financial constraints, intricate mechanisms, clogged membranes, restricted flow rates, and production of byproducts.²³

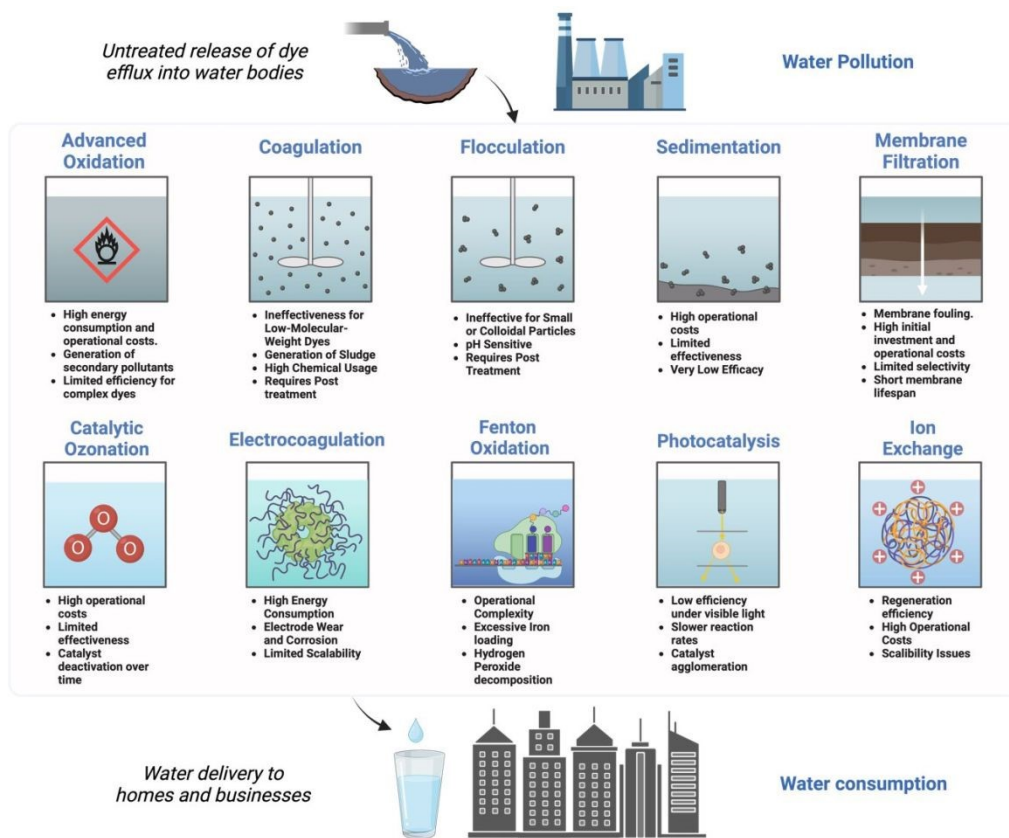


Figure 1. Drawbacks of traditional methods employed for dye removal

Among these methods, adsorption is considered as one of the effective substitute techniques for de-colorizing wastewater owing to its easy handling, affordability, sustainability, and quick water treatment.^{24–31} Furthermore, during the regeneration process, adsorption stops the creation of hazardous chemicals, which results in secondary contamination. For efficient adsorption, adsorbents with appropriate functionality and large surface area are usually utilized for the adsorption process. Few porous materials MOF, activated carbon, zeolites, chitosan,

and kaolinite) were built as adsorbents for environmental contaminants.^{32,33} Hydrogel materials are also used as a superior adsorbent for the elimination of water-based contaminants.^{34,35}

The research community has shown substantial interest in 2D materials owing to their distinct chemical and physical properties, which set them apart from their bulk counterparts. This difference became particularly evident after the groundbreaking discovery of graphene through mechanical exfoliation into single layers.³⁶ Following the graphene's discovery, various 2D materials, including metal oxides, metal hydroxides, hexagonal boron nitrides, and TMDs, have been identified and demonstrated their capability across various applications.^{37–41} These 2D materials are low-dimensional materials possessing enormous surface areas and have been recognized as the best adsorbents for a variety of contaminants. Examples of these materials include carbon-based nanomaterials such as carbon nanotubes (CNTs) and graphene, ordered mesoporous silica, and phosphorenes.^{42–44}

A number of nanomaterials have lately shown great potential in water purification due to their notable physicochemical properties. Among them, MXenes are an innovative family of cutting-edge nanomaterials with promising applications in water purification and material science. They are also referred to as 2-D transition metal carbides, carbonitrides or nitrides. MXene's unique design, fine structure, remarkable stability, notable oxidation and chemical resistance, high conductivity, and environmental friendliness have piqued the curiosity of researchers recently.⁴⁵ They are ideal candidates for use in wastewater treatment applications due to their enhanced surface area and availability of several functional moieties, such as –OH and –O, on the MXene surface.⁴⁶ Their varied chemical composition, photo-catalytic capabilities, 2D layered architecture, and active metallic hydroxide sites have made these materials stand out as excellent candidates for use in water purification systems.⁴⁷ The MXenes-based materials are also very useful in the adsorption of various organic dyes which are toxic to the

environment. Additionally, MXenes serve as raw materials for the creation of nanostructured MXene membranes, demonstrating beneficial usage in wastewater treatment methods.^{48,49}

This review article addresses the potential use of MXenes, 2D transition metal carbides and nitrides in improving dye adsorption for wastewater treatment. MXenes are characterized by their unique surface chemistry, increased surface area, and superior conductivity, which positions them a prime choice to eliminate hazardous dyes from industrial effluents. In this article, the advancements in MXene-based adsorbents, including the physicochemical features, adsorption mechanisms that improve the efficacy of MXenes in dye removal operations, and the design and techniques of synthesis for these adsorbents are discussed. Additionally, it highlights recent progress in integrating MXenes into composite materials and membrane systems to optimize performance. Furthermore, the regeneration, recyclability, challenges and recommendations are also addressed for a sustainable environment. This review explores the viability of MXenes as an eco-friendly and sustainable approach for water pollution, paving the way for future investigation and expansion in sustainable wastewater management technologies.

2. Engineering structural and physicochemical properties of MXenes and related nanosorbents employed for dye removal

2.1. Fundamental structure of MXenes and their nanoadsorbents

MXenes are derived from the MAX phases, which are ternary compounds of carbides or nitrides. They follow with the common formula $M_{n+1}AX_n$, where M signifies a transition metal (Cr, Ti), A corresponds to an element either from the group 13 or 14 of the periodic table (e.g., Si, Al), X indicates nitrogen or carbon and n is typically 1, 2, or 3. These phases are characterized by densely arranged M layers, with X atoms occupying the octahedral sites within the layered hexagonal MAX phases. However, strong acids can easily etch away the A-layer due to the greater strength of M-X bonds compared to M-A bonds. After etching, the

resulting MXene can be expressed as $M_{n+1}X_nT_x$, where T signifies surface terminal groups such

as $-OH$, $-O$, and $-F$, and so on, and x is termination number. This 2-D material, which shares similarities with graphene, was given the name "MXene" because of its structure. The suffix "-ene" is taken from the word "graphene," while "MX" is derived from the material's structure. Additionally, there are a lot of edges and void spaces between the various layers, which help adsorbates to diffuse and allows integration with nanomaterials or polymers. Examples of widely used MXenes are Mo_2CT_x , T_2CT_x , $T_3C_2T_x$, and so on.⁵⁰

The fundamental MAX phase and MXenes have the same hexagonal crystal structure. Typically, MAX phases are expressed as $M_{n+1}AX_n$ ($n = 1-3$), which yields M_2AX (211), M_3AX_2 (312), and M_4AX_3 (413) (**Figure 2a**).^{51,52} The "X" atoms fill the octahedral spaces created by the arrangement of "M" atoms of transition metal organizing into octahedra in all MAX phases, resulting in M_6X interspersed with "A" element sheets and M_6X overlapping with "A" element sheets.⁵³ The only thing that separates the (211), (312), and (413) phases are the numbers of the M atom layers between A atom layer. Conclusively, the MAX phase consists of alternative layers of MX and A. Ti_3AlC_2 has a unit cell that resembles a hexagon and a five-atomic sheet structure. Among the five atomic sheets, three Ti sublayers containing carbon atoms are located at the "octahedral interstitial sites," and a reactive Al layer links the two adjacent layers. The surface terminating groups zone, the intralayer skeleton, and the interlayer make up the structure of $Ti_3C_2T_x$.⁵⁴

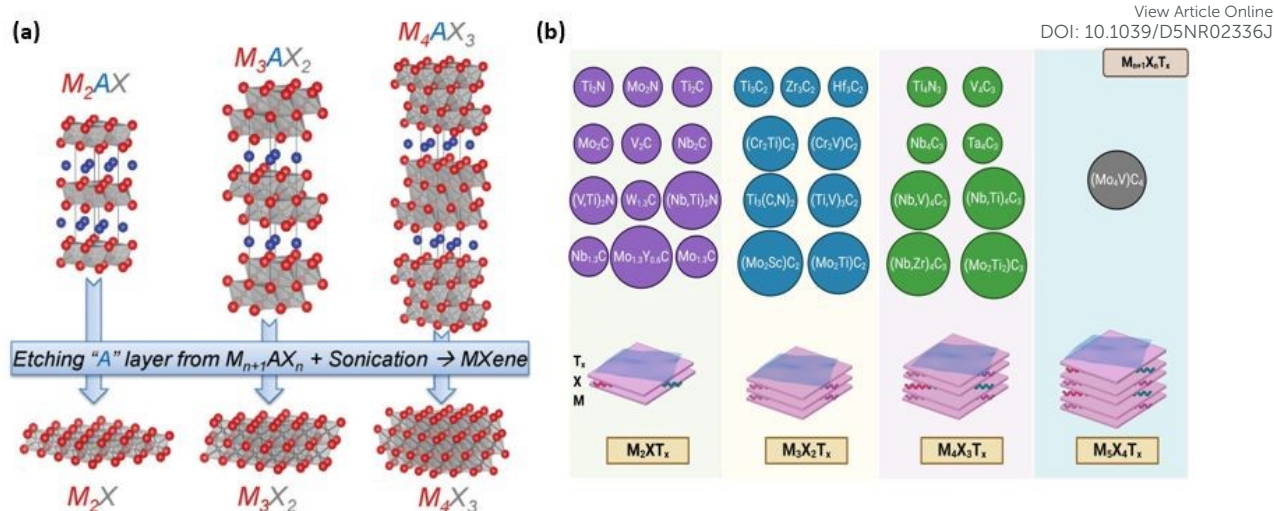


Figure 2. (a) The structural arrangement of MAX phases and their associated MXenes. Reproduced with permission from Ref.⁵² Copyright (2013) John Wiley & Sons. (b) Various examples of different MAX phases.

2.2. Physicochemical properties of MXenes and their nanosorbents

The prominent properties of MXene include its tunable high Young modulus, band gap, and thermal and electric conductivities. Notably, the hydrophilic surfaces of MXenes, characterized by strong metallic conductivities, differentiate themselves from most 2D materials, such as graphene.^{55–57} Finally, to optimize the properties and performance of their applications, various strategies can be employed, including (i) composition adjustments (such as formation of solid solution and variation of “M” and “X” elements), (ii) surface functionalization (achieved through thermal and chemical treatments), and (iii) structural and morphological modifications.^{58–60} The primary features of the MXenes family are outlined below.

2.2.1. Mechanical attributes of MXenes for effective adsorption

The mechanical properties of MXenes are crucial for their effectiveness as adsorbents for dye removal. Young's modulus, a critical indicator of mechanical strength, assesses a material's rigidity and its ability to resist elastic deformation. MXenes are widely recognized for their high Young's modulus values, generally spanning from tens to hundreds of gigapascals (GPa).

For example, the $\text{Ti}_3\text{C}_2\text{T}_x$ MXene has Young's modulus of approximately 330 GPa, while other

[View Article Online
DOI: 10.1039/D5NR02336J](#)

MXenes, such as V_2C and Nb_2C , also exhibit similarly high values.⁶¹ MXene membranes with 7 nm tip radius, demonstrate an effective Young's modulus and a tensile strength of 333 ± 30 GPa and 17.3 ± 1.6 GPa respectively. Additionally, the Young's modulus of Ti_3C_2 is 502 GPa, as determined through molecular dynamics simulations.^{62,63} The layer thickness significantly affects the tensile strength of MXene. Luo *et al.* demonstrated that with the increase in thickness of the MXene film from 2.30 to 17.0 μm , the elastic modulus decreases from 17 GPa to 8 GPa, and the tensile strength reduces from 61 MPa to 36 MPa.⁶⁴ In addition to possessing a high Young's modulus, MXenes exhibit robust physical properties. MXenes exhibit tensile strengths typically ranging from several hundred to several thousand megapascals (MPa), indicating considerable robustness. For example, $\text{Ti}_3\text{C}_2\text{T}_x$ MXene is reported to possess a strength of approximately 400 MPa.⁶⁵ Liang *et al.* demonstrated that addition of 3 wt% MXene enhanced the fracture mechanical Strength of ceramics by $7.6 \text{ MPa} \cdot \text{m}^{1/2}$, marking a 36% increase compared to unmodified ceramics.⁶⁶

This mechanical robustness is coupled with excellent flexibility due to their layered structure, which allows MXenes to bend and deform without compromising their structural integrity. Such properties are advantageous in wastewater treatment, where maintaining functionality under different conditions is essential. Flexibility is another essential aspect of mechanical behavior. MXenes have a layered structure that imparts a degree of flexibility, allowing them to bend and distort. The specific mechanical properties of MXenes can vary based on factors such as composition, doping, production methods, and the existence of defects or functional groups. Owing to their versatility, MXenes are appealing prospects for application in the adsorption of dyes.⁶⁷

2.2.2. Electronic and electrical properties aiding to effective dye removal

MXenes have distinct electronic and electrical properties that greatly improve their efficacy in dye adsorption applications. Modifying the stoichiometry, functional unit, or solid solution formation of MXenes can modify two of their primary attributes of interest: their electric and electronic properties. MXenes' metallic or semi-metallic conductivity allows for quick electron transfer processes, which can increase dye-adsorbent surface interactions. This conductivity facilitates charge transfer, promotes electrostatic interactions, and may improve the adsorption kinetics of anionic or cationic dyes. Experimentally, the pressed MXene discs exhibited electrical conductivities comparable to those of multi-layered graphene (with resistance varying from 22 to 339 Ω , based on the chemical formula and 'n' index) and surpassed those of reduced graphene oxide (rGO) and CNTs.^{52,68} Furthermore, the values of resistivity were found to increase with the functional groups and number of layers.^{55,69,70} The calculated conductivities typically exhibit higher values than those measured experimentally.⁷¹

The electrical conductivity of $\text{Ti}_3\text{C}_2\text{Tx}$ ranged from 850 to 9880 S/cm, which can be attributed to variations in (i) defect concentration, (ii) surface functional groups, (iii) delamination yield, (iv) d-spacing between MXene flakes, and (v) lateral diameters influenced by the etching technique used.^{72,73} Generally, reduced HF content and etching durations produce MXenes with less flaws and higher lateral dimensions, resulting in enhanced electronic conductivity (for instance, bigger flake sizes yielded conductivities five times greater than those of smaller MXenes).⁷⁴ Furthermore, environmental humidity may affect their conductivities,⁷⁵ indicating potential uses for relative humidity sensing materials.^{76,77} An effective method to improve electrical characteristics is surface modification using alkaline and thermal treatments. They demonstrate conductivities that rise by up to two orders of magnitude. This augmentation results from the modification and/or elimination of functional moieties and embedded molecules.^{78–80} Also, the functional groups present on the surface might result in localized electronic states, which boost adsorption capacity *via* enhanced chemical interactions. The

ability to control these electrical properties via chemical modifications or by changing the composition of MXenes enables tailored performance in various dye removal conditions. Overall, the favorable electrical properties of MXenes contribute to their potential as excellent adsorbents in wastewater treatment applications.

2.2.3. Optical attributes aiding to effective dye removal efficacies

MXenes have unique optical characteristics that make them ideal for dye adsorption applications. Their metallic conductivity and configurable bandgap enable efficient interaction with light, making them ideal for photocatalytic reactions. The functional moieties present on the MXene's surface can also affect light absorption, allowing for selective interactions with certain dyes based on their absorption spectra. Furthermore, the layered structure of MXenes can provide plasmonic effects, which increase the local electromagnetic fields around the material, enabling dye adsorption. This combination of optical features not only improves dye removal effectiveness but also provides opportunities for the progress of new materials for environmental remediation and sensing applications.^{52,81}

2.2.4. pH-Responsive surface chemistry of MXenes and its role in selective dye removal

MXene surface charge behavior and zeta potential variations across different pH conditions represent a critical yet underexplored aspect that significantly influences dye selectivity in adsorption applications. The surface terminations of MXenes (primarily -OH, -O, and -F groups) exhibit pH-dependent protonation and deprotonation behaviors, leading to dynamic changes in surface charge density and zeta potential values. Under acidic conditions, MXenes typically exhibit positive zeta potentials due to the protonation of surface hydroxyl groups, whereas alkaline environments promote deprotonation, resulting in increasingly negative surface charges. This pH-responsive behavior directly governs the electrostatic interactions between MXene surfaces and ionic dyes, where cationic dyes show enhanced adsorption at higher pH values when MXene surfaces are negatively charged, and anionic dyes preferentially

adsorb under acidic conditions when surfaces carry positive charges. Despite its fundamental importance for rational design of selective dye removal systems, systematic investigations correlating MXene surface charge characteristics with dye selectivity mechanisms across comprehensive pH ranges remain limited, representing a significant knowledge gap that hinders optimization of MXene-based water treatment technologies.^{60,82,83}

2.2.5. Adsorptive attributes of MXenes and nanosorbents make them ideal adsorbents

The adsorption properties influence the performance of MXene-based adsorbent in removing colors from mixtures. Factors such as hydrophilicity, specific surface area (SSA), toxicity, porosity, uniformity, and various functional groups on MXene adsorbent surface are key determinant in adsorption of dye.

2.2.5.1. Enlarged specific surface area for high adsorption

Adsorption is often a surface process; thus, as an adsorbent's SSA increases, the number of pollutants absorbed also increases. By increasing surface area, several more active sites might be accessible for the likely adsorption of dyes. Usually, a large SSA provides additional active sites dedicated to the adsorption of pollutants, leading to a higher adsorption capacity. These nanomaterials' large SSA and negative surfaces of MXenes have made it possible for them to demonstrate possible adsorption capabilities.⁸⁴

2.2.5.2. Abundant surface functional groups for better adsorption

The functional groups on MXene-derived adsorbents, which are readily available, can significantly contribute to the removal of dyes from aquatic environments. This is due to the robust binding interactions between the molecules of the cationic dye and the negatively charged functional moieties on the MXene adsorbents. These interactions frequently lead to an increase in the amount of dye that is taken up by the adsorbents. Similarly, the existence of surface-bound positive functional groups on MXene-derived adsorbents promotes the adsorption of anionic dyes through electrostatic interaction (attractive) between the oppositely

charged species. Since different surface functional moieties gives different chemical and physical features of MXenes, their availability plays significant part in the utilization of MXene-based adsorbents. Additionally, the molecular intercalations or cations of tiny organic interlayer spacing also enhance the material's capacity for adsorption for MXene adsorbents. The increased interlayer space can explain this; consequently, increased analyte exposure occurs with interlayer gaps and functional divisions.⁸⁵

2.2.5.3. Significant wettability aiding efficient adsorption

Another aspect that substantially affects an adsorbent surface's power for adsorption is its wettability. The wettability of MXene-based adsorbents can significantly influence selective dye uptake. Wet etching technique utilizing (in situ) hydrogen fluoride is the most widely used synthetic method for producing MXenes. This procedure gives the surface of the 2D sheets a spectrum of O and OH containing moieties, making them hydrophilic.⁸⁶ As a result, MXenes show remarkable alignment with liquid procedure in an aqueous media, underscoring their increased capability for forming material hybrids and managing wettability in systems.⁸⁷ Essentially, a liquid droplet's ability to wet on the MXene surface depends on the interaction at the solid-liquid phases. Some of the additional factors that affect this interaction are electrostatic interactions, H-bonding, and van der Waals interactions.

2.2.5.4. Improving stability for practical prospects of nanosorbents

One of the main problems researchers face with MXenes is its stability. Density functional tight-binding calculations, supported by formation and cohesive energy studies as well as ab initio simulations, have demonstrated that MXenes are stable. Specifically, hydroxylated MXene derivatives with varying atomic distributions of nitrogen (N) and carbon (C) represent stable phases with favorable thermodynamic properties. However, under real reaction conditions, the stability of MXenes and their surface topologies remains unknown.⁸⁸ Transition metal-containing layered MXenes have a remarkable combination of excellent metallic

conductivity and rich, adaptable surface chemistry. MXenes become thermodynamically metastable as a result of this. Additionally, it is anticipated that MXenes' larger surface energy and low resistance to oxidation in oxygenated aqueous environments, even at room temperature, will lessen the electrical conductivity and passivate the reactive-interface.⁸⁸ Furthermore, after storing delaminated $\text{Ti}_3\text{C}_2\text{T}_x$ MXene for two weeks, MXenes usually undergo oxidation, such as MXene titania layer oxidation to anatase TiO_2 , which results in a color shift to off-white from greenish-black.⁸⁹ $\text{Ti}_3\text{C}_2\text{T}_x$, on the other hand, was shown to be stable in an argon or hydrogen environment up to 1473 K, demonstrating that it is able to maintain its stability even at higher temperatures.⁶⁹ Thermal stability of MXenes ($\text{Ti}_3\text{C}_2\text{T}_x$) powders is demonstrated to be as low as 200 °C in oxygen, and as high as 800 °C in argon atmosphere. At 200 °C in oxygen, MXenes surface oxidizes to produce amorphous carbon and anatase TiO_2 .^{69,90} Initially, the surfaces of MXene oxidize to form anatase crystals, preventing further oxidation. Then, as a result of the anatase's enhanced O_2 diffusion, the leftover MXene was gradually oxidized at higher temperatures until the anatase converted all of the MXene to CO_2 , TiO_2 , and rutile.⁶⁹

2.2.5.5. Toxicity related to MXene nanosystems

The toxicity profile of titanium-based MXenes presents a complex landscape requiring comprehensive evaluation across multiple biological systems and temporal scales. While non-toxic degradation products including C, N, and Ti breakdown into CO_2 , N_2 , and Ti compounds that are safe in trace amounts,⁹¹ the true group toxicity of MXenes remains challenging to ascertain due to their varied compound classes and significant heterogeneity in X or M elements and surface chemistry (T_x).⁹² $\text{Ti}_3\text{C}_2\text{T}_x$ demonstrates concentration-dependent cytotoxicity with differential effects on normal versus cancerous cell lines. Studies reveal higher toxicity against cancerous cells (A549 and A375) compared to normal cell lines (MRC-5 and HaCaT).^{93,94} Neural stem cell studies indicate no observable adverse effects at 12.5

$\mu\text{g/mL}$ but significant cytotoxicity at $25 \mu\text{g/mL}$ with compromised cell membrane integrity.⁹⁵

The primary toxicity mechanisms involve oxidative stress pathways generating reactive oxygen species (ROS), leading to cellular membrane damage and mitochondrial dysfunction.⁹⁶

Surface termination chemistry significantly influences MXene biocompatibility profiles. Fluorinated $\text{Ti}_3\text{C}_2\text{Tx}$ synthesized via conventional HF etching exhibits enhanced cytotoxicity due to fluoride ion release, which promotes ROS generation.⁹⁷ Halogen-free $\text{Ti}_3\text{C}_2\text{Tx}$ produced through NaOH-based etching demonstrates superior biocompatibility with no noticeable cytotoxicity even at high concentrations. PEGylation alters protein corona formation and cellular uptake mechanisms, with PEGylated MXenes showing modified biocompatibility profiles.⁹⁸

Environmental persistence studies reveal $\text{Ti}_3\text{C}_2\text{Tx}$ stability in aquatic media for at least 4 days at concentrations of 5-20 mg/L, with no dissolution detected over 42 days.⁹⁹ Aquatic organism studies using zebrafish embryo models indicate LC_{50} values of $257.46 \mu\text{g/mL}$, classifying $\text{Ti}_3\text{C}_2\text{Tx}$ as "practically non-toxic" under acute exposure conditions.¹⁰⁰ However, chronic exposure effects including developmental abnormalities and behavioral changes remain poorly characterized. Metabolomic analysis in *Daphnia magna* reveals metabolic disruption at sublethal concentrations, indicating potential ecosystem-level impacts.¹⁰¹ MXene environmental behavior involves complex transformation pathways influenced by water chemistry and redox conditions. Aggregation processes in natural waters alter bioavailability, while photodegradation generates titanium dioxide nanoparticles with unknown ecological implications.⁹⁹ Oxidative degradation over weeks to months may produce metabolites with different toxicity profiles compared to parent materials.

Comprehensive safety assessment using Safe and Sustainable by Design (SSbD) framework suggests $\text{Ti}_3\text{C}_2\text{Tx}$ can be safe and sustainable when properly designed and applied.⁹⁹ Life cycle assessment (LCA) studies identify synthesis impacts as major environmental concerns,

particularly titanium precursor production and hazardous chemical usage.¹⁰² Green synthesis alternatives using electrochemical etching reduce environmental impact but require systematic toxicity evaluation. Current regulatory frameworks lack MXene-specific guidelines, creating knowledge gaps for commercial applications. Standardized testing protocols addressing unique physicochemical properties are needed for comprehensive risk assessment. Risk mitigation strategies include surface engineering for reduced toxicity, biocompatible coating systems, and real-time monitoring for environmental release detection. Critical research needs include long-term exposure studies, mechanistic toxicology investigations, and ecosystem-level impact assessments. Predictive toxicology models incorporating machine learning approaches can accelerate safety evaluation while reducing animal testing requirements. Integration of advanced characterization techniques will provide mechanistic insights essential for safe-by-design approaches.

3. Methods for the synthesis of MXenes and their nanosorbents for dye removal

Most MXenes originate from MAX phase, in which A atoms are embedded in MX layers while M and X atoms positioned at hexagonal crystal's centre and apex, respectively. After eliminating A atoms from MAX phases, MX layers could be maintained by utilizing this "laminar" structure. However, unlike graphene, which rely on weak van der Waals forces to preserve the structure, the strong interlayer bonding in MXenes prevents mechanical exfoliation, making it impossible to produce 2D MXenes through this method.¹⁰³ Numerous methods have been introduced so far to prepare MXenes, which have numerous advantages and disadvantages (**Figure 3**).

Methods for preparing 2D Mxenes

Advantages and Disadvantages

HF/ in situ HF Etching Method	Molten Salt Method	Electrochemical Etching	Electrochemical Etching
Advantages	Advantages	Advantages	Advantages
<ul style="list-style-type: none"> • Easy to use • Widely Applicable 	<ul style="list-style-type: none"> • Improves Safety • Reduced difficulty and cost of Waste liquid treatment 	<ul style="list-style-type: none"> • High efficiency • High yield • Low cost 	<ul style="list-style-type: none"> • Large lateral size; • Extremely low defect concentration
Disadvantages	Disadvantages	Disadvantages	Disadvantages
<ul style="list-style-type: none"> • Hazardous • Harmful to the Environment 	<ul style="list-style-type: none"> • Unclear formation mechanism for Cl-MXene • Longer etching time • Higher reaction temperature 	<ul style="list-style-type: none"> • Excessive etching may destroy MXene structure • Limited Material Range 	<ul style="list-style-type: none"> • Low efficiency • Complicated process

Figure 3. Advantages and Disadvantages of various methods of 2D Mxenes.

3.1. Top-down approaches

Utilizing precursors is a key part of the top-down technique for the synthesis of MXenes. Although ScAl_3C_3 , $\text{Hf}_3(\text{Al, Si})_4\text{C}_6$, and $\text{Zr}_3\text{Al}_3\text{C}_5$, are examples of non-MAX structures, Ti_3AlC_2 and Ti_2AlC are examples of structures that are frequently found in MAX. At the moment, MAX is the precursor that is used the most frequently in the production of MXene. In MAX phase, strength of M-X bonds is greater than that of M-A bonds. Multi-layered MXenes are produced as a result of the breaking of the M-A connection in MAX during the synthesis process. This also results in element A being etched away from the parent structure. These multilayered MXenes are subsequently delaminated to yield single-layered MXenes. MXene's surface produces terminal groups like -OH, -F, and -O, to stabilize its structure. Mechanical stripping is commonly used in top-down methods of synthesis for 2D materials. Mechanical stripping alone is ineffective for breaking the precursor material's M-A bonds. Consequently, chemical stripping is the method of choice for the production of MXenes, whereas mechanical stripping is solely utilized for the production of single-layered MXenes by

the manufacturer. Various etching methods can disrupt M-A bonds: electrochemical, alkali base, fluoride, and lewis acid molten salt.

3.1.1. HF/*in-situ* HF-etching method

The two primary methods for preparing MXene are HF and in situ HF-etching (**Figure 4a**).¹⁰⁴ The loosely layered accordion-like MXene structure was initially described by Gogotsi and colleagues, who selectively etched Al from bulk Ti_3AlC_2 in HF solution (50 wt%).¹⁰⁵ HF broke the Ti-Al bonds in the Al layers, dissolving them and releasing a high volume of H_2 . As a result, the reaction started off with a powerful bubbling phenomenon. Additionally, a large number of functional moieties, like -F, -OH, and -O moieties, were joined to the surface of Ti atoms, giving rise to high hydrophilicity and distinctive electrochemical properties. Following this, HF etching was used to successfully exfoliate Ti_2CT_x , V_2CT_x , and Mo_2CT_x .^{106–108} It should be mentioned that the MAX phase's structural characteristics determine the etching conditions. Ti_2CT_x only needed to be treated for 10 hours in 40-wt% HF, but Nb_2AlC needed 90 hours of etching time in 50-wt% HF. The outcomes were verified using theoretical approaches. The calculation findings confirmed that, in order to etch Al from Nb_2AlC rather than Ti_2AlC , a longer period and greater concentrations of HF solution are required. This is due to the fact that the bond energy of Nb–Al, which is 1.21 eV, marginally greater than Ti–Al, which is 0.98 eV respectively.¹⁰⁹ It is important to note, though, that an overly aggressive etching process will produce more surface flaws, which could adversely affect the characteristics of MXene sheets.¹¹⁰ Successful Al layer delamination significantly reduces the interlayer force, facilitating the easy separation of MXene layers from their neighbouring ones.

Many attempts have been made to create safer and milder production methods for HF due to its significant toxicity and high danger. Using a combination of HCl and LiF rather than HF solution allowed for production of few-layer MXene with fewer surface flaws and greater interlayer spacing in 2014.¹¹¹ H^+ and F^- were liberated during the etching process to create HF

in situ. Al atoms were replaced by intercalated metal ions and H₂O molecules, which encouraged the interlayered gap to expand and the interlayered interaction to diminish. Significantly, by adjusting the quantity of LiF and HCl, this new technique made it possible to regulate the size and quality of sheets.¹¹² The original etchant is also substituted with mixtures of acid (H₂SO₄) and other fluoride salts (KF, NaF, and CaF₂). The presence of -F groups further restrict the application of MXene in electrochemical fields, and the generation of HF cannot be entirely prevented by using these fluorinated salts.¹¹³ Furthermore, a variety of organic compounds, including tetramethylammonium hydroxide (TMAOH) and dimethyl sulphoxide (DMSO), was used as intercalation agent for converting the multi-layer MXene into a few-layer MXene. The intercalants enable stacked multi-layer MXene to delaminate into a few-layer or monolayer sheet through subsequent shaking or ultrasonography treatment.^{70,114}

3.1.2. Molten salt etching method

Both *in situ* HF and HF etching are effective methods for generating carbides MXene, although they perform poorly when etching nitrides MXene. Two concepts were put out to illustrate the challenges involved in manufacturing nitrides MXene. Initially, the computational results indicated that Ti_{n+1}N_n had a lower cohesive energy than Ti_{n+1}C_n, indicating lower stability. The energy required to form Ti_{n+1}N_n is likewise greater than Ti_{n+1}C_n, indicating that the Al atoms were firmly bound in Ti_{n+1}AlN_n structure.¹¹⁵ Gogotsi *et al.* used a combination of molten salt as etchant to produce nitrides MXene to get around these issues.¹¹⁶ In specific, Ti₄AlN₃ was initially mixed with molten salt (29 wt% LiF, 59 wt% KF, 12 wt% NaF) in mass ratio of 1 : 1, and heated at 550 °C for 30 minutes in Ar atmosphere. After that, more washing with H₂SO₄ and deionised water was needed to eliminate the fluorides that contained aluminum. The prominent broad peak (002) of Ti₄N₃T_x shifted from 7.6° to 6.3°, as corroborated by XRD data, showing an extended interlayer distance. The EDX results also showed that no Al atom was seen, indicating that nitrides MXene was successfully etched using molten salt.

3.1.3. Fluorine-free method

Li and colleagues explained an alkali hydrothermal treatment process that yields high-purity multilayer MXene without the use of fluorine.¹¹⁷ Al(oxide) hydroxides can dissolve completely at high temperatures and concentrations of NaOH. Additional delamination using DMSO or TMAOH together with ultrasound approach can aid in the production of a few-layer MXene with smaller diameters.¹¹⁸ In contrast to fluorine-assisted approaches, there are more O-containing groups rather than –F groups dispersed on the surface, which could improve the electrochemical operation. Treatment with alkali prevents the production of HF. However, harsh environments might damage the internal structure and increase surface flaws. There is another method of creating MXene sheets besides conventional wet chemical etching, which is electrochemical etching. Yang and colleagues created an electrochemical etching technique using an organic system mixture of NH_4Cl and TMAOH.¹¹⁹ The counter electrode and working electrode were made of two bulk pieces, and only working electrode was etched.

Chloride ions functioned as the Ti-Al bond breaker at a constant applied potential of 5 V, and the NH_4OH that was produced assisted in extending the edge. Compared to the conventional HF-etched MXene, the exfoliated sheets had an average lateral size of nearly 2 μm and were primarily single or double layers. Furthermore, $\text{Ti}_3\text{C}_2\text{T}_x$ sheets generated through electrochemical etching often have a stacked architecture that is comparable to that of bulk Ti_3AlC_2 without exhibiting any obvious expansion. This is due to the fact that the reaction process does not include the release of a significant amount of gas. It should be mentioned that the outcome of etched MXene is also greatly influenced by the choice of electrolytes. For instance, electrochemical treatment in solutions containing NaCl and HCl invariably produces amorphous carbon, which obstructs additional etching.¹²⁰ Sun and colleagues discovered that when MAX was treated with 2 M HCl aqueous electrolyte, a three-layer structural composite

was produced.¹²¹ The components of this hybrid were unetched MAX, carbon-derived carbides (CDCs), and MXene, which required additional purification in order to get pure MXene sheets. Above all, using particular etching techniques such as molten salt etching, HF etching, and other fluorine-free approaches, MXenes could be extracted from bulk MAX phases by exploiting the difference in intensities between M–X and M–A bonds. It should be mentioned that the M–A bond energies had a significant impact on the etching conditions, with higher etching times and etchant concentrations needed for stronger M–A bond. Furthermore, the etching rate and reaction conditions are significantly influenced by the size of MAX particles.¹⁰⁵ Attrition milling the MAX powder beforehand could significantly cut down on etching time while maintaining overall yield.

3.2. Bottom-up approaches

Apart from the etching approach described above, various alternative bottom-up techniques have been developed to build ultrathin 2D highly crystalline MXene particularly for Mo₂C materials. These techniques include chemical vapor deposition (CVD) method, template method, PEPLD.^{122–126}

3.2.1. Chemical vapor deposition method

CVD was utilized by Ren *et al.* to successfully generate ultrathin two-dimensional α -Mo₂C crystals, with few nanometers thickness and lateral dimensions of up to 100 μ m (**Figure 4c**). This procedure required the use of methane over bilayer substrate made of copper and molybdenum foils. Further, this CVD process has been expanded to produce ultrathin TaC and WC crystals from additional transition metals such as Ta and W. Notably, this approach has the benefit of producing MXenes with large lateral diameters and few flaws, which substantially simplifies the analysis of their intrinsic properties.¹²⁵ Despite the fact that the fabrication of MXene monolayers has not yet been achieved through this method, it presents the possibility of future research and advancement in bottom-up approach for synthesis of

MXene. MXene thickness and form can be controlled very precisely by the use of CVD. On

View Article Online
DOI: 10.1039/D5NR02336J

the other hand, this procedure calls for highly specialized machinery and individuals who have received adequate training.¹⁰⁵

3.2.2. Plasma-enhanced pulsed laser deposition method

The PELPD system is a step up from traditional pulsed laser deposition systems. The very initial ultrathin films of Mo₂C synthesized using PELPD, made with methane plasma as the source of carbon, interacted with Mo vapor produced by pulsed laser. Utilizing sapphire substrate that was heated upto 700 °C, this reaction was carried out in order to generate films of high-quality with thickness that can be altered by modifying the pulse rate of laser.^{122,123}

3.2.3. Template method

To create 2D MoN, a salt-templated technique was employed. In this process, hexagonal 2D NaCl crystals coated with MoO₃ were first prepared, and then NH₃ was used to ammoniate them at 650 °C (**Figure 4d**). As a result, 2D MoN@NaCl powder, in which MoN species combined with the NaCl matrix, were successfully synthesized. 2-D nanosheets of MoN were produced by removing the NaCl using deionized water afterward.¹²³ The high yield of the template approach is its main benefit over CVD. This method also provides the capacity to precisely regulate the surface functional moieties. It is crucial to recognize that energy input is necessary for the precursor to be converted into nitride or carbide, which adds to energy consumption.¹²⁴

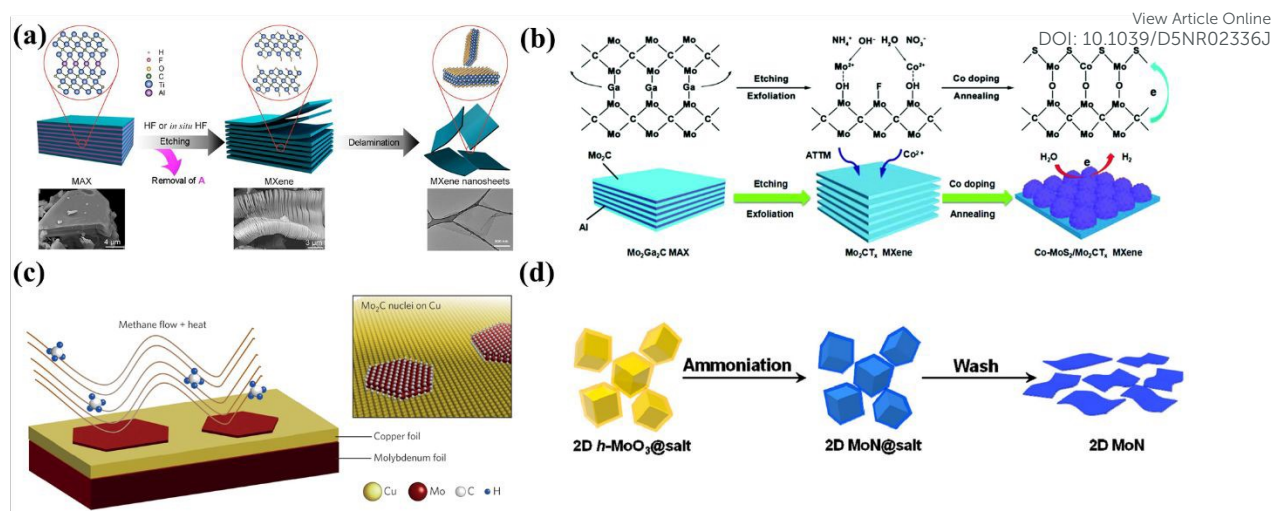


Figure 4. (a) Illustration of the process of etching and delamination of MXene. Reproduced with permission from Ref.¹⁰⁴ Copyright 2019, Elsevier. (b) The schematic diagram for synthesizing the Co-MoS₂/Mo₂CT_x nanohybrids. Reproduced with permission from Ref.¹⁰⁶ (c) CVD growth of large-area α -Mo₂C thin layer on Cu substrate. Reproduced with permission from Ref.¹²⁶ Copyright 2015, Springer Nature. (d) Schematic of synthesis of 2D MoN. Reproduced with permission from Ref.¹²³ Copyright 2015, American Chemical Society.

4. Rational engineering of MXene-based materials for enhanced dye removal performance

The rational engineering of MXene-based materials for enhanced dye removal performance represents a systematic approach to designing and optimizing these advanced adsorbents through targeted modifications that address specific limitations and enhance desired properties. As the field of MXene-based water treatment technologies has evolved, researchers have developed sophisticated strategies that go beyond the use of pristine MXenes to create engineered materials with superior performance characteristics. These rational design approaches are guided by a fundamental understanding of structure-property relationships, adsorption mechanisms, and the specific requirements for effective dye removal from aqueous environments. The engineering strategies encompass four primary categories: surface

functionalization to introduce particular chemical interactions, interlayer engineering to optimize structural accessibility, composite formation to achieve synergistic effects, and morphological control to enhance practical implementation. Each of these approaches addresses different aspects of the dye adsorption process, from molecular-level interactions to macroscopic material handling and system integration. A comparative analysis of published literature reveals several vital aspects when examining the efficiency of various MXene-based materials in dye adsorption (**Table 1**). The information includes adsorption capacity or removal efficiency, experimental conditions, and the type of adsorption isotherms and kinetics models applied for removing different dyes from the aqueous environment using MXene-based materials. This comprehensive evaluation demonstrates that rational engineering approaches have successfully achieved remarkable improvements in adsorption performance, with engineered MXene-based materials exhibiting significantly enhanced adsorption capacities representing orders of magnitude enhancement compared to pristine MXenes. The systematic design and optimization of these materials not only advance our fundamental understanding of MXene chemistry and physics but also provide practical pathways toward the development of commercially viable water treatment technologies capable of addressing the growing global challenge of dye-contaminated wastewater.

4.1. Surface Functionalization Strategies

Surface functionalization is a key method for improving the adsorption capabilities of MXenes by changing their surface chemistry and charge properties. The natural surface terminations of MXenes (-F, -OH, =O) create reactive sites for various chemical modifications, allowing the addition of specific functional groups that can greatly enhance their selectivity, capacity, and stability for dye removal. These methods aim to modify the surface features of MXenes without significantly altering their layered structure, thus maintaining their unique 2D properties while adding new functionalities. Surface functionalization techniques include chemical

modifications through covalent bonding of organic groups, alkali treatments to change surface terminations, organic coupling reactions to attach complex molecular structures, and surfactant modifications to adjust surface charge and hydrophilicity. Each approach provides distinct benefits, such as boosting electrostatic interactions, hydrogen bonding, π - π interactions, and other molecular interactions that affect dye adsorption. Successful surface functionalization not only improves adsorption performance but also enables the creation of pH-responsive materials, selective adsorbents for specific dyes, and systems with better regeneration ability, making them highly useful for practical water treatment.

Li and co-authors effectively synthesized Nb_2CT_x MXene with a particular surface area by etching Nb_2AlC with hydrofluoric acid (**Figure 5a**). The produced Nb_2CT_x MXene is highly effective at adsorbing methylene Blue (MB) and methyl orange (MO) dyes, achieving maximum capacity exceeding 500 mg/g . For starting concentrations of 100 and 200 mg/g , ~99% MO dye may be removed in ~30 min (**Figure 5 d and e**). However, MB dye removal requires just 5 min of contact time. Furthermore, the adsorption process of Nb_2CT_x MXene is governed by a pseudo-second-order kinetics model (**Figure 5 b and c**), with chemisorption at the surface absorption active sites serving as the rate limit.¹²⁷

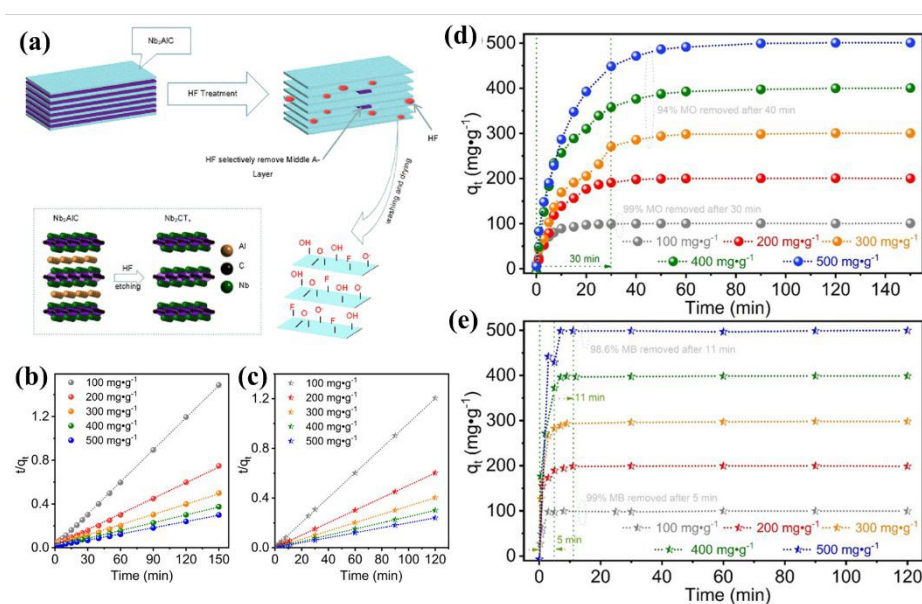


Figure 5: (a) Schematic Diagram of Nb₂CT_x MXene preparation by Etching Nb₂AlC with HF Solution. (b) & (c) Pseudo-second-order kinetics analysis for MO and MB adsorption by Nb₂CT_x at room temperature (d) and (e). Relationship between the adsorption capacity of Nb₂CT_x and contact time at different initial MO and MB concentrations at room temperature, pH = 7, and 1 g/L Nb₂CT_x powder dose. Reproduced with permission from Ref.¹²⁷ Copyright 2021, American Chemical Society.

The elimination of MB and congo red (CR) dyes from wastewater was accomplished by Li *et al.* by the fabrication of AA-alk-MXene-based adsorbent. This was accomplished by attaching acrylic acid (AA) to alkalized single or several layered MXene nanosheets. The influence of pH, temperature, concentration of dye, contact time and AA dosage on adsorption was examined. The process of adsorption used the pseudo-second-order kinetic and langmuir isotherm adsorption model. The highest adsorption capacity of a AA-modified sample (2 ml) for MB and CR was found to be 193.92 mg/g and 264.46 mg/g, respectively. Furthermore, hydrogen bonding, electrostatic attraction, along with interlayer force, are likely the primary driving forces behind the adsorption mechanism of AA-alk-MXene (**Figure 6 a and b**).¹²⁸

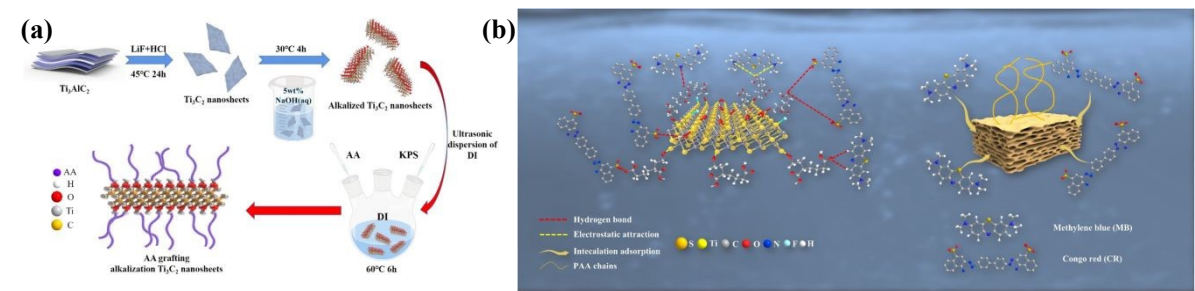


Figure 6: (a) Schematic Diagram for preparing AA-alk-MXene; (b) The adsorption mechanism diagram of AA-alk-MXene for MB and CR. Reproduced with permission from Ref.¹²⁸ Copyright 2022, Elsevier.

By modifying Ti_3C_2 to incorporate sulfonic groups through aromatic coupling-diazotization, Wei *et al.* achieved the fabrication of 2D material MXenes. This was accomplished by removing the Al layer from Ti_3AlC_2 through a simple process. A further investigation into the adsorption behavior of functionalized Ti_3C_2 against MB was conducted under various experimental conditions, including pH, solution temperature, initial MB concentration, and contact time. The results demonstrated that $\text{Ti}_3\text{C}_2\text{-SO}_3\text{H}$ achieved an adsorption performance of 111.11 mg/g. Kinetic and isotherm analyses discovered that the pseudo-first-order and the Langmuir isotherm adsorption models were appropriate for explaining the experimental data. The deposition of MB onto adsorbent surfaces was endothermic, while dye adsorption is most effective when the aqueous solution is alkaline (**Figure 7**).¹²⁹

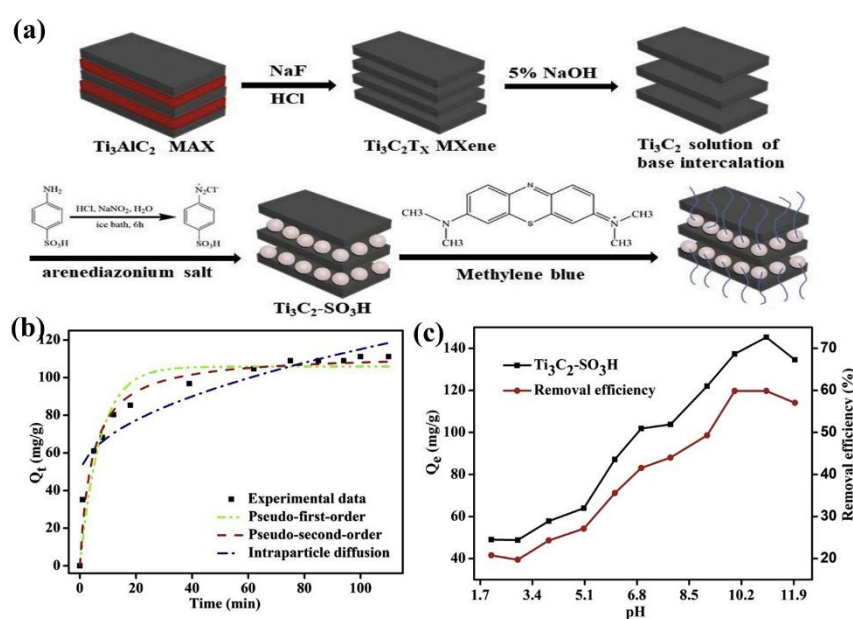


Figure 7: (a) Schematic diagram for the preparation of $\text{Ti}_3\text{C}_2\text{-SO}_3\text{H}$ for MB removal. (b) The kinetic curve of $\text{Ti}_3\text{C}_2\text{-SO}_3\text{H}$ adsorption MB. (c) Effect of pH; on the adsorption of MB onto $\text{Ti}_3\text{C}_2\text{-SO}_3\text{H}$. Reproduced with permission from Ref.¹²⁹ Copyright 2019, Elsevier.

Kelishami *et al.* designed a cetyltrimethylammonium bromide (CTAB)-modified multi-layered $\text{Ti}_3\text{C}_2\text{T}_x$ MXene (CMM) from Ti_3AlC_2 precursor and was employed to remove MO (**Figure 8**

a and b). This material adsorbent was resulted from an electrostatic combination between the cationic surfactant solution (CTAB) and negatively charged $\text{Ti}_3\text{C}_2\text{T}_x$ nanosheets. The accessible active sites were exposed as a result of this, which resulted in an increase in the spacing between the nanosheets and an increase in adsorption efficiency. The adsorbents were analyzed by using a few analytical techniques, and the impact of various parameters (contact time, pH, loading adsorbent, and initial concentration of dye) was investigated. The results of this study demonstrated that MO adsorbs CMM to its maximum capacity at an adsorbent dosage of 0.83 g/L, a contact time of 90 minutes, and a solution pH of 3. The results of the adsorption experiment were most accurately represented by the pseudo-second-order kinetic model ($R^2 = 0.9924$) and the Langmuir isotherm ($R^2 = 0.9990$). Approximately 213.00 mg/g was the maximum amount of adsorption capacity that MO possessed. There is a possibility that the MO adsorption mechanism on CMM involves many interactions, including electrostatic adsorption, π -cation interactions, and hydrogen bonding.¹³⁰

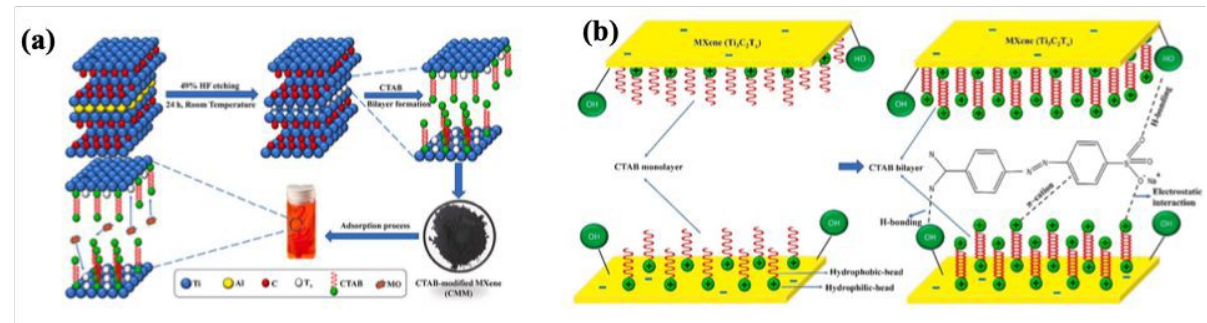


Figure 8. (a) Illustration diagram for the intercalation of CTAB in MXene (CMM) for the adsorption of MO; (b) CTAB monolayer and bilayer formation on MXene ($\text{Ti}_3\text{C}_2\text{T}_x$) sheets and adsorption mechanisms of MO by MXene sheets. Reproduced with permission from Ref.¹³⁰ Copyright 2024, Elsevier.

4.2. Interlayer Engineering and Spacing Modification

Interlayer engineering and spacing modification represent critical strategies for optimizing the structural architecture of MXenes to enhance their dye adsorption capabilities. The layered nature of MXenes, with interlayer spaces typically ranging from 0.98 to 1.5 nm in their pristine form, provides unique opportunities for structural manipulation to accommodate different dye molecules and improve accessibility to adsorption sites. These approaches focus on controlling the interlayer distance through various techniques that either expand, maintain, or systematically modify the spacing between MXene layers. Interlayer expansion techniques involve the insertion of molecules or ions that physically separate the layers, creating larger void spaces for enhanced accommodation of dye molecules. Ion intercalation methods utilize cations or anions to penetrate between layers, causing structural swelling and increased surface accessibility. Delamination strategies aim to entirely or partially separate multi-layered MXene structures into individual or few-layer nanosheets, maximizing the available surface area. Pillaring approaches involve the insertion of rigid molecular or ionic species that act as structural supports, maintaining controlled interlayer distances while preventing restacking. These interlayer engineering strategies are particularly effective because they directly address the accessibility limitations inherent in layered materials, enabling larger dye molecules to penetrate the interlayer galleries and access previously unavailable adsorption sites. The controlled modification of interlayer spacing also facilitates size-selective adsorption, improves mass transfer kinetics, and enhances the overall adsorption capacity by creating a three-dimensional network of accessible adsorption sites throughout the material structure.

Gogotsi *et al.* tested $\text{Ti}_3\text{C}_2\text{T}_x$ stacked sheets bound by hydrogen bonds and/or van der Waals interactions for the adsorption of MB dye. $\text{Ti}_3\text{C}_2\text{T}_x$ showed adsorption capacity of 39 mg/g for MB. The adsorption of MB on $\text{Ti}_3\text{C}_2\text{T}_x$ was most closely with Freundlich isotherm model.¹³¹

Through the use of alkali solution, ZhengMing *et al.* described a straightforward method for increasing the interlayer gap of $\text{Ti}_3\text{C}_2\text{T}_x$ while modulating the surface functional groups of the

material (**Figure 9a**).¹³² Using LiOH, the approach is able to enhance the spacing between layers by 29% in $\text{Ti}_3\text{C}_2\text{T}_x$ MXene. Additionally, the modification of functional groups involves the transformation of -F into -OH. NaOH- $\text{Ti}_3\text{C}_2\text{T}_x$ and LiOH- $\text{Ti}_3\text{C}_2\text{T}_x$ MXenes are able to adsorb MB more quickly compared to other types of MXene adsorbents. Notably, NaOH- $\text{Ti}_3\text{C}_2\text{T}_x$ has the maximum ability to adsorb MB, capacity of 189 mg/g, attributed to the combination of intercalation adsorption and surface adsorption of the MXene (**Figure 9b**). The High-resolution transmission electron microscopy (HRTEM) images (**Figure 9c, d, and e**) reveal significant structural modifications following alkaline metal ion intercalation in LiOH- $\text{Ti}_3\text{C}_2\text{T}_x$, NaOH- $\text{Ti}_3\text{C}_2\text{T}_x$, and KOH- $\text{Ti}_3\text{C}_2\text{T}_x$ systems. The intercalation process involves alkaline metal ions (Li^+ , Na^+ , K^+) inserting between MXene layers, causing interlayer spacing expansion through electrostatic interactions and hydration shell formation. Structural expansion mechanisms include: direct ion insertion where alkaline cations occupy interlayer galleries, creating physical separation between $\text{Ti}_3\text{C}_2\text{T}_x$ sheets; hydration-induced swelling as intercalated ions attract water molecules, forming hydration shells that further increase interlayer distance; and surface functionalization changes where alkaline treatment converts surface -F terminations to -OH groups, enhancing hydrophilicity and water uptake. The measured interlayer spacings show progressive expansion: LiOH- $\text{Ti}_3\text{C}_2\text{T}_x$ (~1.22-1.65 nm), NaOH- $\text{Ti}_3\text{C}_2\text{T}_x$ (~1.16-2.0 nm), and KOH- $\text{Ti}_3\text{C}_2\text{T}_x$ (~1.40-1.73 nm), correlating with ionic radius differences ($\text{Li}^+ < \text{Na}^+ < \text{K}^+$) and hydration characteristics. This structural expansion directly contributes to enhanced adsorption capacity by increasing accessible surface area and creating larger pore channels for dye molecule accommodation, explaining the superior MB adsorption performance observed in alkaline-modified MXene systems.

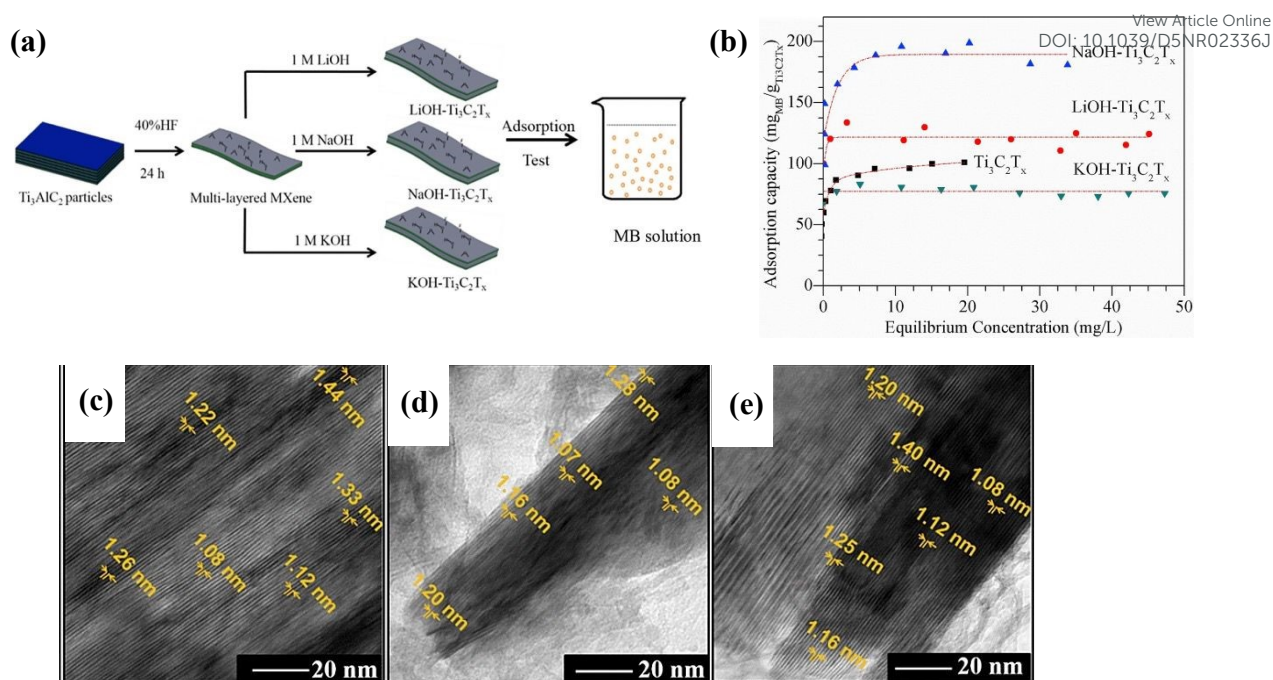


Figure 9: (a) Illustration diagram for the fabrication of different Alkali- $\text{Ti}_3\text{C}_2\text{T}_x$ towards adsorption of MB dye. (b) Adsorption isotherms of MB on $\text{Ti}_3\text{C}_2\text{T}_x$, $\text{LiOH-Ti}_3\text{C}_2\text{T}_x$, $\text{NaOH-Ti}_3\text{C}_2\text{T}_x$ and $\text{KOH-Ti}_3\text{C}_2\text{T}_x$. HRTEM images of (c) $\text{LiOH-Ti}_3\text{C}_2\text{T}_x$, (d): $\text{NaOH-Ti}_3\text{C}_2\text{T}_x$ and (e): $\text{KOH-Ti}_3\text{C}_2\text{T}_x$. Reproduced with permission from Ref.¹³² Copyright 2017, Elsevier.

Yu and co-workers developed a novel hydrothermal method utilizing less toxic etching agents such as NaBF_4 , HCl for the synthesis of Ti_3C_2 MXene ($h\text{-Ti}_3\text{C}_2$). Because of slow-release mechanism during hydrothermal, $h\text{-Ti}_3\text{C}_2$ has a higher lattice parameter c , and a longer interlayer distance, as well as a better SSA than $t\text{-Ti}_3\text{C}_2$. The hydrothermal etching method avoids high-concentration HF and is more effective in synthesizing Ti_3C_2 flakes. Furthermore, the etching method can be used for other MXene compositions, such as Nb_2C and $h\text{-MXenes}$ shows superior adsorption performance for MB, with a capacity of 24 mg/g .¹³³ Cagnetta and colleagues synthesized $\text{Ti}_3\text{C}_2\text{T}_x$ MXene layers pillared with terephthalate using an innovative MC etching approach that involved exfoliating a titanium MAX phase with a small volume of concentrated hydrofluoric acid using a high-energy ball mill. The obtained material has a

greater SSA and strong adsorption capability of MB of 209 mg/g because of wider interlayer space between free carboxylate groups of terephthalate and MXene sheets. Also, dye adsorption with the material is best explained by pseudo-second-order model.¹³⁴

Yang *et al.* produced a suspension of $\text{Ti}_3\text{C}_2\text{T}_x$ MXene nanosheets using the intercalation and delamination of multi-layered $\text{Ti}_3\text{C}_2\text{T}_x$ utilizing TMAOH. The prepared material showed excellent adsorption of cationic MB dye. The highest adsorption capacity, noted at 318 K, reached 1026 mg/g. This performance best fits with pseudo-second-order kinetic and Freundlich isotherm models. The mechanism of adsorption is mainly attributed to the ion exchange and electrostatic attraction for MB removal.¹³⁵ By intercalating GO into an Alk-MXene layer, Li and the authors were able to create a novel AMXGO absorbent. This absorbent demonstrated a high level of efficiency in the elimination of MG and anionic CR (**Figure 10**). The results of the FTIR, XRD, and SEM investigations showed that the AMXGO absorbent possesses a characteristic 3D layer-by-layer structure with plentiful oxygen-bearing groups, and that its heat stability has greatly improved. Based on the results of the BET analysis, it was determined that the AMXGO1 adsorbent possesses a greater SSA ($16.686 \text{ m}^2/\text{g}$) and pore volume ($0.04733 \text{ cm}^3/\text{g}$). It was discovered that the performance of adsorption was dependent on the mass ratio of Alk-MXene to GO, the starting dye concentration, pH, contact time, and temperature. The AMXGO1 absorbent, which had a mass ratio of 3:1, had the maximum capacity to adsorb 1111.6 mg/g of MG and 1133.7 mg/g of CR, and it had dye removal rates that were greater than 92%. Both pseudo-second-order kinetic and Freundlich isotherm models are utilized to describe the adsorption behaviour of AMXGO1 for both CR and MG.¹³⁶

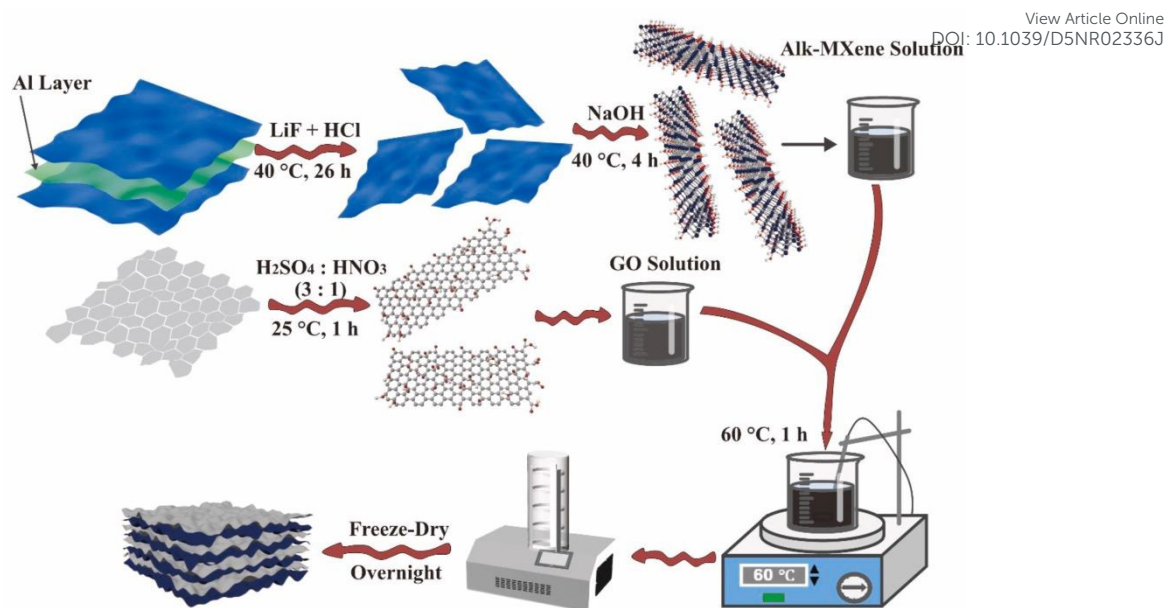


Figure 10: Diagram for the preparation of AMXGO. Reproduced with permission from Ref.¹³⁶

Copyright 2024, Elsevier.

4.3. Composite Formation Strategies

Composite formation strategies represent a versatile and powerful approach to developing advanced MXene-based adsorbents by synergistically combining the unique properties of MXenes with complementary materials to achieve enhanced dye removal performance. These strategies leverage the principle that the integration of different materials can create synergistic effects that surpass the individual performance of constituent components, resulting in composites with superior adsorption capacities, improved selectivity, enhanced stability, and additional functionalities such as magnetic separability or pH responsiveness. The composite formation approaches can be systematically categorized based on the nature of the secondary materials integrated with MXenes. MXene-organic composites involve the combination of MXenes with organic polymers, biomaterials, or carbon-based materials, creating hybrid systems that benefit from the conductivity and surface chemistry of MXenes while gaining enhanced mechanical properties, biocompatibility, or specific functional groups from the

organic components. MXene-inorganic composites integrate MXenes with metal oxides, hydroxides, or other inorganic materials, often resulting in enhanced adsorption capacity through increased surface area, additional adsorption sites, or new interaction mechanisms such as magnetic separation capabilities. Multi-hybrid systems represent the most sophisticated approach, combining MXenes with multiple different material types to create complex architectures that integrate the advantages of various components, such as combining organic polymers for flexibility, inorganic nanoparticles for functionality, and MXenes for conductivity and surface area. These composite formation strategies not only enhance the fundamental adsorption properties but also address practical considerations such as material recovery, regeneration efficiency, mechanical stability, and cost-effectiveness, making them particularly attractive for real-world water treatment applications where multiple performance criteria must be simultaneously optimized.

Peng *et al.* effectively synthesized MXene-based core-shell composites, MXene-COOH@-(PEI/PAA)_n, using layer-by-layer technique. Furthermore, these nanocomposites were studied using spectral and morphological techniques, revealing that they contain more reaction sites and mesoporous structures. The produced composites were able to efficiently adsorb MB dye after approximately 200 minutes, showing that the generated composites might be used as a highly efficient adsorbent. The observed data are well matched with pseudo-second-order model and show a significant correlation coefficient of $R^2 > 0.99$, indicating that the core-shell composites have outstanding adsorption capabilities.¹³⁷

The PHGC/MXene that was created by Zhang *et al.* (**Figure 11 a and b**) exhibited remarkable a strong selectivity and cycle stability for ionic dyes across a range of pH levels. PHGC/MXene shown exceptional adsorption selectivity and great pH-responsiveness in the mixed dyes system. It was able to adsorb MB at a pH of 11.0, and methyl blue (AB93) at pH 2.0, achieving maximum adsorption capacities of 555.56 mg/g and 207.47 mg/g, respectively. The adsorption

kinetics for these dyes were found to be in agreement with the two-level kinetic model that was proposed, while Langmuir model demonstrated a good fit for adsorption isotherms being studied. It was determined that electrostatic adsorption and hydrogen bonding were the primary processes responsible for the adsorption process, with van der Waals forces also making a contribution. Despite undergoing 12 rounds of desorption and regeneration, the clearance rates for MB and AB93 remained more than 90%.¹³⁸

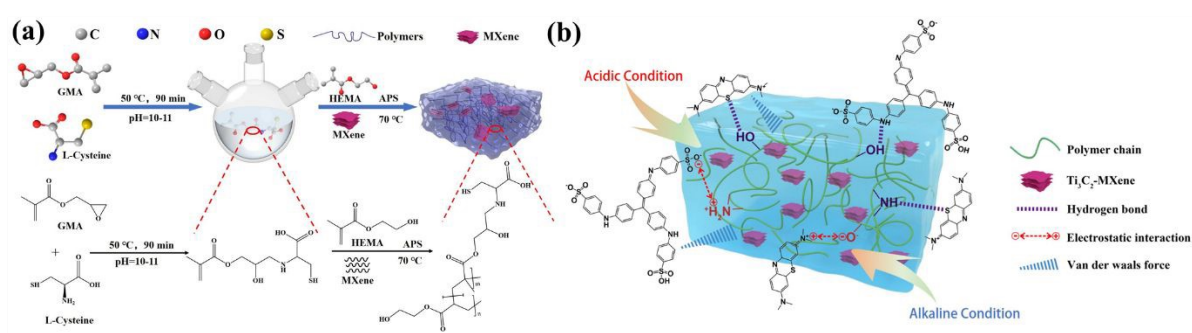


Figure 11. (a) Schematic preparation of PHGC/MXene hydrogel; (b) Adsorption mechanism diagram of PHGC/MXene for AB93 or MB. Reproduced with permission from Ref.¹³⁸ Copyright 2019, Elsevier.

The amino-functionalized bacterial cellulose/Ti₃C₂T_x MXene (ABC/MX) composites were developed by Wen and his colleagues by the utilization of an electrostatic self-assembly technique that comprised modifications of polydopamine (PDA) and polyethyleneimine (PEI) (**Figure 12a**). Based on the findings of this research, the effective insertion of amino groups strengthens the interfacial contacts between nanofibers of BC and nanosheets of Ti₃C₂T_x, it also enhances the number of active sites for adsorption. With a maximal ability to adsorb 1103.7 mg/g of CR, the results demonstrate that the composite possesses a remarkable removal efficiency.¹³⁹ Using a chemical etching approach, Wang *et al.* created a few-layer MXene. Subsequently, PEI was grafted onto the surface of the MXene with the assistance of glutaraldehyde-assisted crosslinking (**Figure 12b**). The adsorption properties of water-soluble

dyes were extensively studied. The results indicated that grafting PEI may improve MXene exfoliation as well as adsorption capacities. The modified MXene showed a remarkable ability to adsorb 909.1 mg/g of MO. **Figure 12c** reveals the binding mechanism between the components of the MPEI composites. The pseudo-second-order kinetic and Langmuir isothermal adsorption model are the best appropriate to the adsorption processes of MO, which are spontaneously endothermic and chemisorption.¹⁴⁰

Wang and co-authors designed a novel CoFe₂O₄/CS composite-supported onto alk-MXene magnetic adsorbent *via* hydrothermal and self-assembly approach (**Figure 12d**). Adding CoFe₂O₄/CS to alk-MXene can significantly increase the capacity to adsorb anionic and cationic dyes. The prepared material showed high adsorption capacity upto 1333.9, 537.6, and 2095.9 mg/g for rhodamine B (RhB), malachite green (MG), and CR dyes, respectively. The higher adsorption performance of the composites is attributed to synergistic effect of hydrogen bonding, π - π interaction, and electrostatic interaction.¹⁴¹

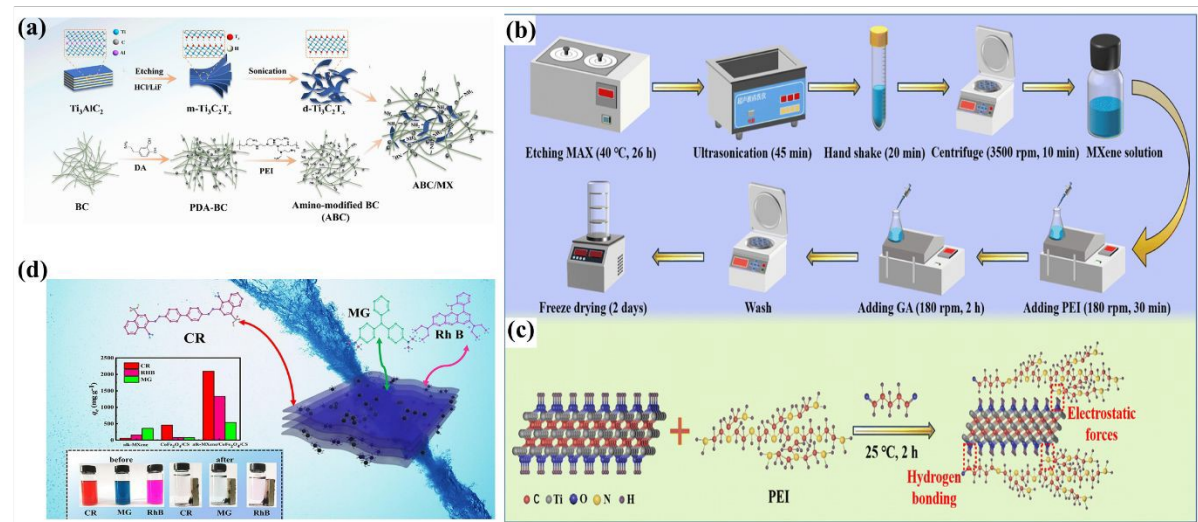


Figure 12: (a) Schematic diagram of the preparation of ABC/MX composite. Reproduced with permission from Ref.¹³⁹ Copyright 2024, Elsevier. (b) Synthesis procedures of the MPEI composites and (c) Diagram of the inter-component microscopic combination mechanism in MPEI composites. Reproduced with permission from Ref.¹⁴⁰ Copyright 2023, Royal Society of

Chemistry. (d) Adsorption capacity of different dyes onto alk-MXene/CoFe₂O₄/CS composite. View Article Online
DOI: 10.1039/D5NR02336J

Reproduced with permission from Ref.¹⁴¹ Copyright 2023, Elsevier.

Zhang *et al.* used an in-situ growing technique to create a new 2D MXene coated with Fe₃O₄. The prepared material was analyzed for MB dye adsorption at different temperatures. This material exhibits superparamagnetic characteristics and a typical 2D lamellar structure. The elimination of MB occurred as endothermic process, as evidenced by maximum elimination capacity of 11.68 mg/g and 91.93% decolorization efficiency at 55 °C, considerably surpassing the performance at lower temperatures. Additionally, at high temperatures (40 and 55 °C), the adsorption isotherm demonstrated that the model which best fits for removal method of MB is Freundlich isotherm, but at low temperatures (25 °C), the Langmuir isotherm fit best. Through electrostatic attraction and hydrogen bonding at high temperatures, Ti-OH groups on the material's surface enhance MB decolorization. At 25 °C, surface adsorption by electrostatic interaction aids in the elimination of MB (**Figure 13**).¹⁴²

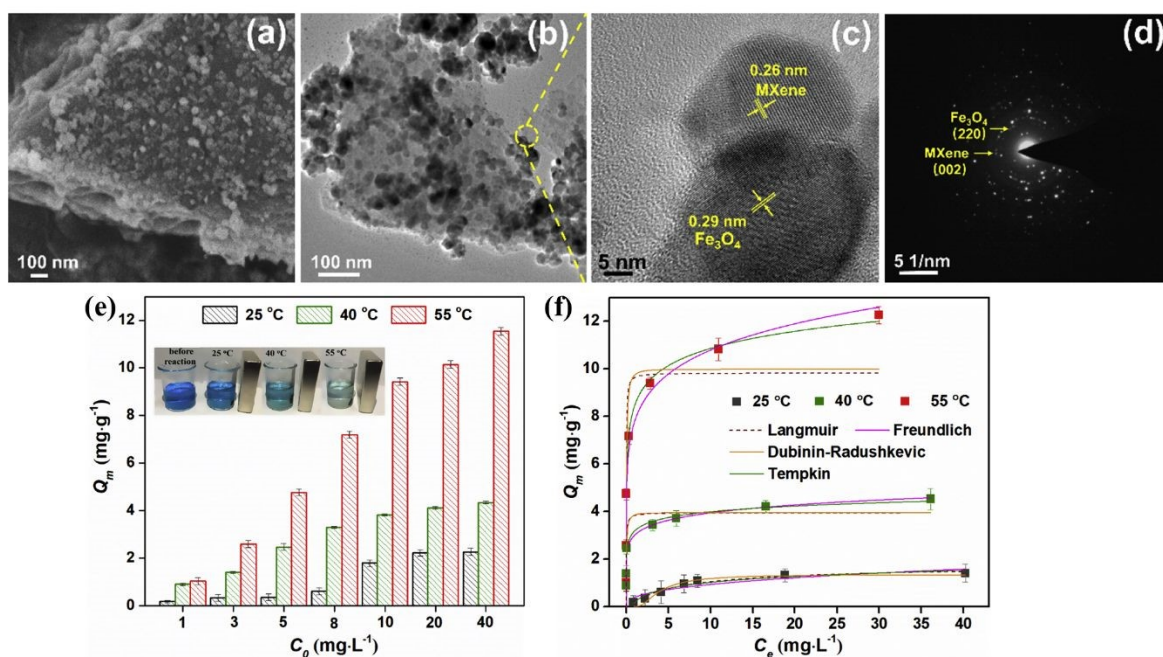


Figure 13: (a) SEM, (b) TEM, (c) HRTEM, (d) SAED pattern of 2D-MX@Fe₃O₄ nanocomposites. (e) The removal capacity of MB over 2D-MX@Fe₃O₄ at 25, 40 and 55 °C. (f) Adsorption isotherm of 2D-MX@Fe₃O₄ for MB removal. Reproduced with permission from Ref.¹⁴² Copyright 2019, Elsevier.

Eltaweil *et al.* fabricated Ti₃C₂T_x/NiFeMn-LDH@Gel composites in order to remove organic CR dye synthesized *via* cross-linking reaction by incorporating Ti₃C₂T_x MXene and NiFeMn-LDH into gelatin (**Figure 14a**). The results shown that the adsorption ability of Ti₃C₂T_x/NiFeMn-LDH@Gel towards CR was significantly enhanced by raising the Ti₃C₂T_x content in the matrix to 10%. With a q_{\max} value of 588.24 mg/g, the Freundlich model offered the best explanation for adsorption of CR. Moreover, pseudo-second-order model was determined to be best for studying the adsorption kinetics of CR accompanied. The remarkable recyclability over multiple cycles confirms the composite's sustainability.¹⁴³

Using a macroporous polymeric support, Yang *et al.* were able to effectively generate a flexible, rigid, and porous MXene/COF hybrid flake. This flake is characterized by the presence of three 2D COF flakes that are bridged covalently on the surface of the MXene by the process of in-situ growth. COFs (TpTAPB, TpBD, TpPa) were synthesized via Schiff-base reactions using 1,3,5-triformylphloroglucinol with 1,3,5- tris(4-aminophenyl) benzene, benzidine and p-phenylenediamine monomers (**Figure 14b**). Further, interlayer of MXene (Ti₃C₂T_x) nanosheets expands adjacent interlayer spacing and introduces numerous sieving pores when COFs are intercalated into it. The optimized MXene/TpTAPB hybrid membrane when utilized for eliminating organic dyes, it exhibits a removal efficiency of 96.4% for AB93, 98.2% for CR, 97.2% for MO and 98.7% for chrome black T.¹⁴⁴

Wang *et al.* developed alk-MXene/ZIF composite, with small ZIF particles in situ synthesized on interlayer and on the alk-MXene surface (**Figure 14c**). In the meantime, stable intercalation

framework is produced, allowing dye molecules to transfer mass more quickly. Adding ZIF particles increases the adsorption functional groups and SSA in alk-MXene/ZIF composite. The composites achieved excellent adsorption values, with maximum capacity of 7111.3 and 539.7 mg/g for MG and CR, respectively. The impact of coexisting ions, temperature, concentration, contact time, and pH on the adsorption performance were studied. Adsorption kinetics studies demonstrated that dye adsorption onto the composite surface is consistent with Elovich and pseudo-second-order kinetic models. Additionally, the adsorption mechanism of adsorbent is mainly due to chemisorption.¹⁴⁵

By integrating few-layer MXene and hydrophilic biomaterial DASNP, followed by immobilization of DASNP onto few-layer MXene through dialdehyde-based cross-linking technique, Li et al. were able to generate a novel environmentally friendly composite material known as DSP-M (**Figure 14d**). The findings indicate that DSP-M had outstanding adsorption efficiency for both adsorbates. Further, Langmuir maximum adsorption capacity for monomer adsorption for RhB was measured to be 678.19 mg/L, while the capacity for CR was measured to be 754.41 mg/L. These results were in agreement with the pseudo-second-order, intraparticle diffusion, and Langmuir models. For the purpose of conducting additional research on the adsorptive mechanism, the statistical model of physics was utilized. The DSP-M characteristics post-adsorption and findings of the simulation suggest that the RhB and CR removal by DSP-M occurred predominantly through physical adsorption mechanism involving van der Waals, electrostatic force, and hydrogen bonding.¹⁴⁶

Wang and co-authors designed a ZnS/CuFe₂O₄/MXene (ZSCFOM) composites featuring ternary heterostructures *via* solvothermal approach to efficiently adsorb azo dyes. The composite primarily achieved azo dyes adsorption via electrostatic interactions and hydrogen bonding, with maximum capacity to adsorb 377 mg/g for DBM and 390 mg/g for DBRN. The

pseudo-second-order and Langmuir model were used to characterize the adsorption properties of ZSCFOM, suggesting that adsorbate forms a monolayer on the ZSCFOM surface.¹⁴⁷

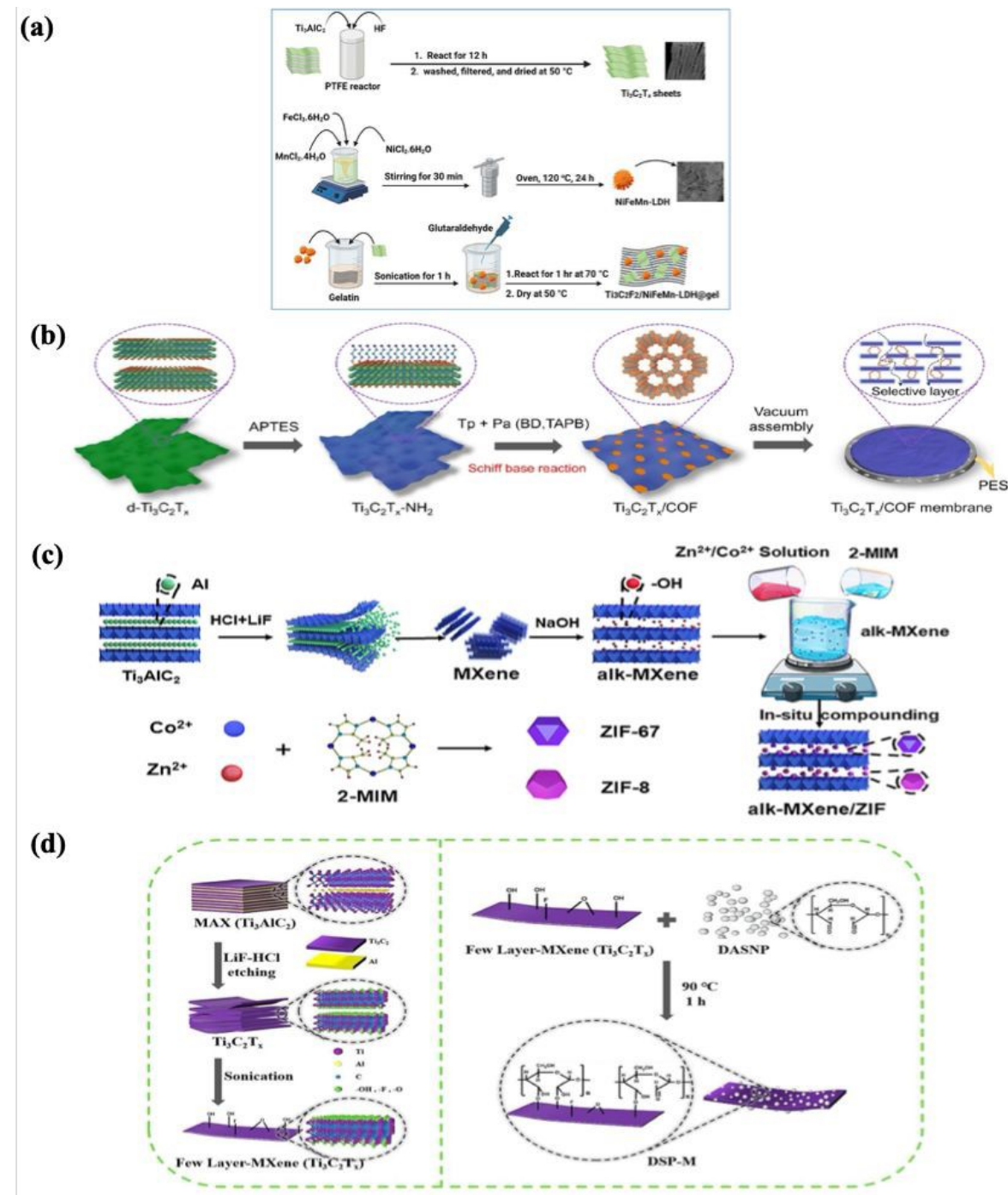


Figure 14: (a) A schematic presentation for the synthesis of $\text{Ti}_3\text{C}_2\text{T}_x/\text{NiFeMn-LDH@Gel}$ composite. Reproduced with permission from Ref.¹⁴³ Copyright 2024, Elsevier. (b) Schematic illustration of the separation mechanism of MXene/COF in the dye wastewater purification process. Reproduced with permission from Ref.¹⁴⁴ Copyright 2024, Elsevier. (c) Schematic

preparation process of alk-MXene/ZIF composite. Reproduced with permission from Ref.¹⁴⁵ View Article Online
DOI: 10.1039/D5NR02336J

Copyright 2024, Elsevier. (d) Schematic illustration for the step-wise synthesis of DSP-M composite. Reproduced with permission from Ref.¹⁴⁶ Copyright 2023, Elsevier.

Moreover, green methods have also been adopted to design MXene-based nano adsorbents. Ijaz *et al.* developed an efficient and rapid Fe₂O₃/BC/MXene composite by functionalizing *Shorea faguettiana* biochar with Fe₂O₃ and MXene for selective adsorption. XPS and FTIR revealed that the Fe₂O₃/BC/MXene composites had more surface functional groups (F⁻, C=O, CN, NH, and OH⁻) than the original biochar. The characterization revealed that the intended modified BC had a high MB adsorption capacity in wastewater. At 293 K, MB showed a q_m value of 899.03 mg/g. The adsorption followed a pseudo-second-order model ($R^2 = 1$) and the Langmuir isotherm. Surface electrostatic forces and hydrogen bonding helped to remove MB more efficiently. This demonstrates monolayer adsorption on the Fe₂O₃/BC/MXene composite, which is regulated by chemical adsorption.¹⁴⁸

An effective, fast, and selective adsorption of MB was achieved by Imtiaz *et al.* through the development of Ni₃(HITP)₂/MXene/CS. This was accomplished by functionalizing chitosan biopolymer with MXene and 2D MOFs (Ni₃(HITP)₂). The TEM image clearly shows irregularly-shaped MOFs and spherical CS particles adhered to the MXene surface. At 298 K, MB had a maximum adsorption capability of 424.99 mg/g, 400.59 mg/g at 308 K, and 305.80 mg/g at 318 K. The adsorption of MB on Ni₃(HITP)₂/MXene/CS composite followed the pseudo-second-order kinetic and Langmuir models. The composite has -OH, -F, -O, and N groups, which allow for effective MB absorption *via* hydrogen bonding, electrostatic attraction, and complexation interaction.¹⁴⁹

4.4. Morphological and Structural Control

Morphological and structural control strategies focus on engineering the macroscopic architecture and three-dimensional organization of MXene-based materials to optimize their performance in dye adsorption applications. Unlike surface functionalization or interlayer modifications that primarily alter chemical properties or nanoscale structure, these approaches target the overall physical form, porosity, and architectural arrangement of MXene materials to enhance mass transfer, improve accessibility, and facilitate practical implementation in water treatment systems. The controlled manipulation of morphology enables the creation of materials with tailored pore structures, enhanced mechanical properties, and optimized flow characteristics that are essential for real-world applications. Membrane fabrication represents a critical approach for creating selective barriers with controlled permeability and high surface area-to-volume ratios, enabling efficient dye removal while maintaining structural integrity under operational conditions. Aerogel formation involves the development of ultra-lightweight, highly porous three-dimensional networks that maximize surface accessibility while providing excellent adsorption kinetics through interconnected pore channels. Nanofiber integration focuses on incorporating MXenes into fibrous architectures that combine high surface area with excellent mechanical flexibility and easy handling characteristics. Three-dimensional architecture design encompasses the creation of complex hierarchical structures that integrate multiple length scales, from nanoscale MXene sheets to macroscopic frameworks, enabling optimized mass transfer pathways and enhanced adsorption site utilization. These morphological control strategies are particularly valuable because they address critical practical considerations such as pressure drop in flow-through systems, ease of material recovery and regeneration, mechanical durability under operational stresses, and scalability for industrial applications. By controlling the overall architecture and form factor of MXene-based adsorbents, these approaches bridge the gap between fundamental material

properties and practical implementation requirements, enabling the development of efficient, robust, and economically viable water treatment technologies.

Purkayastha and co-author used vacuum filtering to produce 2D $\text{Ti}_3\text{C}_2\text{T}_x$ MXene on porous PAN membrane, demonstrating its effective adsorption of MB. MX-PAN had an adsorption effectiveness of 85%, compared to 12% achieved by PAN membrane. Adsorption efficiency increased dramatically after manufacturing PAN membrane along with $\text{Ti}_3\text{C}_2\text{T}_x$ MXene nanoflakes.¹⁵⁰ Zhang *et al.* combined SA with d- $\text{Ti}_3\text{C}_2\text{T}_x$ nanosheets (MXene), then employed electrospinning and subsequent Ca^{2+} -mediated crosslinking for production of various SA/MXene NMs. The impact of MXene in NMs on MB adsorption ability were examined. SA/MXene NMs exhibited the ability to adsorb 440 mg/g of MB at the optimal MXene concentration comprising 0.74 wt.%, surpassing electrospun SA NMs, pristine MXene, or SA/MXene composite beads with equivalent MXene content. Moreover, the optimal SA/MXene NMs demonstrated high reusability. The Langmuir and pseudo-second-order model were in good agreement with the results, indicating monolayer adsorption aligned with the mechanism of chemical adsorption.¹⁵¹

By using cross-linking approaches to incorporate PEI and amino-functionalized $\text{Ti}_3\text{C}_2\text{T}_x$ into SA aerogel matrix, Wang *et al.* created the MXene/PEI-modified SA aerogel. The plentiful active PEI groups, together with the reduction capabilities of MXene, considerably enhance the adsorption capacity of 3568 mg/g for CR, attributed to the robust electrostatic attraction along with the synergistic effects of intercalation and surface adsorption. The results showed that adsorption process of CR aligned well with pseudo-second-order kinetic and Langmuir isotherm model. The mechanical strength of the aerogel was greatly enhanced by the double-network structure composed of polymeric PEI and SA, allowing for easy recycling without secondary contamination, with only a slight reduction in capacity following five cycles.¹⁵²

The innovative nanocomposite hydrogel of ZIF-8@IL-MXene/Poly(N-isopropylacrylamide) (NIPAM), which was fabricated by Xiong and his co-authors, is capable of successfully adsorbing crystal violet (CV) from wastewater (**Figure 15a**). The formation of composite hydrogel IL-MXene/PNIPAM was accomplished through in-situ polymerization by grafting IL onto MXene surface and subsequently introduced into solutions of NIPAM monomer. This process was completed in a single step. Utilizing in-situ formation of ZIF-8 on pore walls of composite hydrogels, ZIF-8@IL-MXene/PNIPAM were produced. The prepared nanocomposite hydrogel displayed maximum adsorption capacities for CV of 325.03 mg/g under ambient temperature, with the reducing to 91% following five cycles of adsorption-desorption. The results are in accordance with Freundlich and pseudo-second-order kinetics models, based on several interactions between molecules of adsorbent and hydrogel.¹⁵³

By self-assembling CNTs, CTAB and MXene nanosheets, Ding *et al.* were able to synthesize a unique CMC three-dimensional composite. In order to determine whether or not the produced material could adsorb AO7, CR, and MO the material was tested. In comparison to CNTs and MXene, the CMC composite had a greater capacity for adsorption of AO7, CR, and MO with maximum capacity to adsorb 367.9, 628.5, and 294.2 mg/g, respectively. As the temperature increased, the adsorption capabilities for AO7 and MO by CMC composite reduced, whereas the adsorption capabilities of CR increased. When it comes to the process of adsorption, the hydrogen bonding, π - π electron-donor-acceptor, and electrostatic interactions were all crucial contributors. The energy distribution of sites analysis revealed that the CMC composite possessed more adsorption active sites than MXene and CNTs. As a result, CMC composites possessed better adsorption capabilities for the anionic dyes that were being studied. It is possible that the changes in adsorption patterns for the anionic dyes can be attributed to the availability of the adsorption sites as well as the changes in the heterogeneity of the site on the CMC surface. Based on the findings of the approximate site energy distribution analysis, it was

discovered that the CMC composite has a greater number of adsorption active sites compared to MXene and CNTs. This indicates that the CMC composite possesses a superior adsorption capability for specific anionic dyes. The amount of accessible adsorption sites and the change in site heterogeneity on the CMC surface are two factors that can be attributed to the differences in adsorption behaviors that occur between three anionic dyes from different compounds (**Figure 15b-f**).¹⁵⁴

Wang and co-authors developed an innovative approach to modify the electrospun polylactic acid fibrous membrane, improving its adaptability for treatment of wastewater under challenging conditions. PLA fibre membranes were initially coated with PDA, followed by deposition of MXene facilitated by PDA (**Figure 15g**). The as-prepared SC-PLA/PDA/MXene membranes proved effective for MB adsorption, with maximum capacity to adsorb 434.8 mg/g. The MB adsorption by the membrane aligns closely with the pseudo-second-order kinetic and Langmuir models. The above circumstance also indicates that chemisorption predominates in the MB elimination process. In essence, the membrane and MB molecules exhibit π - π interaction and electrostatic attraction.¹⁵⁵

Xing *et al.* fabricated TiVCT_x MXene/graphene nanosheet-based aerogels, named TiVCT_x/GAs, via a simple self-assembly hydrothermal process, followed by freeze-drying (**Figure 15h**). Combining bimetallic MXene and graphene aerogel in TiVCT_x/GAs provides a remarkable broad-spectrum dye removal capability from wastewater. TiVCT_x/GAs effectively adsorb different dyes, with capacities of 319.67, 229.97, 303.45, and 217.87 mg/g for MB, CR, RB, and MO, respectively. Kinetics and thermodynamics studies confirm that the process of adsorption follows pseudo-second-order kinetic and Langmuir adsorption models.¹⁵⁶

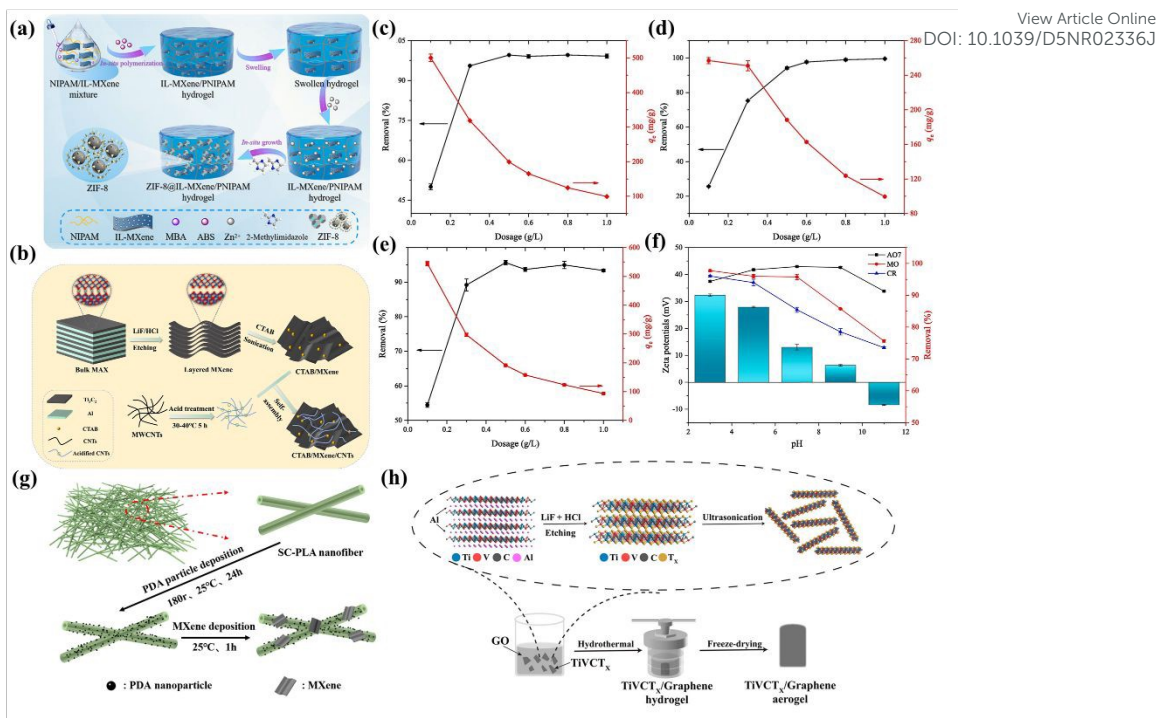


Figure 15: (a) Schematic illustration of ZIF-8 grown in situ in composite hydrogels. Reproduced with permission from Ref.¹⁵³ Copyright 2024, Elsevier. (b) Scheme of the preparation process of the CMC composite. (c), (d) & (e) Effect of adsorbent dosage on the removal efficiency and adsorption capacity (q_e) of AO7, MO, and CR. (f) effect of pH on the adsorption and zeta potentials of the CMC composite at different pH values. Reproduced with permission from Ref.¹⁵⁴ Copyright 2024, Elsevier. (g) Fabrication procedures of composite fibers. Reproduced with permission from Ref.¹⁵⁵ Copyright 2024, Elsevier. (h) Preparation Process of TiVCT_x/Gas. Reproduced with permission from Ref.¹⁵⁶ Copyright 2024, Elsevier.

MXene/carbon foam (MCF) hybrid aerogel was synthesized by Li and co-authors using Ti₃C₂T_x-MXene and MF. Both cationic and anionic dyes were used to investigate the removal properties of the MCF. Several different methods of characterization were utilized in order to examine the physicochemical properties of MCF. Additionally, statistical physics models were utilized in order to gain a deeper comprehension of dye adsorption mechanism that it possesses. MCF was shown to have outstanding adsorptive efficiency against the harmful dyes CR and

MB, with adsorption capacities of 647.75 mg/g and 356.97 mg/g respectively. According to the findings, these capacities were better fitted for Langmuir and pseudo-second-order kinetic models. In addition, the saturated multilayer model was utilized in order to explore the molecular process that underlies the adsorption systems of MCF-MB and MCF-CR components. Through a process that involved multi-anchoring (303 and 318 K), single connection (333 K), and mixed adsorption orientation, the findings of the numerical simulation demonstrate that MCF adsorbed the MB molecules in the form of dimers. In contrast, CR molecules were adsorbed as monomers through a process that included mixed adsorption orientation (333 K), multi-anchored and pure non-parallel adsorption directions (303 K and 318 K), and adsorption directions that were not parallel to one another.¹⁵⁷

Electrostatic self-assembly of 2D MXene nanosheets and biomass-activated carbon was used by Li *et al.* to create a heterostructure adsorbent that they referred to as CMAC composite. This was accomplished in the presence of a CTAB. This method prevented the re-stacking of MXene nanosheets, which resulted in a reduction in the multilayer plate structure of MXene and an increase in the layer spacing. This resulted in an increase in exposure of accessible active sites, which made adsorption performance even more significantly improved. As a consequence of the tests, it was shown that CMAC possessed an exceptional adsorption efficiency for CR, with adsorption capacities of 1264.032 mg/g. The Langmuir, intraparticle diffusion and pseudo-second-order kinetic models suit the dye adsorption data well. The adsorption mechanism is attributed to the combination of hydrogen bonding, physical adsorption, and electrostatic interactions.¹⁵⁸

Li *et al.* developed a straightforward and eco-friendly foaming technique in order to produce a macroporous cellulose nanocrystals (CNC)/MXene/polyvinyl alcohol (PVA) (C-CMP) foam that possessed exceptional adsorption capabilities. Glutaraldehyde was utilized as a crosslinker to enhance the adsorption effectiveness of MB dye. The adsorption experiment revealed that

MB has a maximum adsorption capacity of 239.92 mg/g. The adsorption performance corresponded well to Langmuir isotherm and pseudo-second-order kinetic models. Thermodynamic studies showed that the process of adsorption was spontaneous and endothermic. The study demonstrated that the adsorption between MB and C-CMP was due to electrostatic interaction.¹⁵⁹

[View Article Online](#)
DOI: 10.1039/D5NR02336J

Table 1: Comparison of different MXene-based materials for adsorption of various dyes.

MXene	Dye	Adsorption capacity/ % Removal efficiency	Experimental Conditions	Isotherms/ kinetics	Regeneration	Toxicity Evaluation
$\text{Ti}_3\text{C}_2\text{T}_x^{131}$	MB	39	C_0 (MB) = 0.05 mg/ml, 25 °C, 20 h	Freundlich	<ul style="list-style-type: none"> • $\text{Ti}_3\text{C}_2\text{T}_x$ gradually oxidises to TiO_2 and $\text{Ti}(\text{OH})_4$ in water, limiting reusability. • Structural changes (layer expansion and disorder) occur after 20 h in dye solution. • Material is not stable for long-term aqueous applications or storage. 	<ul style="list-style-type: none"> • No direct cytotoxicity or ecotoxicity tests were reported. • Possible formation of TiO_2 NPs and fluoride leaching may raise concerns. • Further studies needed to assess environmental and biological safety.
$\text{NaOH-Ti}_3\text{C}_2\text{T}_x^{132}$	MB	189	25 °C, pH = 6–6.5	Langmuir/PSO	<ul style="list-style-type: none"> • No regeneration or reuse tests were conducted. 	<ul style="list-style-type: none"> • No cytotoxicity, ecotoxicity, or leaching tests were included.
$\text{LiOH-Ti}_3\text{C}_2\text{T}_x^{132}$	MB	121	25 °C, pH = 6–6.5	Langmuir/PSO	<ul style="list-style-type: none"> • Material performance stability over multiple cycles not studied. 	<ul style="list-style-type: none"> • Alkaline treatment may reduce fluoride (-F) groups, potentially
$\text{KOH-Ti}_3\text{C}_2\text{T}_x^{132}$	MB	77	25 °C, pH = 6–6.5	Langmuir/PSO		

					<ul style="list-style-type: none"> • Suggests need for future work on recyclability. 	<p>improving biocompatibility.</p> <ul style="list-style-type: none"> • Safety and environmental impact not evaluated.
$h\text{-Ti}_3\text{C}_2^{133}$	MB	24	2 h	-	<ul style="list-style-type: none"> • No regeneration, desorption, or reuse cycles were tested or discussed. • Long-term stability of the MXenes in dye removal applications not evaluated. • Future studies should assess recyclability to validate practical applicability. 	<ul style="list-style-type: none"> • No direct toxicity, cytocompatibility, or environmental safety evaluations made. • Indirect benefit: hydrothermal route avoids toxic HF, reducing synthesis hazards. • Leaching or stability of AlF_3 by-products not assessed.
$\text{Nb}_2\text{CT}_x^{127}$	MB	526.32	$C_0 = 100\text{--}500$ mg/L, 25 °C, pH = 7, dose = 1 g/L, 700 rpm	PSO	<ul style="list-style-type: none"> • No regeneration/reusability cycles tested. • Long-term performance stability and recyclability are not addressed. 	<ul style="list-style-type: none"> • No toxicity (cytotoxicity or ecotoxicity) or leaching studies reported. • HF used for etching may pose safety concerns

					<ul style="list-style-type: none"> • Future studies should focus on desorption efficiency and material durability. 	<p>unless thoroughly washed and neutralised.</p> <ul style="list-style-type: none"> • Environmental and biological safety remain unexplored.
PAA ₂ alk-MXene ¹²⁸	MB	193.92	C ₀ = 60–90 mg/L, 25–55 °C, pH = 2–10	Langmuir/ PSO	<ul style="list-style-type: none"> • The adsorbent AA2-alk-MXene maintained over 85% dye removal efficiency after five adsorption–desorption cycles. 	<ul style="list-style-type: none"> • No direct cytotoxicity or ecotoxicity tests were reported in the study.
PAA ₂ alk-MXene ¹²⁸	CR	264.46	C ₀ = 60–90 mg/L, 25–55 °C, pH = 2–10	Langmuir/ PSO	<ul style="list-style-type: none"> • Ethanol was used as the desorbing agent. • Good reusability and structural stability. 	<ul style="list-style-type: none"> • Use of mild reagents like AA and NaOH suggests potentially low toxicity, although this was not experimentally verified. • Biocompatibility and environmental safety remain unexplored.
Ti ₃ C ₂ –SO ₃ H ¹²⁹	MB	111.11	T = 25 °C, pH = 7, dosage = 10 mg, C ₀ = 50 mg/L	Langmuir/ PSO	<ul style="list-style-type: none"> • Regeneration or reuse experiments were not conducted. • Long-term adsorbent stability was not assessed. • No adsorption–desorption cycles reported. 	<ul style="list-style-type: none"> • Did not evaluate toxicity, cytotoxicity, or leaching risks. • Use of NaF and arenediazonium salts may pose safety concerns.

						<ul style="list-style-type: none"> • Environmental impact and biocompatibility remain unexplored.
MXene-COOH@ $(\text{PEI/PAA})_n$ ¹³⁷	MB	81.9672	$C_0 = 0\text{--}3\text{ mg/L}$, 25 °C, dose = 10 mg/50 mL	Langmuir/ PSO	<ul style="list-style-type: none"> • The removal efficiency decreased from 85.6% to 64.4% after 8 cycles. • The material showed good stability and reusability. 	<ul style="list-style-type: none"> • Environmental safety and leaching of components were not assessed. • The synthesis avoids heavy metals, but toxicity remains unevaluated.
PHGC/MXene ¹³⁸	MB	555.56	$C_0 = 50\text{--}100\text{ mg/L}$, 298-308 K, pH = 11	Langmuir/ PSO	<ul style="list-style-type: none"> • PHGC/MXene hydrogel maintained over 90% removal efficiency for AB93 and MB after 12 regeneration cycles. • NaHCO_3 and HCl were effective desorption agents for AB93 and MB, respectively. • The material showed excellent reusability and economic regeneration. 	<ul style="list-style-type: none"> • No <i>in vivo</i> or <i>in vitro</i> toxicity study was reported. • Environmental impact and cytocompatibility were not evaluated. • Safety validation is lacking for biomedical or large-scale applications.
cetyltrimethylammonium bromide-modified multi-	MO	213	$C_0 = 10\text{--}500\text{ mg/L}$, 298 K,	Langmuir/ PSO	<ul style="list-style-type: none"> • Adsorption capacity decreased slightly from 25.52 	<ul style="list-style-type: none"> • No direct toxicity assessment (e.g.,

layered $\text{Ti}_3\text{C}_2\text{Tx}$ MXene (CMM) ¹³⁰			pH= 3–12, dose = 0–3.33 g/L		<p>mg/g to 14.3 mg/g after 5 cycles.</p> <ul style="list-style-type: none"> • Ethanol used for desorption demonstrated effective dye elution. • CMM maintained commendable reusability and structural integrity. 	<p>cytotoxicity, ecotoxicity) was conducted in the study.</p> <ul style="list-style-type: none"> • Implicit safety suggested via use of ethanol in desorption and absence of harmful leachates.
ABC/MX composite ¹³⁹	CR	1103.7	$C_0 = 50\text{--}500$ mg/L, pH = 1–11, 300 K–330 K, dose = 0.4 g/L	Freundlich model	<ul style="list-style-type: none"> • CR: High stability and reusability; >95% removal retained after 5 cycles. • Cr(VI): Performance dropped significantly from 88.44% to 55.53% after 1 cycle. 	<ul style="list-style-type: none"> • No <i>in vitro</i>, <i>in vivo</i>, or ecotoxicity tests were performed. • However, authors emphasised that: • Bacterial cellulose (BC) is a renewable, biodegradable, and non-toxic biopolymer. • Desorbed Cr(VI) is treated with Fe(II) to form precipitates, reducing secondary pollution risk.

						<ul style="list-style-type: none">• Suggests low environmental burden under controlled usage but lacks direct toxicity proof
MXene-PEI ¹⁴⁰	MO	909.1	C ₀ =120-300 mg/L, 328 K, pH=3	Langmuir/ PSO	<ul style="list-style-type: none">• High stability and reusability over 5 cycles: MB: Removal decreased from 89.7% → 85.3% Cr(VI): Removal decreased from 93.4% → 87.2%• Structural Integrity: Maintained porous architecture and adsorption capacity.	<ul style="list-style-type: none">• No <i>in vitro</i> or <i>in vivo</i> toxicity tests.• Materials (MXene, chitosan, alginate) are described as biocompatible and eco-friendly.• No harmful by-products or leaching reported.• Indicates low environmental impact but lacks formal toxicological validation.
MX-PAN membrane ¹⁵⁰	MB	-	C ₀ = 10 mg/L, 25 °C, pH= 7	-	<ul style="list-style-type: none">• Reusability: After 5 adsorption–desorption cycles: Cr(VI): Removal decreased from 91.7% to 86.3%	<ul style="list-style-type: none">• No explicit cytotoxicity or environmental toxicity tests conducted.• Components (MXene, lignocellulose, CNF) are

					<p>MB: Removal declined from 95.4% to 89.5%.</p> <ul style="list-style-type: none"> Retained adsorption capability and structure, demonstrating excellent recyclability. 	<p>natural or biocompatible.</p> <ul style="list-style-type: none"> Emphasis on green synthesis and biodegradability. Suggests low toxicity potential, but lacks empirical toxicology evidence.
SA/MXene nanofiber membranes ¹⁵¹	MB	440	$C_0 = 50\text{--}220$ mg/L, 98 K–323 K, pH= 2–11, dose = 1–5 mg	Langmuir/PSO	<ul style="list-style-type: none"> Performance Over Cycles: After 5 adsorption–desorption cycles: Cr(VI): Decreased from 93.6% → 84.7% MB: Decreased from 91.2% → 85.2% Observation: Slight decline but excellent reusability and structural robustness. 	<ul style="list-style-type: none"> No direct cytotoxicity or environmental toxicity data. MXene and attapulgite considered relatively biocompatible materials. Use of mild regenerants (ethanol, NaOH) supports low environmental burden. Long-term stability of MXene against oxidation not discussed in toxicological terms.

Ti ₃ C ₂ T _x bound with terephthalate (T-MX) ¹³⁴	MB	209	pH=7, RT, 100 mg/L	PSO	<ul style="list-style-type: none"> • Unique regeneration method: Spent T-MX (after MB adsorption) is reconverted into MAX phase by adding only Al powder and applying mechanochemical (MC) ball milling. • The MAX phase is then re-etched into MXene, confirming the closed-loop recyclability of the material. • Pollutants and terephthalate pillars are carbonised and reused as carbon source in the MAX phase. 	<ul style="list-style-type: none"> • No cytotoxicity or environmental safety data were presented. • Concerns noted: • Potential contamination from milling tools (Fe, alloying metals) under acidic HF etching. • These may bind to reactive Ti sites, requiring further toxicological investigation. • Materials used (MXene, terephthalate) are otherwise not inherently toxic, and MC synthesis is solvent-free and greener.
TMAOH delaminated Ti ₃ C ₂ T _x MXene nanosheets ¹³⁵	MB	1026	C ₀ = 20–80 mg/L, 318 K, pH=6, dose = 0.01–0.06 g/L	Freundlich / PSO	<ul style="list-style-type: none"> • Reusability was tested over 5 cycles using 1 M NaOH for desorption. 	<ul style="list-style-type: none"> • No direct cytotoxicity or ecotoxicity tests were reported.

					<ul style="list-style-type: none"> • Stable performance for 3 cycles with no significant loss in adsorption capacity. • Slight drop after 3rd cycle likely due to material loss and structural degradation (ultrathin layers disrupted). 	<ul style="list-style-type: none"> • Regeneration using NaOH and sedimentation by flocculation suggest potential for safe separation, but further biological evaluations are necessary for real-world application.
MXene/PEI modified sodium alginate aerogel (MPA) ¹⁵²	CR	3568	Adsorbent dose:10 mg	Langmuir/PSO	<ul style="list-style-type: none"> • MPA demonstrated excellent recyclability with 16.3% capacity loss for Cr(VI) after 5 cycles and only 4.29% loss for CR after 5 cycles. • The adsorbent maintained 83.7% Cr(VI) removal capacity and 95.71% CR removal efficiency after five regeneration cycles using NaOH/NaCl and ethanol desorption methods respectively. 	<ul style="list-style-type: none"> • No toxicity assessment or environmental impact evaluation was conducted in this study. • MPA exhibited outstanding antibacterial properties with 99.99% bacterial killing efficiency against both <i>E. coli</i> and <i>S. aureus</i> after 2 hours exposure.

alk-MXene/CoFe ₂ O ₄ /CS ¹⁴¹	MB	537.63	C ₀ = 17–50 mg/L, 22–47 °C, pH = 2–12, dose = 10 mg/25 mL	Langmuir/ PSO	<ul style="list-style-type: none"> The adsorbent demonstrated excellent recyclability with >80% removal efficiency maintained for RhB and MG dyes after 5 cycles, while CR retained ~66% efficiency. Magnetic separation using NdFeB magnet enabled easy recovery from aqueous solutions, with ethanol used as desorption agent for regeneration cycles. 	<ul style="list-style-type: none"> No toxicity assessment or environmental impact evaluation was conducted in this study. The paper focused solely on adsorption performance without investigating potential environmental or health impacts of the synthesized materials.
alk-MXene/CoFe ₂ O ₄ /CS ¹⁴¹	RhB	1333.86	C ₀ = 5–10 mg/L, 22–47 °C, pH = 2–12, dose = 10 mg/25 mL	Langmuir/ PSO		
alk-MXene/CoFe ₂ O ₄ /CS ¹⁴¹	CR	2095.9	C ₀ = 5–10 mg/L, 22–47 °C, pH = 2–12, dose = 10 mg/25 mL	Langmuir/ PSO		
MXene (Ti ₃ C ₂)/Fe ₃ O ₄ ¹⁴²	MB	9.85	C ₀ = 1–40 mg/L, 25–55 °C, dose = 1 g/L	Freundlich isotherm	<ul style="list-style-type: none"> No regeneration or recyclability studies were conducted in this research. The study focused solely on adsorption performance at different temperatures without investigating the reusability of the 2D-MX@Fe₃O₄ adsorbent. 	<ul style="list-style-type: none"> No toxicity assessment or environmental impact evaluation was performed in this study. The research concentrated on adsorption mechanisms and temperature effects without addressing potential health or environmental risks.

Ti ₃ C ₂ T _x /NiFeMn-LDH@Gel ¹⁴³	CR	588.24	C ₀ = 50–300 mg/L, 298-328 K, pH = 3-9	Freundlich / PSO	<ul style="list-style-type: none"> The composite demonstrated excellent recyclability with 74.94% and 71.72% removal efficiency maintained for Cr(VI) and CR respectively after 5 cycles. Regeneration was achieved using 1 M NaCl/methanol solution with continuous stirring for 2 hours, followed by drying at 50 °C for 8 hours before reuse. 	<ul style="list-style-type: none"> A comprehensive leaching test was conducted using ICP-MS technique to detect potential metal leaching (Ni, Fe, Mn) across pH range 3-9. Results showed almost constant metal content after adsorption processes, confirming the stability and safety of the composite for practical applications without significant metal leaching.
AMXGO ¹³⁶	MG	1111.6	C ₀ = 100-400 mg/L, 298 K-328 K, pH = 2-12	Freundlich / PSO	<ul style="list-style-type: none"> The composite maintained >70% removal efficiency for both MG and CR after 5 cycles. Regeneration used 5 mL detergent + 100 mL DI water, 	<ul style="list-style-type: none"> Zeta potential analysis showed stable surface charge (-20.54 to -52.00 mV, pH 2-12) without harmful ion leaching.

					stirred for 3 hours, washed to neutral pH, then freeze-dried.	<ul style="list-style-type: none"> • XRD and FTIR confirmed no structural degradation after multiple cycles, ensuring material safety.
MXene/COF ¹⁴⁴	MB	96.4%	effective membrane area = ~ 8.0 cm ²	--	<ul style="list-style-type: none"> • The membrane maintained >96% rejection and >243 L/m²·h·bar water permeance after 45 hours of continuous operation. • No specific regeneration process described - membrane showed excellent stability without requiring regeneration protocols. 	<ul style="list-style-type: none"> • XRD analysis confirmed no structural degradation with d-spacing remaining stable at ~1.46 nm after extended operation.
MXene/COF ¹⁴⁴	CR	98.2%	effective membrane area = ~ 8.0 cm ²	--		<ul style="list-style-type: none"> • Membranes showed excellent anti-swelling properties in pH 3-10 conditions, maintaining structural integrity without toxic leaching.
MXene/COF ¹⁴⁴	MO	97.2%	effective membrane area = ~ 8.0 cm ²	--		
alk-MXene/ZIF composites ¹⁴⁵	CR	539.7	298-318 K, pH=8	Elovich/PSO	<ul style="list-style-type: none"> • The composite maintained >85% removal efficiency for all three pollutants (CR, TC, MG) after 5 cycles. 	<ul style="list-style-type: none"> • XRD analysis confirmed stable crystalline structure with no significant peak
alk-MXene/ZIF composites ¹⁴⁵	MG	7111.3	298-318 K, pH=8	Elovich/PSO		

					<ul style="list-style-type: none"> • Regeneration achieved using anhydrous ethanol stirring for 2 hours, followed by deionized water washing and freeze-drying. 	<p>shifts after air exposure for 45 days.</p> <ul style="list-style-type: none"> • Membrane filtration tests showed >90% removal maintained after 5 cycles, demonstrating material safety without toxic leaching.
DSP-M ¹⁴⁶	RhB	678.19	C ₀ = 2–100 mg/L, 30 °C-60 °C, pH= 7	Langmuir/ PSO	<ul style="list-style-type: none"> • The composite maintained stable performance with no specific regeneration protocol described, showing structural integrity after multiple adsorption-desorption cycles. 	<ul style="list-style-type: none"> • XPS analysis confirmed no harmful metal leaching or toxic byproduct formation during adsorption processes.
DSP-M ¹⁴⁶	CR	754.41	5–200 mg/L, 30 °C-60 °C, pH= 7	Langmuir/ PSO	<ul style="list-style-type: none"> • Material stability confirmed through XRD and FTIR analysis showing no structural degradation after repeated use 	<ul style="list-style-type: none"> • Statistical physics modeling confirmed physical adsorption processes (E < 8 kJ/mol) involving safe hydrogen bonding, electrostatic forces, and van der Waals interactions.

ZnS/CuFe ₂ O ₄ /MXene (ZSCFOM) ¹⁴⁷	DBM	377	0.02–4 g/L, 12 h, 75 rpm, 20 °C	Langmuir/PSO	<ul style="list-style-type: none"> • Good reusability with no significant reduction in DBM removal rate after three cycles. • Excellent thermal stability with minimal weight loss (0.23-0.38%) at 25-600 °C. • Magnetic separation capability for easy recovery using CuFe₂O₄ component. 	<ul style="list-style-type: none"> • Successfully applied to real environmental waters (tap, pond, river) with 100% removal of 0.05 g/L dyes. • Photocatalytic process generates environmentally benign products through complete mineralization. • Magnetic properties enable easy separation and recovery, preventing secondary contamination.
ZnS/CuFe ₂ O ₄ /MXene (ZSCFOM) ¹⁴⁷	DBRN	390	0.02–4 g/L, 12 h, 75 rpm, 20 °C	Langmuir/PSO		
PHGC/MXene ¹³⁸	AB93	207.47	C ₀ = 50-100 mg/L, 298-308 K, pH = 2	Langmuir/ PSO	<ul style="list-style-type: none"> • Excellent reusability with removal rates remaining above 90% for AB93 and above 97% for MB after 12 cycles. • Regeneration achieved using 0.1 mol/L NaHCO₃ solution 	<ul style="list-style-type: none"> • No comprehensive toxicity assessment of the PHGC/MXene composite material itself was conducted. • Effective removal of toxic anionic (AB93)

					<p>for AB93 and 0.1 mol/L HCl solution for MB.</p> <ul style="list-style-type: none">• Minimal decrease in performance (less than 3% compared to highest removal rate) demonstrating excellent stability.• Both acidic and alkaline regeneration solutions proved effective for respective dye systems.	<p>and cationic (MB) dyes from contaminated water.</p> <ul style="list-style-type: none">• Successfully tested across different pH ranges (2-12) without significant material degradation.• Non-toxic regeneration process using environmentally acceptable desorption agents (NaHCO₃ and HCl).• No adverse effects on hydrogel structure during multiple regeneration cycles.• Material demonstrated biocompatibility based on constituent components.
--	--	--	--	--	--	---

ZIF-8@IL-MXene/PNIPAM ¹⁵³	CV	325.03	$C_0 = 0.4\text{-}2\text{ mg/L}$, 25-45 °C, pH = 7	Freundlich / PSO	<ul style="list-style-type: none"> • Good reusability with adsorption capacities decreasing to 79%, 91%, and 29% for 4-NP, CV, and Cu^{2+} respectively after five cycles. • Desorption achieved via volume phase transition in deionized water at 35-40 °C (environmentally friendly process). • Decline in Cu^{2+} adsorption due to strong chelation bonds difficult to break through phase transition. 	<ul style="list-style-type: none"> • Environmentally friendly synthesis and desorption processes without organic solvents. • Successfully applied to multifunctional removal of phenols, dyes, and metal ions from industrial wastewater. • VPTT range 33-35 °C enables safe temperature-responsive desorption process. • No toxic byproducts reported during adsorption/desorption cycles.
AMXGO ¹⁵⁴	CR	1133.7	$C_0 = 100\text{-}400\text{ mg/L}$, 298 K-328 K, pH = 2-12	Freundlich/ PSO	<ul style="list-style-type: none"> • Good reusability with removal efficiencies 	<ul style="list-style-type: none"> • No significant effects from common cations

CMC composite ¹⁵⁴	AO7	367.9	$C_0 = 50-500$ mg/L, 25-45 °C, pH = 3-11	Sips/PSO	gradually decreasing over five cycles.	(Na ⁺ , K ⁺ , Ca ²⁺ , Mg ²⁺) and anions (Cl ⁻ , NO ₃ ⁻ , CO ₃ ²⁻ , SO ₄ ²⁻) on dye removal.
CMC composite ¹⁵⁴	MO	294.2	$C_0 = 50-500$ mg/L, 25-45 °C, pH = 3-11	Sips/PSO	<ul style="list-style-type: none"> • AO7 showed least decrease in efficiency, followed by MO and CR after five cycles. • Gradual decrease attributed to incomplete desorption and loss of surface functional groups during regeneration process. 	<ul style="list-style-type: none"> • Successfully tested in different water matrices (deionized, tap, and lake water).
CMC composite ¹⁵⁴	CR	628.5	$C_0 = 50-500$ mg/L, 25-45 °C, pH = 3-11	Sips/PSO		<ul style="list-style-type: none"> • Slightly reduced performance in tap and lake water due to competing ions and organic matter. • Effective removal of carcinogenic, mutagenic, and toxic anionic azo dyes from contaminated water. • No specific toxicity assessment of the CMC composite material itself was conducted.

SC-PLA/PDA/MXene membrane ¹⁵⁵	MB	434.8	$C_0 = 0.5-2 \text{ g/L}$	Langmuir/ PSO	<ul style="list-style-type: none">• Good cycling stability demonstrated over 10 consecutive separation cycles for oil/water separation• Water flux remained stable at 1429.0 L/(m²·h) even after 10 cycles for E-N/W separation• Oil flux maintained at ~1862.0 L/(m²·h) for the first 4 cycles in E-W/N separation, then declined to 1563.3 L/(m²·h) (84.6% retention) after 10 cycles• Alcohol regeneration treatment used between cycles with good recovery performance• Excellent reusability for simultaneous oil and MB removal with water flux maintaining high levels after 6 reuse cycles	<ul style="list-style-type: none">• Biodegradable PLA-based composite material providing eco-friendly alternative to conventional polymer membranes• Eliminates potential secondary pollution from plastic debris entering water systems• No comprehensive toxicity assessment of the composite material conducted• Effective removal of toxic organic pollutants (MB) from contaminated water• Biocompatible polylactide substrate reduces environmental impact compared to
--	----	-------	---------------------------	---------------	---	--

					<ul style="list-style-type: none"> • Minor performance decline attributed to porosity blocking by residual oil during separation process 	non-degradable polymer membranes <ul style="list-style-type: none"> • Polydopamine and MXene components generally considered biocompatible based on literature
$\text{Fe}_2\text{O}_3/\text{BC}/\text{MXene}^{148}$	MB	899.03	$C_0 = 15\text{--}45 \text{ mg/L}$, 293–313 K, pH= 1–11	Langmuir/ PSO	<ul style="list-style-type: none"> • Pb^{2+} sorption capacity: 99.91% → 90.99% after 5 cycles; MB: 98.63% → 89.47%. • Desorption efficiency: Pb^{2+}: 96.8% → 78.32%; MB: 95.08% → 77.40% after 5 cycles. • Easy separation using external magnetic field. 	<ul style="list-style-type: none"> • Biochar-based composite provides sustainable wastewater treatment. • Effectively removes highly toxic lead and MB from water. • Composite material itself not assessed for environmental/health impacts. • Generally considered safe based on literature.
$\text{TiV}_x\text{T}_x/\text{GAs}^{156}$	MB	319.67	298 - 338 K, pH= 1–13	Langmuir/ PSO		

$\text{TiV}_\text{CT}_\text{x}/\text{GAs}^{156}$	RhB	303.45	298 K- 338 K, pH= 1-13	Langmuir/ PSO	<ul style="list-style-type: none">• Excellent cycling stability demonstrated over 5 successive adsorption-desorption cycles.• MB removal rate remained at around 95.8% after five cycles.• High absorption capacity maintained even after five cycles of absorption-squeezing for oil/solvent removal.• Easy regeneration through simple mechanical squeezing due to excellent elasticity of $\text{TiVCT}_\text{x}/\text{GAs}$.	<ul style="list-style-type: none">• Leaching experiments confirmed that $\text{TiV}_\text{CT}_\text{x}/\text{GAs}$ adsorbent does not produce secondary pollution during adsorption process.• Effectively removes highly toxic organic contaminants including dyes and antibiotic drugs from wastewater.• No comprehensive toxicity assessment of the composite material itself conducted.• Biocompatible components generally considered safe for environmental applications.
$\text{TiV}_\text{CT}_\text{x}/\text{GAs}^{156}$	CR	229.97	298 K- 338 K, pH= 1-13	Langmuir/ PSO		
$\text{TiV}_\text{CT}_\text{x}/\text{GAs}^{156}$	MO	217.87	298 K- 338 K, pH= 1-13	Langmuir/ PSO		

MCF hybrid aerogel ¹⁵⁷	MB	356.97	$C_0 = 3\text{--}100$ mg/L, 303 K- 333 K, pH = 11	Langmuir/ PSO	<ul style="list-style-type: none"> • Limited regeneration assessment mentioned in the study. 	<ul style="list-style-type: none"> • No comprehensive toxicity assessment of the MCF composite material conducted.
MCF hybrid aerogel ¹⁵⁷	CR	647.75	$C_0 = 3\text{--}200$ mg/L, 303- 333 K, pH = 6	Langmuir/ PSO	<ul style="list-style-type: none"> • No comprehensive cycling stability evaluation provided. • Brief mention that physical adsorption is beneficial for reversible processes and adsorbent regeneration after desorption. • Statistical physics modeling suggests physical interaction enables regeneration potential. 	<ul style="list-style-type: none"> • Focuses on removing highly toxic contaminants: MB causes DNA structure damage, cancer risk, heart rate acceleration, shock, and tissue necrosis. • CR degradation produces benzidine, a recognized human carcinogen. • MCF designed as environmentally-friendly technology for hazardous dye elimination. • No secondary pollution production during

						adsorption process confirmed through leaching experiments.
$\text{Ni}_3(\text{HITP})_2/\text{MXene}/\text{CS}^{149}$	MB	424.99	10–400 mg/L, 298 K, pH= 2–9	Langmuir/PSO	<ul style="list-style-type: none"> • Five consecutive adsorption-desorption cycles conducted for reusability evaluation. • Composite maintained excellent adsorption rate after five cycles for both Pb(II) and MB. • Chemical adsorption nature may pose challenges for complete regeneration. • Detailed regeneration protocols not clearly presented in main text. 	<ul style="list-style-type: none"> • No comprehensive toxicity assessment of the composite material conducted. • Composite uses biocompatible chitosan biopolymer as base material. • No secondary pollution or leaching studies reported.
MXene with biomass activated carbon (CMAC) ¹⁵⁸	CR	1264.032	$C_0 = 0\text{--}400$ mg/L, 25–75 °C, pH = 6, dose = 10 mg/100 mL	Langmuir/PSO	<ul style="list-style-type: none"> • Desorption and recyclability studies conducted using ethanol as desorbing agent. • CMAC mixed with 100 mL ethanol and stirred at 25 °C for 24 hours. 	<ul style="list-style-type: none"> • No comprehensive toxicity assessment of the CMAC composite material conducted. • Focus on removing highly toxic anionic azo dyes that are

					<ul style="list-style-type: none"> • Good adsorption effect maintained for all three dyes after multiple desorption cycles. • No significant loss of performance after several cycles. • Economic benefit and high stability demonstrated for wastewater treatment applications. 	<p>carcinogenic and mutagenic.</p> <ul style="list-style-type: none"> • CMAC composite uses biomass activated carbon as environmentally friendly base material. • No secondary pollution or environmental impact studies reported.
macroporous cellulose nanocrystals (CNC)/MXene/PVA (C-CMP) ¹⁵⁹	MB	239.92	pH=6, 338 K, 250 mg/L	Langmuir/PSO	<ul style="list-style-type: none"> • Adsorption-desorption experiment conducted for three cycles using 0.1 mol/L HCl for desorption. • MB removal efficiency maintained above 80% after three cycles. • Good recyclability of C-CMP composite foam confirmed. • Slightly decreased efficiency attributed to strong interaction between MB and C-CMP. 	<ul style="list-style-type: none"> • No comprehensive toxicity assessment of the C-CMP composite material conducted. • Focus on removing highly toxic MB which severely affects water transparency and dissolved oxygen. • MB is difficult to degrade due to benzene ring structure and

					<ul style="list-style-type: none">• Residual dye from previous cycles may affect subsequent performance.	<p>accumulates in drainage systems.</p> <ul style="list-style-type: none">• Even 1 mg/L concentration severely impacts water quality.• Composite uses biocompatible materials: cellulose nanocrystals and polyvinyl alcohol.• No environmental impact or secondary pollution studies reported.
Co: concentration of dye						

5. Mechanism of adsorption fundamentals of MXenes-based nano-adsorbents for dyes

When it comes to water filtration, adsorption is among the most effective and economical technologies available. On the basis of variations in the adsorption forces, adsorption is typically divided into two categories: chemical adsorption and physical adsorption. Physical adsorption primarily occurs due to van der Waals forces, which are frequently observed in MXene due to material's large SSA. A number of different processes, including electrostatic interactions, coordination, ion exchange, and hydrogen bonding, are included in chemical adsorption. Due to the fact that $\text{Ti}-\text{C}-\text{O}-$ or $\text{Ti}-\text{C}-\text{OH}-$ groups on MXene have the ability to interact with a wide variety of cations, electrostatic contact is a frequent mechanism in the process of adsorption of MXene. Ion exchange or development of inner-sphere complexes is encouraged by the presence of a considerable number of functional groups and the stratified structure. There are a variety of factors that influence the adsorption mechanisms of MXenes, including the exact kind of MXenes, the properties of pollutants, and the natural environment of the aquatic environment. The adsorption mechanism for $\text{TiVCT}_x/\text{GAs}$, as proposed by Xing *et al.*, is depicted in **Figure 16a**. Integrating H-bonding, $\pi-\pi$ interactions, and electrostatic attraction significantly influences adsorption. The structural features of $\text{TiVCT}_x/\text{GAs}$, such as their porous structure with a large SSA and the abundance of adsorption active sites given by bimetallic layers of TiVCT_x and graphene sheets, also help to enhance the ability of $\text{TiVCT}_x/\text{GAs}$ to adsorb MB dye.¹⁵⁶

Furthermore, Purkayastha and co-authors produced MX-PAN membranes that may bind MB molecules to both F and $\text{OH}/=\text{O}$ terminating groups of MXene. The molecular structure of MB dye is shown in **Figure 16b**. The sulfur (S) or nitrogen (N) atoms in MB, carrying positive charge, classify it as cationic dye. After the aluminum atoms are removed *via* etching from Ti_3AlC_2 (parent powder), various functional groups ($-\text{F}$ and $-\text{OH}/=\text{O}$) attach simultaneously on

surface of $\text{Ti}_3\text{C}_2\text{T}_x$, resulting in negative charge. These negative charges $[\text{Ti-F}]^{-1}$ and $[\text{Ti-O}]^{-1}$ can be cationic species sensors. As shown in **Figure 16c**, MB molecules can interact with both F and OH/=O terminal groups. Therefore, a key mechanism for adsorption of MB dye is electrostatic interaction between positively charged MB molecules and negatively charged $\text{Ti}_3\text{C}_2\text{T}_x$ MXene.¹⁵⁰

Wang *et al.* explained that the adsorption of MG and CR on alk-MXene/ZIF composite could be ascribed to the hydrogen bonding, π - π , and electrostatic interaction. Additionally, the proposed adsorption mechanism is schematically illustrated in **Figure 16d**.¹⁴⁵ To further understand the phenomenon of adsorption, Li *et al.* explained the adsorption process of AMXGO for CR and MG, as shown in **Figure 16e**. AMXGO dye adsorption involves various phenomena, including π - π conjugates, electrostatic force, intercalation adsorption, as well as pore adsorption. Among the most significant impacts is the electrostatic force, which is generated by the negative hydroxyl and carboxyl groups present on GO lamellae and Alk-MXene surfaces, which mix with cationic molecules. π - π conjugates have a considerable effect on CR adsorption because their structure contains six benzene rings, which is more than three in the structure of MG molecule. This also describes why AMXGO has superior adsorption efficacy toward anionic CR. Furthermore, the layer-by-layer structure of Alk-MXene and GO flakes in AMXGO favors intercalation adsorption of either CR or MG molecules. Furthermore, the AMXGO samples include numerous mesoporous pores, that ultimately promote pores adsorption of CR and MG.¹³⁶

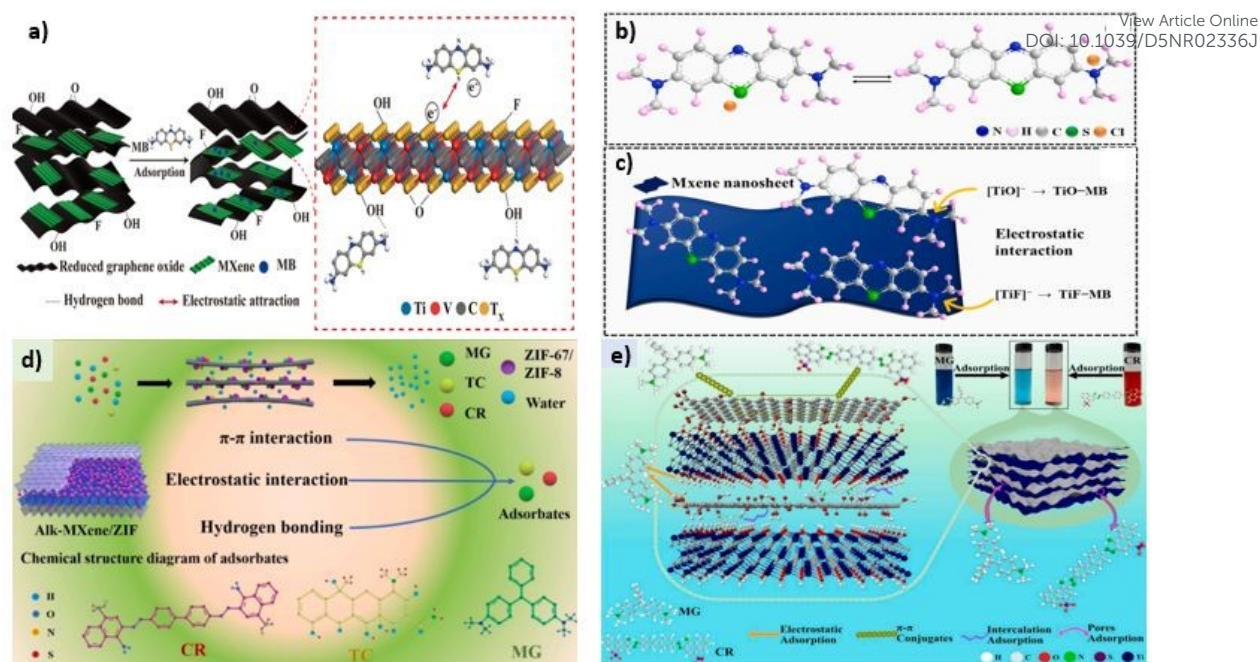


Figure 16: (a) Schematic Illustration of Adsorption Mechanism of TiVCT_x/Gas. Reproduced with permission from Ref.¹⁵⁶ Copyright 2024, American Chemical Society. (b) Molecular structure of MB. Reproduced with permission from Ref.¹⁵⁰ Copyright 2023, Elsevier. (c) Schematic illustration of electrostatic interaction between Ti₃C₂T_x MXene nanosheet and MB dye molecules.¹⁵⁰ Reproduced with permission from Ref.¹⁵⁰ Copyright 2023, Elsevier. (d) Schematic diagram on the adsorption mechanism of the alk-MXene/ZIF adsorbent. Reproduced with permission from Ref.¹⁴⁵ Copyright 2024, Elsevier. (e) Adsorption mechanism of AMXGO adsorbents for MG and CR.¹³⁶ Reproduced with permission from Ref.¹³⁶ Copyright 2024, Elsevier.

While the fundamental adsorption mechanisms have been identified, a comprehensive mechanistic framework reveals the relative contributions and synergistic interactions among different adsorption pathways in MXene-based systems.⁶⁰ Electrostatic interactions represent the primary driving force for cationic dye adsorption, with mechanism efficiency directly correlated to surface charge density and zeta potential values. Ti₃C₂T_x MXenes exhibit highly negative surface charges due to abundant -OH, -O, and -F terminations, creating strong

electrostatic fields capable of attracting cationic species over significant distances.¹⁰⁵ Quantitative analysis reveals that electrostatic contribution accounts for the majority of total adsorption energy for MB and rhodamine B, while representing a smaller fraction for anionic dyes like CR. pH-dependent studies demonstrate optimal electrostatic interactions occur at near-neutral pH, where MXene surface deprotonation maximizes negative charge density while maintaining structural stability. π - π stacking mechanisms show high selectivity toward aromatic dye molecules, with interaction strength proportional to aromatic ring number and electron density distribution. Computational studies using Density Functional Theory (DFT) calculations reveal significant binding energies for benzene ring interactions with $\text{Ti}_3\text{C}_2\text{T}_x$ surfaces, with substantially higher energies for multi-ring systems like CR. Distance-dependent analysis shows optimal π - π interactions occur at specific separations, with parallel orientation providing maximum orbital overlap. MXene surface hybridization enhances π -electron delocalization, creating favorable interaction sites for aromatic dye molecules.¹⁶⁰

Hydrogen bonding exhibits remarkable complexity in MXene-dye systems, involving multiple donor-acceptor combinations and cooperative strengthening effects. Surface -OH and -O groups serve as hydrogen bond acceptors, while dye amino groups (-NH₂) and hydroxyl functionalities act as donors.¹⁶¹ Spectroscopic analysis (FTIR and NMR) reveals moderate hydrogen bond strengths for individual interactions, with significantly enhanced cumulative effects for dyes with multiple bonding sites. Temperature-dependent studies show hydrogen bonding contributions decrease substantially at elevated temperatures, indicating entropy-driven weakening of directional interactions. Ion exchange processes demonstrate high specificity toward charge-to-size ratios and hydration energies of exchangeable species.¹⁶² $\text{Ti}_3\text{C}_2\text{T}_x$ interlayer cations exhibit different exchange affinities for organic cations, with selectivity series: quaternary ammonium > primary ammonium > metal cations. Kinetic analysis reveals two-stage exchange processes: rapid surface exchange followed by slower

interlayer diffusion. Stoichiometric studies confirm equivalent exchange ratios for monovalent dye cations, while multivalent species show complex exchange behaviors involving charge compensation mechanisms.

Physical adsorption through pore filling becomes dominant for microporous MXene derivatives and high molecular weight dyes. Pore size distribution analysis reveals optimal dye accommodation in mesopores, where molecular diffusion remains unrestricted while surface interactions are maximized. Molecular dynamics simulations demonstrate size-selective adsorption, with larger dye molecules showing reduced diffusion rates and surface-limited adsorption.⁶³ Multiple mechanisms operate simultaneously in real adsorption systems, creating cooperative enhancement effects that exceed individual contributions. Electrostatic pre-concentration brings dye molecules into proximity with MXene surfaces, facilitating secondary interactions including π - π stacking and hydrogen bonding. Computational analysis reveals cooperative binding energies significantly higher than additive individual contributions, indicating synergistic stabilization. Sequential mechanism analysis shows electrostatic interactions dominate initial adsorption, followed by π - π stacking at intermediate saturation and pore filling at high saturation. Solution pH dramatically influences mechanism prevalence and adsorption efficiency through surface chemistry modifications and dye speciation changes.¹⁶³

Acidic conditions enhance protonation of MXene surface groups, reducing electrostatic attractions but increasing hydrogen bonding opportunities. Alkaline conditions maximize electrostatic interactions but may destabilize MXene structures through excessive deprotonation. Thermal analysis reveals differential temperature dependencies among adsorption mechanisms, with electrostatic interactions showing minimal temperature dependence, while hydrogen bonding decreases significantly at elevated temperatures. Multi-component systems reveal mechanism-dependent selectivity patterns, with different dyes

competing for specific interaction sites, indicating moderate to intense competition depending on the degree of overlap between mechanisms. This comprehensive mechanistic framework offers quantitative insights into MXene-dye interactions, facilitating the rational design of high-performance adsorbents through targeted mechanism optimization and synergistic enhancement strategies.

6. Regeneration and recyclability of adsorbent

Adsorbents, such as MXene, used for dye adsorption should be recyclable and regenerative due to their practical and sustainable environmental applications. Several approaches have been established to recover the adsorption ability of dye-loaded MXene adsorbents for reuse.¹³⁴ Thermal regeneration comprises heating the adsorbents to encourage the desorption of dyes that have been absorbed. Chemical regeneration uses regenerants like alkalis, acids, organic solvents, or complexing agents to desorb the dyes from the adsorbent surface specifically.^{164,165} Another approach is electrochemical regeneration, which uses an electrical potential to accelerate desorption with the advantage of selectivity and in situ regeneration. When the regenerant solution and dye-loaded adsorbents are mixed, and suitable desorption conditions are sustained, batch systems can perform these processes. The effectiveness of the regeneration is evaluated based on the amount of dye removed and the recovery of adsorption capacity. MXene adsorbents' long-term viability as cost-efficient and sustainable solutions for dye removal applications is partially due to their effective regeneration and recyclability.^{83,166} For instance, the recyclability of $\text{Ti}_3\text{C}_2\text{T}_x/\text{NiFeMn-LDH@Gel}$ was demonstrated after five times of recycling and it was observed the removal ratio of $\text{Ti}_3\text{C}_2\text{T}_x/\text{NiFeMn-LDH@Gel}$ for CR adsorption remained at 71.72%, displaying the effective regeneration property for $\text{Ti}_3\text{C}_2\text{T}_x/\text{NiFeMn-LDH@Gel}$ as shown in **Figure 17a**.¹⁴³ Likewise, the cyclic stability of $\text{TiVCT}_x/\text{GAs}$, as illustrated in **Figure 17b**, highlights its remarkable performance in dye adsorption applications. Over five cycles of the absorption-squeezing process, the material

consistently maintains a high absorption capacity, indicating its durability and effectiveness in removing contaminants from wastewater.¹⁵⁶ The utilization of NaHCO_3 solution as a desorption agent for PHGC/MXene/AB93 results in a negligible reduction in adsorption capacity of PHGC/MXene for AB93, even following 12 cycles of adsorption and desorption. The elimination rate is around 94% (**Figure 17c**), with variations not exceeding 1.5%. Upon utilizing hydrochloric acid solution as desorption agent for PHGC/MXene/MB, the PHGC/MXene's adsorption capacity for MB decreases by a minimal amount after 12 cycles of adsorption and desorption, while the efficiency of removal remains consistently higher than 97% (**Figure 17d**). The results suggest that the removal rate decreases by at least three percent throughout the course of the twelve cycles in comparison to its highest value. This suggests that PHGC/MXene hydrogel excels in both alkaline and acidic environments, demonstrating its versatility. In the case of PHGC/MXene/AB93 and PHGC/MXene/MB, respectively, solutions of sodium bicarbonate and hydrochloric acid demonstrate effective desorption characteristics. As a result, PHGC/MXene hydrogel is a stable, efficient, and renewable adsorbent that may be utilized for the treatment of wastewater that contains AB93 or MB.¹³⁸

View Article Online
DOI: 10.1039/D5NR02336J

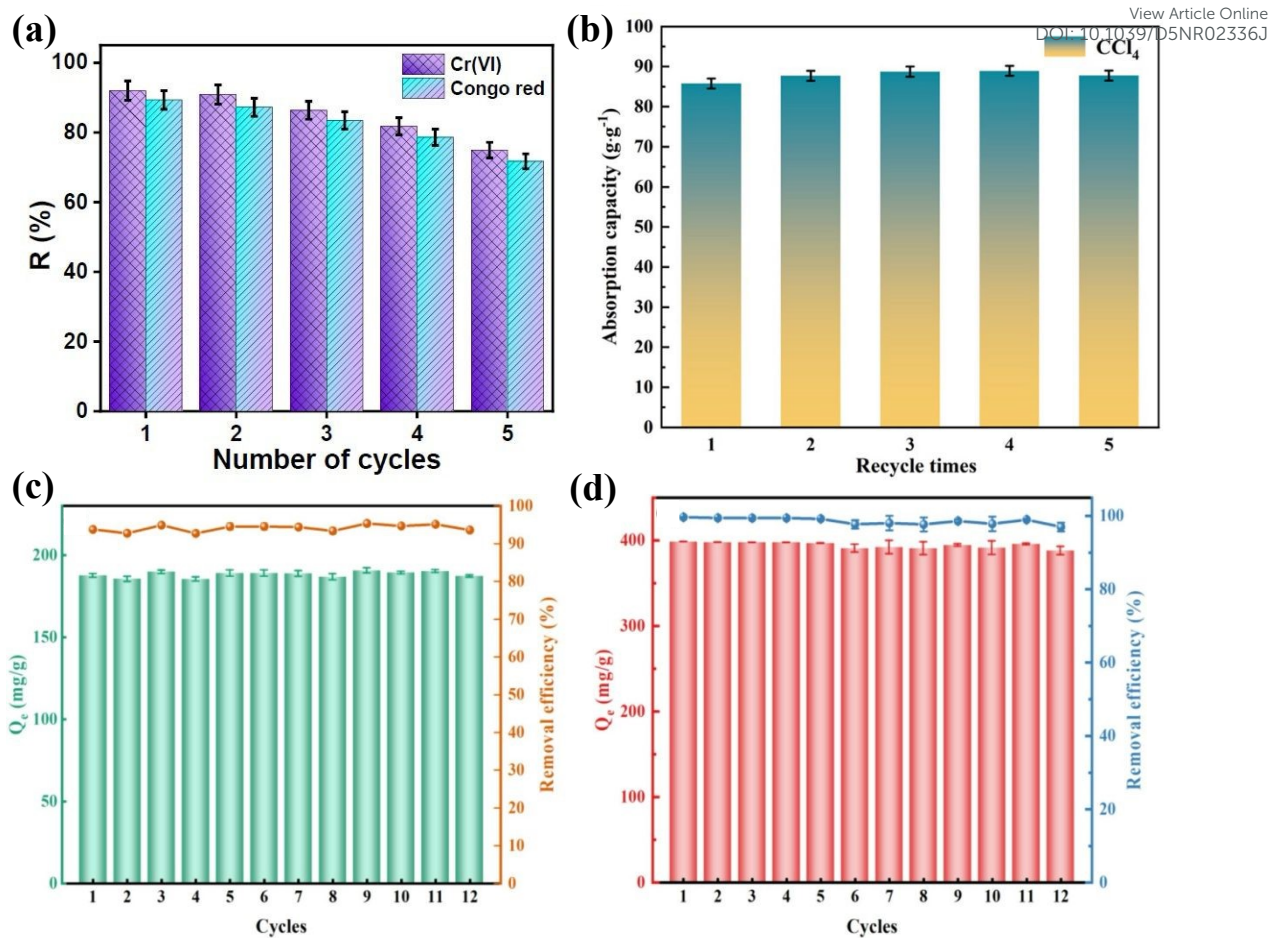


Figure 17: Reusability tests for (a) $\text{Ti}_3\text{C}_2\text{T}_x/\text{NiFeMn-LDH@Gel}$ against Cr (VI) and CR. Reproduced with permission from Ref.¹⁴³ Copyright 2024, Elsevier. (b) $\text{TiVCT}_x/\text{Gas}$ against CCl_4 . Reproduced with permission from Ref.¹⁵⁶ Copyright 2024, American Chemical Society. Regeneration studies of (c) AB93 and (d) MB by PHGC/MXene. Reproduced with permission from Ref.¹³⁸ Copyright 2024, Elsevier.

Table 2: Key strengths and limitations of $\text{Ti}_3\text{C}_2\text{T}_x$ MXene for dye adsorption and photocatalysis

MXene	• Positive Insights	• Negative Insights
$\text{Ti}_3\text{C}_2\text{T}_x^{131}$	<ul style="list-style-type: none"> • First report on MXene for dye removal & photocatalysis. • High MB adsorption via electrostatic interaction. • Effective UV-driven dye degradation (MB & AB80). • Strong binding (irreversible adsorption). • Good fit with Freundlich model (heterogeneous sites). 	<ul style="list-style-type: none"> • Poor stability in water; oxidises to TiO_2. • No toxicity or environmental safety data. • Moderate adsorption capacity (~ 39 mg/g). • Complex mechanisms; needs further clarification. • No real wastewater or reuse tests.
NaOH/LiOH/KOH- $\text{Ti}_3\text{C}_2\text{T}_x^{132}$	<ul style="list-style-type: none"> • Alkali treatment (NaOH, LiOH) increased interlayer spacing (up to 29%). • Surface functionalisation ($-\text{F} \rightarrow -\text{OH}$) improved adsorption capacity. • NaOH-$\text{Ti}_3\text{C}_2\text{T}_x$ showed highest MB adsorption capacity (189 mg/g). • Follows Langmuir model, indicating monolayer adsorption. • Faster dye removal rates compared to untreated MXene. 	<ul style="list-style-type: none"> • No data on reusability or long-term performance. • Lack of toxicity and safety assessment. • Some variants (e.g. KOH-$\text{Ti}_3\text{C}_2\text{T}_x$) showed lower capacity due to agglomeration. • Intercalation effects not uniform; morphology-dependent performance.
$h\text{-Ti}_3\text{C}_2^{133}$	<ul style="list-style-type: none"> • Developed a fluoride-free, HF-free hydrothermal synthesis route using NaBF_4/HCl. • Resulting MXenes ($h\text{-Ti}_3\text{C}_2$, $h\text{-Nb}_2\text{C}$) had higher surface area and better exfoliation. • Improved adsorption performance for MB over HF-etched MXenes. 	<ul style="list-style-type: none"> • No reusability or recyclability tests conducted. • No quantification of maximum adsorption capacity (only removal % shown). • Performance tested only for MB; limited scope (e.g. no heavy metals, real water). • No mechanistic insight into selectivity or adsorption modelling (e.g. isotherms).

	<ul style="list-style-type: none"> • Larger interlayer spacing and higher BET surface area (44.6 vs. 8.9 m²/g). • Broader applicability: method extended to Nb₂C MXene synthesis. 	<ul style="list-style-type: none"> • Adsorption only moderate (~24 mg/g for MB) compared to other MXenes.
Nb ₂ CT _x ¹²⁷	<ul style="list-style-type: none"> • High specific surface area (~44.69 m²/g) and layered morphology support efficient adsorption. • Very high adsorption capacities: MB = 526 mg/g, MO = 500 mg/g. • Follows pseudo-second-order kinetics, indicating chemisorption at active sites. • Faster adsorption for MB (99% removal in 5–11 min). • Excellent efficiency for both cationic and anionic dyes. 	<ul style="list-style-type: none"> • No data on regeneration, recyclability, or real wastewater testing. • Adsorption isotherms (Langmuir, Freundlich) did not fit well; mechanism modelling limited. • Slight surface oxidation observed; long-term MXene stability not assessed.
PAA ₂ alk-MXene ¹²⁸	<ul style="list-style-type: none"> • Adsorbent showed high adsorption capacities of 264.46 mg/g for CR and 193.92 mg/g for MB. • Adsorption followed the Langmuir isotherm and pseudo-second-order kinetics. • The material retained its adsorption efficiency after multiple cycles. • Surface functionalisation introduced beneficial –COOH and –OH groups and increased interlayer spacing. 	<ul style="list-style-type: none"> • The study did not evaluate performance in real wastewater or multi-component dye systems. • Toxicity or leaching of components was not assessed. • Only two dyes (MB and CR) were tested, limiting the generality of the findings.
Ti ₃ C ₂ –SO ₃ H ¹²⁹	<ul style="list-style-type: none"> • Functionalisation with sulfonic groups increased adsorption capacity from 21.10 mg/g to 111.11 mg/g. 	<ul style="list-style-type: none"> • No regeneration or recyclability testing was conducted.

	<ul style="list-style-type: none"> • Adsorption followed Langmuir isotherm and pseudo-second-order kinetics. • Adsorption capacity reached 723.35 mg/g with increased MB concentration. • Surface chemistry and interlayer spacing were enhanced through diazonium modification. 	<ul style="list-style-type: none"> • The study only tested MB; no multicomponent or real wastewater systems. • Safety and environmental aspects were not addressed. • Adsorbent stability and scalability were not discussed.
MXene-COOH@(PEI/PAA) _n ¹³⁷	<ul style="list-style-type: none"> • Adsorption followed pseudo-second-order kinetics and Langmuir isotherm (monolayer adsorption). • Good selectivity and performance across three dyes (MB, ST, NR). • Composites are easily separable and structurally stable. 	<ul style="list-style-type: none"> • Adsorption tested only in single dye systems, not in complex wastewater. • Decline in adsorption capacity upon recycling may limit long-term use. • Synthesis and LbL process may be time-consuming at industrial scale.
PHGC/MXene ¹³⁸	<ul style="list-style-type: none"> • PHGC/MXene hydrogel exhibited pH-responsive selectivity, with adsorption capacities of 555.56 mg/g for MB and 207.47 mg/g for AB93. • High reusability and performance across acidic and alkaline conditions. • The system demonstrated rapid adsorption and strong ionic dye interaction. 	<ul style="list-style-type: none"> • No real wastewater or multi-dye solution testing was conducted. • Potential biodegradability or leaching behaviour of MXene was not assessed. • Toxicity and environmental compatibility remain unexplored.
cetyltrimethylammonium bromide-modified multi-layered Ti ₃ C ₂ Tx MXene (CMM) ¹³⁰	<ul style="list-style-type: none"> • High adsorption capacity: up to 213.00 mg/g. • Effective in a broad pH range, especially at pH 3. • Adsorption follows Langmuir isotherm and pseudo-second-order kinetics. 	<ul style="list-style-type: none"> • Surface area decreased after CTAB modification (from 5.02 to 2.06 m²/g). • No biological toxicity or environmental risk data provided.

	<ul style="list-style-type: none"> • Mechanisms include electrostatic attraction, π-cation interaction, and hydrogen bonding. • Maintains functionality in presence of common co-existing ions. 	<ul style="list-style-type: none"> • Decreased adsorption efficiency after multiple reuse cycles.
ABC/MX composite ¹³⁹	<ul style="list-style-type: none"> • Electrostatic attraction, reduction, chelation, hydrogen bonding. • Excellent selectivity and ion interference resistance. • Thermally enhanced adsorption (endothermic; capacity \uparrow with temperature). • Stable for real-world application: Minimal impact from co-ions and long-term storage. 	<ul style="list-style-type: none"> • Cr(VI) regeneration is limited due to MXene oxidation. • No cytotoxicity or leaching data; safety in biomedical or food applications not assured. • Performance slightly affected by HPO_4^{2-} due to competitive adsorption. • MXene's known susceptibility to oxidation may limit long-term use in oxidative environments. • Complex DFT-supported adsorption models require experimental validation in multicomponent matrices.
MXene-PEI ¹⁴⁰	<ul style="list-style-type: none"> • Fast adsorption kinetics: Equilibrium within 20–60 min. • Mechanisms: Electrostatic attraction, redox reaction ($\text{Cr(VI)} \rightarrow \text{Cr(III)}$), π-π stacking, hydrogen bonding. • Thermally and mechanically stable structure. • Effective even in the presence of competing ions. • Easy handling and reusability due to aerogel form. 	<ul style="list-style-type: none"> • No biological toxicity evaluation for MXene oxidation products or long-term exposure. • Oxidation of MXene over cycles not deeply discussed. • Desorption agents (ethanol, NaOH) could impact cost or scalability. • No real wastewater or multi-contaminant system testing.

MX-PAN membrane ¹⁵⁰	<ul style="list-style-type: none"> • Fast kinetics: Equilibrium achieved in 30–60 min. • Mechanisms: Electrostatic interactions, hydrogen bonding, π-π interactions, redox transformation. • Excellent mechanical strength and porosity from aerogel architecture. • Effective in presence of co-existing ions (Cl^-, SO_4^{2-}, CO_3^{2-}). • Scalable and sustainable fabrication method using wood waste and green chemistry. 	<ul style="list-style-type: none"> • No biological or environmental toxicity validation of MXene degradation products. • Oxidation stability of MXene during long-term use not addressed. • Real wastewater validation not included. • Performance slightly decreased with coexisting PO_4^{3-} ions.
TMAOH delaminated $\text{Ti}_3\text{C}_2\text{T}_x$ MXene nanosheets ¹³⁵	<ul style="list-style-type: none"> • Exceptional adsorption capacity of 1026 mg/g at 318 K, among the highest reported for MXenes. • Fast adsorption kinetics, reaching equilibrium in 10 minutes. • Mechanism confirmed: electrostatic interaction and ion exchange ($\text{TMA}^+ \leftrightarrow \text{MB}^+$) dominate. • Highly dispersible suspension prevents restacking, ensuring active surface availability. • High performance in MNM (membrane form): up to 96% removal efficiency with good dye flux (52 L/m²·h at 0.6 mg/cm² loading). • Good tolerance to pH range (2–10) and monovalent salts. 	<ul style="list-style-type: none"> • Performance decreases in presence of multivalent cations (Ca^{2+}, Al^{3+}) due to competition and electrostatic shielding. • Adsorption capacity decreases slightly after several reuse cycles due to partial loss and delamination damage. • No real wastewater or biological testing provided, performance in complex matrices remains unproven. • Freeze-drying reduces performance, dry-state materials are less effective due to aggregation.
alk-MXene/ CoFe_2O_4 /CS ¹⁴¹	<ul style="list-style-type: none"> • Ultra-high adsorption capacities achieved: 2095.9 mg/g for CR, 1333.9 mg/g for Rhodamine B, and 537.6 mg/g for Malachite Green, among the highest reported for similar adsorbents. 	<ul style="list-style-type: none"> • Limited recyclability scope with significant capacity loss for anionic dyes (34% loss for CR vs <20% for cationic dyes) indicating preferential performance toward cationic species.

	<ul style="list-style-type: none"> • The system demonstrated versatility in removing both cationic and anionic dyes simultaneously with rapid kinetics (equilibrium within 60-120 minutes) and excellent magnetic separability. • Multiple synergistic mechanisms including electrostatic interaction, π-π stacking, and hydrogen bonding provided comprehensive dye removal capability with good structural stability after cycling. 	<ul style="list-style-type: none"> • No environmental safety assessment conducted, and complex multi-step synthesis process involving multiple components (alkalized MXene, CoFe_2O_4, chitosan) may limit practical scalability and cost-effectiveness.
MXene (Ti_3C_2)/ Fe_3O_4 ¹⁴²	<ul style="list-style-type: none"> • Temperature-enhanced performance with 91.93% removal efficiency at 55 °C compared to lower temperatures, demonstrating excellent high-temperature adsorption capability (11.68 mg/g maximum capacity). • The system exhibited superparamagnetic properties (20.3 emu/g) enabling easy magnetic separation and recovery from aqueous solutions with good stability (zeta potential -48 mV). • Multiple adsorption mechanisms identified including electrostatic attraction, hydrogen bonding ($\text{Ti-OH}\cdots\text{N}$), and surface interactions, with temperature-dependent mechanism shifts from physisorption (25 °C) to chemisorption (55 °C). 	<ul style="list-style-type: none"> • Limited scope with testing only on single cationic dye (MB) and no comprehensive evaluation across different dye types or real wastewater conditions. • No recyclability assessment conducted, leaving questions about long-term performance, stability, and practical applicability, with potential concerns about magnetic material leaching and structural integrity over multiple cycles.
AMXGO ¹³⁶	<ul style="list-style-type: none"> • Ultra-high adsorption capacities: 1111.6 mg/g for MG and 1133.7 mg/g for CR, among highest for MXene-based adsorbents. 	<ul style="list-style-type: none"> • Limited real-world testing - only synthetic single-dye solutions, not actual industrial wastewater.

	<ul style="list-style-type: none"> • Excellent versatility with >92% removal for both cationic and anionic dyes, plus selective separation capability. • Multiple adsorption mechanisms with 3.5x surface area increase compared to pristine MXene. 	<ul style="list-style-type: none"> • Complex multi-step synthesis and long equilibrium times (24-48 hours) limit scalability and cost-effectiveness.
ZIF-8@IL-MXene/PNIPAM ¹⁵³	<ul style="list-style-type: none"> • First hydrogel achieving simultaneous high-efficiency adsorption of phenols, dyes, and metal ions (198.40, 325.03, and 285.65 mg/g respectively). • Excellent mechanical properties withstanding ten repeated compressions without damage. • 100× increase in specific surface area through ZIF-8 incorporation. • Novel ionic liquid grafting approach for MXene stabilization and functionality. 	<ul style="list-style-type: none"> • Complex multi-step synthesis requiring precise control of ZIF-8 growth conditions and IL grafting. • Significant decrease in Cu²⁺ regeneration efficiency (29% after 5 cycles) due to irreversible chelation. • Limited scalability due to multiple synthesis stages and specialized materials (ionic liquids, ZIF-8 precursors). • Reduced swelling ratios with ZIF-8 growth potentially limiting accessibility to binding sites.
SC-PLA/PDA/MXene membrane ¹⁵⁵	<ul style="list-style-type: none"> • Outstanding dual functionality combining excellent oil/water separation and organic dye adsorption capabilities. • High flux performance with maximum water flux of 3009.2 L/(m²·h) and oil flux of 6397.9 L/(m²·h) for pure liquids. • Exceptional MB adsorption capacity of 434.8 mg/g following Langmuir model. • Excellent photothermal conversion ability enhancing separation efficiency under light irradiation (water flux: 9428.4 L/(m²·h), oil flux: 12498.1 L/(m²·h)). 	<ul style="list-style-type: none"> • Complex multi-step synthesis involving electrospinning, polydopamine self-polymerization, and MXene deposition requiring precise control. • Limited long-term stability assessment under continuous industrial operating conditions. • Gradual performance decline in oil flux during extended cycling due to irreversible pore blocking by residual oil.

	<ul style="list-style-type: none"> • Superior amphiphilic properties enabling effective separation of different emulsion types (oil-in-water and water-in-oil). • Novel polydopamine-assisted MXene deposition strategy ensuring uniform distribution and stable attachment. • Simultaneous removal capability for both oil and organic pollutants in single-step process. • Ultrahigh oil/water separation efficiency of 99.12% with excellent selectivity. • Good mechanical properties with tensile strength above 4.5 MPa maintaining structural integrity. 	<ul style="list-style-type: none"> • Temperature and light dependency for optimal performance may limit operational flexibility in varying environmental conditions. • No comprehensive economic analysis or cost-effectiveness evaluation compared to conventional separation methods. • Limited testing on real industrial wastewater with complex compositions - most studies conducted using synthetic solutions. • Potential scalability challenges for large-scale industrial applications not thoroughly addressed. • Performance optimization requires specific conditions (pH, temperature, light irradiation) which may complicate real-world implementation. • Incomplete removal during regeneration treatment leading to gradual accumulation of contaminants affecting long-term performance.
$\text{TiV}_\text{C}\text{T}_\text{X}/\text{GAs}^{156}$	<ul style="list-style-type: none"> • Outstanding broad-spectrum removal capabilities: 319.67, 303.45, 229.97, 217.87, and 283.38 mg/g for MB, RhB, CR, MO, and TCH respectively. • Superior performance compared to other adsorbents in comparative analysis. 	<ul style="list-style-type: none"> • Complex multi-step synthesis involving hydrothermal treatment, freeze-drying, and hazardous HF acid for MXene preparation. • Limited long-term stability assessment with only 5-cycle regeneration study.

	<ul style="list-style-type: none">• Excellent compatibility with harsh environments including wastewater containing multiple dyes/drugs and inorganic salts.• Remarkable photothermal conversion ability reaching 95.0 °C within 1 min under sunlight irradiation.• Large absorption capacity for oils and solvents ranging from 40-90 g/g.• Spontaneous and endothermic adsorption process following Langmuir model and pseudo-second-order kinetics.	<ul style="list-style-type: none">• Performance dependency on pH, temperature, and light conditions may limit operational flexibility.• No comprehensive economic analysis or cost-effectiveness evaluation provided.• Mostly tested on synthetic wastewater rather than real industrial effluents.• Endothermic nature requires higher temperatures for optimal performance which may increase operational costs.
--	---	---

7. Comparative insights into the advantages and limitations of $\text{Ti}_3\text{C}_2\text{T}_x$ MXene in dye adsorption and photocatalytic applications

A comprehensive analysis of $\text{Ti}_3\text{C}_2\text{T}_x$ MXene variants and their performance characteristics is presented in **Table 2**, highlighting both positive insights and critical limitations across different modification strategies. $\text{Ti}_3\text{C}_2\text{T}_x$ MXene represents a groundbreaking milestone as the first reported MXene system for dye removal and photocatalysis applications, establishing the foundation for an entire class of 2D materials in environmental remediation. The material exhibits exceptional electrostatic interaction capabilities with cationic dyes, particularly MB, by leveraging its inherent negative surface charge and rich surface chemistry to achieve a strong binding affinity. This electrostatic mechanism proves highly effective for irreversible adsorption, indicating robust dye-MXene interactions that prevent desorption under mild conditions.¹³¹

Photocatalytic versatility emerges as a distinctive advantage, with $\text{Ti}_3\text{C}_2\text{T}_x$ exhibiting effective UV-driven dye degradation for both MB and AB80, demonstrating dual functionality beyond conventional adsorbents. The heterogeneous adsorption behavior, confirmed through excellent Freundlich model fitting, indicates the presence of multiple binding sites with varying energies, providing flexibility in accommodating diverse dye molecules. This multi-site adsorption mechanism contributes to the material's broad applicability across different dye classes and concentrations.¹³¹ Performance enhancement through strategic modifications demonstrates remarkable capabilities through surface functionalization strategies that dramatically amplify $\text{Ti}_3\text{C}_2\text{T}_x$ performance. Alkali treatments using NaOH, LiOH, and KOH achieve remarkable improvements, with NaOH-treated $\text{Ti}_3\text{C}_2\text{T}_x$ demonstrating an exceptional adsorption capacity of 189 mg/g for MB, representing a nearly five-fold increase over the pristine material. This enhancement stems from interlayer spacing expansion (up to 29% increase) and surface

chemistry modification through fluoride-to-hydroxyl group conversion ($-F \rightarrow -OH$), creating more favorable binding sites.¹³² Fluoride-free synthesis approaches using $NaBF_4/HCl$ represent a significant advancement,¹³³ producing $h-Ti_3C_2$ with superior surface area (44.6 vs. 8.9 m^2/g) and enhanced exfoliation characteristics. This environmentally safer synthesis route eliminates hazardous HF usage while achieving better performance for MB adsorption, addressing both environmental concerns and performance requirements. The Langmuir model compliance in modified systems indicates a transition to monolayer adsorption, suggesting a more uniform distribution of binding sites.

Chemical functionalization through sulfonic acid modification ($Ti_3C_2-SO_3H$) showcases dramatic capacity enhancement from 21.10 to 111.11 mg/g , with concentration-dependent performance reaching 723.35 mg/g under optimized conditions. This diazonium-mediated surface modification enhances both surface chemistry and interlayer spacing, creating highly active adsorption sites.¹²⁹ Surfactant modification using cetyltrimethylammonium bromide (CTAB) achieves 213.00 mg/g capacity while maintaining broad pH tolerance, particularly effective at pH 3.¹³⁰ Critical performance limitations and stability challenges reveal that oxidative instability represents the most significant limitation of $Ti_3C_2T_x$ systems, with poor stability in aqueous environments leading to oxidation to TiO_2 .¹³¹ This fundamental degradation pathway compromises long-term performance and material integrity, particularly problematic for continuous water treatment applications. The oxidation susceptibility extends across all $Ti_3C_2T_x$ variants, indicating a materials-level challenge requiring protective strategies or alternative compositions.

The limited adsorption capacity in its pristine form presents significant competitive disadvantages, with the baseline $Ti_3C_2T_x$ achieving only ~ 39 mg/g , substantially lower than that of high-performing adsorbents.¹³¹ Even modified variants like $h-Ti_3C_2$ show moderate performance (~ 24 mg/g), indicating inherent capacity limitations that require extensive

modification for competitive performance.¹³³ Surface area reduction following certain modifications, such as CTAB treatment (5.02 to 2.06 m²/g), demonstrates trade-offs between functionalization and accessible surface area.¹³⁰ Mechanistic complexity across Ti₃C₂T_x systems requires further clarification,¹³¹ with multiple interaction pathways including electrostatic attraction, π -cation interactions, hydrogen bonding,¹³⁰ and ion exchange contributing to overall performance. This complexity makes performance prediction and optimization challenging, particularly in multi-component systems where competitive interactions may alter dominant mechanisms. Scalability and practical implementation barriers pose significant challenges, particularly due to the complexity of synthesis, which requires multi-step modifications. Alkali treatments,¹³² chemical functionalization,¹²⁹ and surfactant modifications¹³⁰ introduce additional processing steps, chemical consumption, and potential environmental concerns. The time-consuming nature of layer-by-layer assembly and precise control requirements for modification procedures limit industrial scalability and cost-effectiveness.¹³⁷

Regeneration limitations across Ti₃C₂T_x systems present economic and environmental concerns. Decreased adsorption efficiency after multiple reuse cycles, observed in CTAB-modified systems, indicates structural degradation or irreversible binding.¹³⁰ Desorption agent requirements (ethanol, NaOH) increase operational costs and waste generation, while incomplete regeneration leads to a gradual decline in performance. Real-world validation gaps represent critical knowledge deficits, with most studies conducted using synthetic single-dye solutions rather than complex industrial wastewaters. Performance degradation in the presence of multivalent cations (Ca²⁺, Al³⁺) and competitive anions highlights selectivity challenges in realistic water matrices. No comprehensive real wastewater testing limits practical applicability assessment.

Environmental and safety considerations highlight critical research gaps, with the assessment of toxicity and biocompatibility representing urgent needs. No systematic evaluation of $\text{Ti}_3\text{C}_2\text{T}_x$'s environmental impact or human health effects exists, while the toxicity of oxidation products, leaching behavior, and long-term environmental fate remain uncharacterized, raising concerns about its widespread deployment. Surface modification agents, such as CTAB and sulfonic acid groups, introduce additional chemical complexity, requiring safety evaluation. HF-based synthesis environmental concerns necessitate safer alternatives, with fluoride-free routes showing promise but requiring further optimization.¹³³ Waste generation from synthesis processes and regeneration procedures requires a comprehensive life cycle assessment to evaluate their overall environmental impact. Challenges associated with disposing of spent MXene materials and their oxidation products necessitate a systematic investigation.

Future directions and innovation opportunities suggest that enhancing oxidative stability represents the highest priority research direction, requiring protective coating strategies, alloy composition optimization, or control of operational conditions. Encapsulation approaches, such as those using protective polymer layers or composite formation with stable matrices, could address degradation issues while maintaining functional performance. Performance optimization strategies should focus on synergistic modification approaches combining interlayer engineering, surface functionalization, and morphological control. AI-guided design can accelerate composition-structure-property relationships discovery, enabling rational optimization of $\text{Ti}_3\text{C}_2\text{T}_x$ variants for specific applications. Scale-up engineering focusing on continuous flow systems, automated synthesis procedures, and regeneration optimization will bridge the laboratory-to-industry gap. Economic feasibility studies incorporating material costs, processing requirements, and performance benefits are essential for commercial viability assessment. Comprehensive environmental impact evaluation through life cycle assessment

View Article Online
DOI: 10.1039/D5NR02336J

will guide sustainable development and regulatory compliance for $\text{Ti}_3\text{C}_2\text{T}_x$ -based water treatment technologies.

8. Benchmarking MXene-based adsorbents against established materials for sustainable dye remediation

To compare performance and demonstrate MXenes' potential in wastewater treatment, **Table 3** provides a detailed quantitative comparison of 2D MXenes with well-known adsorbents, including MOFs, COFs, activated carbon, graphene-based materials, and CNTs for dye removal. The data, sourced from peer-reviewed studies between 2004 and 2024, highlights the outstanding adsorption abilities of MXene-based adsorbents under various conditions. TMAOH- $\text{Ti}_3\text{C}_2\text{T}_x$ achieved the highest adsorption capacity of 1026 mg/g for MB, a 2.5 times increase over commercial activated carbon (400 mg/g) and a significant edge over GO (250-300 mg/g) and multi-walled CNTs (400 mg/g) in similar settings.^{135,167} Likewise, MXene/biomass activated carbon composites showed excellent performance for CR, removing over 1400 mg/g, much higher than commercial activated carbon (500 mg/g) and functionalized CNTs (500 mg/g).^{158,168} MXenes' top performance comes from their unique dual adsorption process that includes surface adsorption and intercalation, along with abundant surface functional groups (-OH, =O, -F), and adjustable surface chemistry that fosters strong electrostatic interactions with both cationic and anionic dyes. MXenes show quick kinetics, reaching equilibrium in 5-120 minutes versus 60-300 minutes for traditional adsorbents, and they can be reused with over 90% efficiency after multiple cycles. Although MOFs and COFs perform well in some cases, like TpStb- SO_3Na COF achieving high capacities for certain cationic dyes, MXenes offer greater versatility, faster kinetics, and wider applicability across diverse dye types and conditions, making them the most promising new adsorbents for sustainable wastewater treatment.¹⁶⁹

Table 3: Adsorption capacities of MXenes vs. conventional adsorbents for organic dyes

Adsorbent Material	Dye	Adsorption Capacity (mg/g)	Contact Time	pH	Temp (°C)	Initial conc. (mg/L)
MXenes (2D Transition Metal Carbides)						
TMAOH- Ti ₃ C ₂ Tx ¹³⁵	MB	1026	Rapid	7	45	100
Ti ₃ C ₂ Tx@Sodium Alginate ¹⁷⁰	MB	969	60 min	10	25	300
Ti ₃ C ₂ Tx/Carbon Foam ¹⁵⁷	MB	357	120 min	7	30	200
Ti ₃ C ₂ Tx/Carbon Foam ¹⁵⁷	CR	648	120 min	7	30	300
MXene/Biomass AC ¹⁵⁸	CR	>1400	180 min	7	25	500
NaOH-Ti ₃ C ₂ Tx ¹³²	MB	189	120 min	7	25	100
Ti ₃ C ₂ Tx/Loofah Carbon ¹⁶⁸	MB	175	60 min	7	25	200
Ti ₃ C ₂ Tx/Loofah Carbon ¹⁶⁸	CR	93	60 min	7	25	150
Activated Carbon						
Commercial PAC (Norit) ¹⁶⁷	MB	400	120 min	6-7	25	200
Commercial PAC (Norit) ¹⁶⁷	CR	500	120 min	6-7	25	250
Tea Seed Shell AC ¹⁷¹	MB	325	180 min	6-7	25	200
Water-activated AC ¹⁷²	MB	149	5 min	6.5- 7	25	100
Palm Kernel Shell AC ¹⁷³	MB	15	60 min	7	25	100
Ashitaba Waste AC ¹⁷⁴	CR	200-300	180 min	7	25	200
Walnut Shell AC ¹⁷⁴	MB	150-200	180 min	7	25	150
Graphene-based Materials						
Graphene Oxide ¹⁷⁵	MB	250-300	60 min	7	25	100

View Article Online
DOI: 10.1039/D5NR02336J

Graphene Oxide ¹⁷⁴	Rhodamine B	200-250	60 min	7	25	100
GO-AC Composite ¹⁷⁶	MB	300-400	120 min	7	25	200
CNTs						
Multi-walled CNTs ¹⁶⁷	MB	400	120 min	6-7	25	200
Multi-walled CNTs ¹⁶⁷	CR	500	120 min	6-7	25	250
Functionalized CNTs ¹⁷⁷	MB	350-450	90 min	7	25	150
Metal-Organic Frameworks (MOFs)						
ZIF-67/GO composite ¹⁷⁸	Malachite Green	250-350	180 min	7	25	200
Al-based MOF ¹⁷⁹	MB	180-250	120 min	7	25	100
MOF-199 ¹⁸⁰	Various odorants	22.6 ± 42.3	60 min	7	25	Variable
Covalent Organic Frameworks (COFs)						
TpStb-SO ₃ Na COF ¹⁶⁹	Cationic dyes	400-500	60 min	7	25	200
Various COFs ¹⁸¹	MB	200-400	120 min	7	25	100-300

9. Challenges, recommendations and future prospectives

Although MXene-based materials are often employed to remove dyes in the environment, studies on these materials are still in their initial phases due to the numerous problems encountered by researchers. The theoretical concept of using MXene-based materials has expanded faster, but the experimental aspect remains slower. However, several challenging issues still need to be carefully considered. In order to realize their real-world relevance and commercial viability in large-scale water treatment applications, it will be necessary to take future steps toward scaling up MXenes and nanocomposites based on MXene.

Current MXene-based dye removal technologies operate at Technology Readiness Level (TRL) 3-4, characterized by laboratory-scale proof-of-concept and component validation in

controlled environments.⁶⁰ While fundamental adsorption mechanisms are well-understood and performance optimization has been demonstrated in synthetic solutions, significant gaps remain in real-world validation, system integration, and scalable manufacturing processes.¹⁸² Real wastewater performance presents the most critical challenge, as industrial effluents contain complex mixtures of organic contaminants, salts, suspended particles, heavy metals, and fluctuating pH that can drastically reduce MXene adsorption capacity and selectivity compared to single-component laboratory studies. Fouling mechanisms from biological wastes, organic matter, and inorganic scaling create surface deactivation and pore blockage, reducing recyclable capacity over operational cycles.⁸⁹ Cost and scalability barriers arise from expensive, hazardous synthesis methods using HF or LiF/HCl, with material costs of \$50-200/kg compared to \$1-10/kg for conventional adsorbents.¹⁸³ Environmental impact assessment through Life Cycle Analysis (LCA) reveals carbon footprints of 5-15 kg CO₂ equivalent per kg MXene, primarily from energy-intensive synthesis processes.¹⁰² Advancement to TRL 6-7 requires pilot-scale demonstrations, comprehensive techno-economic analysis, and development of green synthesis alternatives to establish commercial feasibility.

Several vital areas require attention to fully harness the capabilities of MXene-based materials in dye removal and other applications:

1. **Improvements in the etching procedure:** Traditional etching methods for synthesizing MXenes often employ hazardous chemicals that can harm the environment. Therefore, exploring and creating more ecologically friendly techniques for the etching process is critical. This transition could make MXene production safer and more sustainable and increase its appeal for industrial applications in which environmental restrictions are growing more stringent.

2. **Research on toxicity:** Another critical area of exploration is the potential toxicity of MXene-based materials. Understanding how these materials interact with the environment and human health is essential, especially for therapeutic applications. Comprehensive studies assessing the biocompatibility and environmental impact of MXenes will help establish safety protocols and regulatory frameworks, ensuring their responsible use in various applications, including medicine and environmental remediation.
3. **Surface characterization:** The surface characteristics of MXene-based materials play a significant role in their adsorption abilities. Gaining a deeper understanding of these properties, including surface area, functional groups, and morphology, can lead to modifications that enhance their performance in dye removal. Tailoring the surface chemistry of MXenes could optimize their interaction with various dye molecules, thereby improving their efficiency as adsorbents (**Figure 18**).
4. **Lifespan of recycled materials and advanced integration strategies:** Finally, further research is needed to evaluate the lifespan and reusability of recycled MXene-based materials in real applications. Understanding how these materials degrade over time and how they operate after several cycles of usage is critical to determining their feasibility in long-term applications. Investigating to create methods for the regeneration of MXenes could considerably improve their use in various applications, including wastewater treatment, energy storage, and sensing technologies. Integrating AI and ML can transform the development of MXene materials. These technologies may be utilized to forecast material degradation trends, enhance synthesis procedures, and formulate more effective recycling methods. ML models may evaluate massive datasets to discover trends and recommend ideal settings for material regeneration, therefore eliminating trial-and-error experimentation.

5. **Performance in real wastewater:** The majority of MXene research has been carried out using artificial dye solutions in controlled lab settings. Real wastewater streams, on the other hand, are far more complicated and frequently include a combination of organic contaminants, salts, suspended particles, heavy metals, and fluctuating pH. These conflicting elements have the potential to drastically lower MXenes' adsorption capability and selectivity. Therefore, assessing MXene-based systems in realistic wastewater environments must be a top priority for future research in order to confirm their resilience, effectiveness, and longevity.
6. **Fouling and long-term stability:** MXenes are prone to fouling from biological wastes, organic matter, and other wastewater particles, which can result in surface deactivation, pore blockage, and decreased recyclable capacity. To ensure constant performance across several cycles, fouling must be addressed via surface functionalization, hybrid coating techniques, or integration with antifouling polymers. Additionally, MXene degradation under extended exposure to aquatic environments, particularly under variable redox conditions, remains a significant but little-studied problem.
7. **Cost and scalability:** The top-down etching techniques that use dangerous chemicals like HF or LiF/HCl are among the current MXene production methods that are expensive, dangerous, and challenging to scale. Additionally, the purification and post-synthesis delamination processes require a lot of energy and time. To move MXene manufacturing from laboratory to commercial scale, it will be essential to develop low-cost, scalable, and environmentally friendly synthesis methods, such as electrochemical etching, green exfoliation processes, and continuous flow systems.
8. **Environmental impact and sustainability:** MXenes are intriguing prospects for green remediation solutions, but their total environmental impact must be carefully evaluated. To assess energy use, chemical use, emissions, and end-of-life disposal or recyclability, LCA

studies are crucial. To guarantee environmental and regulatory compliance, issues with leaching, nanoparticle release, and ecotoxicity should also be addressed using thorough risk assessment frameworks. Furthermore, performing a LCA is essential for identifying the environmental impacts of MXene-based materials throughout their life span, from synthesis to disposal. Such a technique guarantees that the materials are sustainable and effective, in agreement with the overall green chemistry initiatives. Evaluating LCA would make MXenes more attractive for firms embracing eco-friendly technology.

For biomedical and environmental applications, *in vivo* cytotoxicity analysis is significant in determining the toxicity of MXenes. Such tests would ensure the safer use of MXenes in real-world applications, such as sensing and wastewater treatment, and guarantee no risk to human health or ecosystems. Advanced characterization solutions including real-time monitoring capabilities, molecular docking studies, and computational simulation technologies, combined with emerging force measurement techniques and advanced X-ray methodologies, could significantly improve MXene system activity and reusability assessment. Force measurement approaches, particularly atomic force microscopy (AFM) and nanoindentation techniques, enable precise quantification of interfacial interactions between MXene surfaces and target molecules, providing critical insights into adsorption mechanisms at the nanoscale level. These force-based methodologies can map surface heterogeneity, measure adhesion forces, and characterize mechanical properties evolution during cycling processes, offering unprecedented understanding of structure-property relationships in MXene systems.¹⁸⁴

Although MXene-based materials hold great promise for environmental applications, addressing these challenges through focused research will be crucial for translating theoretical advancements into practical solutions. By improving synthesis methods, assessing toxicity, understanding surface properties, and evaluating lifespan, the full potential of MXenes can be realized, paving the way for innovative approaches to dye removal and other environmental

challenges. Despite years of investigation on MXene, these materials are still in their early phases of development. Standardization is still required to produce MXene, an attractive material with stable characteristics, including higher biocompatibility, uniform dispersion, prolonged strength, and higher efficiency compared to other 2D materials.⁶⁰ Industry-academia collaboration is essential for developing large-scale MXene-based materials, including encapsulated adsorbents, membranes, and electrodes, with increased hazardous removal efficiency. This will enable the production and deployment of low-cost MXene-based adsorbent solutions for wastewater treatment in residential and commercial areas.

Artificial Intelligence (AI) and Machine Learning (ML) technologies offer transformative potential for advancing MXene-based water treatment systems through multiple specific applications.¹⁸⁵ Machine learning algorithms can predict optimal MXene compositions and surface functionalization strategies by analyzing structure-property relationships from experimental datasets, with Density Functional Theory (DFT) calculations combined with ML models enabling screening of thousands of potential MXene variants to identify high-performance candidates before experimental synthesis.¹⁸⁶ Gaussian Process Regression and Random Forest algorithms have been successfully applied to predict adsorption capacities based on surface area, functional group density, and interlayer spacing parameters,¹⁸⁷ while neural network models can optimize synthesis conditions, including etching time, temperature, and chemical concentrations to achieve target material properties.¹⁸⁸ Support Vector Machine (SVM) and Artificial Neural Network (ANN) models demonstrate capability in predicting dye removal efficiency based on water quality parameters including pH, ionic strength, competing ions, and dye concentrations,¹⁸⁹ with ensemble learning methods such as XGBoost and Random Forest showing superior accuracy in predicting breakthrough curves and saturation points for MXene-based filtration systems.¹⁹⁰

Real-time process optimization represents another critical application area, where adaptive control algorithms integrated with IoT sensor networks enable dynamic optimization of treatment parameters.¹⁹¹ Reinforcement learning agents can continuously adjust flow rates, pH levels, and regeneration cycles based on real-time performance feedback, while digital twin models combining physics-based simulations with ML algorithms provide predictive maintenance capabilities and optimal operational strategies.¹⁹² Deep learning architectures including Convolutional Neural Networks (CNNs) can analyze microscopy images to predict material degradation and performance decline over operational cycles,¹⁹³ with computer vision systems powered by deep learning enabling effluent quality analysis through spectroscopic data interpretation. Time-series forecasting models using LSTM networks predict treatment system performance and identify potential failures before critical thresholds are reached,¹⁹⁴ while anomaly detection algorithms monitor unusual patterns in adsorption behavior that may indicate material degradation or system malfunction.

5G technology enables ultra-low latency communication between distributed sensor networks and central control systems, facilitating real-time optimization of multiple treatment units, while edge computing capabilities allow on-site ML inference for immediate decision-making without cloud dependency.¹⁹⁵ IoT sensors equipped with selective dye detection capabilities provide high-resolution monitoring of specific contaminants, enabling precision treatment protocols that automatically adjust based on real-time water quality parameters.¹⁹⁶ Cloud-based platforms integrate multi-site data for comprehensive performance analysis and predictive modeling, with blockchain technology ensuring data integrity and traceability for regulatory compliance and performance verification. Specific implementation examples include predictive maintenance models that analyze pressure drop patterns, flow rate variations, and energy consumption trends to schedule optimal regeneration cycles, and multi-objective

optimization algorithms that balance treatment efficiency, energy consumption, and operational costs to minimize total system expenses.¹⁹⁷

Future prospects include quantum machine learning algorithms that may accelerate materials discovery by exploring vast chemical spaces more efficiently than classical computers, automated laboratory systems guided by AI algorithms conducting high-throughput synthesis and screening experiments with minimal human intervention, and integration of genomics data with ML models to predict ecological impacts and optimize MXene designs for environmental compatibility.¹⁹⁸ Federated learning frameworks enable collaborative model training across multiple treatment facilities while preserving data privacy and proprietary information, while augmented reality interfaces provide operators with real-time system status and maintenance guidance through smart glasses and mobile applications.¹⁹⁹ This comprehensive AI/ML integration represents a paradigm shift toward intelligent water treatment systems that continuously learn, adapt, and optimize their performance, ultimately enabling more efficient, cost-effective, and sustainable MXene-based environmental remediation technologies capable of autonomous operation and predictive performance optimization across diverse water treatment scenarios.

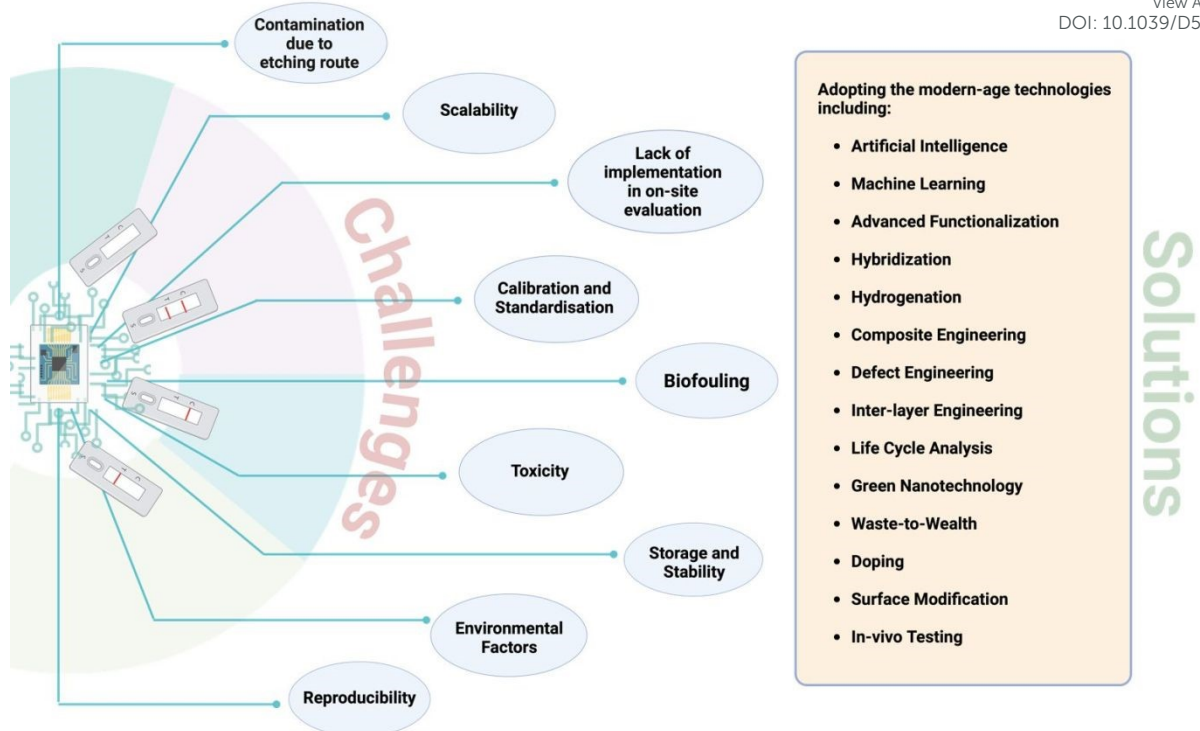


Figure 18. Challenges and Solutions for employing MXene-based materials in the adsorption of dyes

10. Conclusion

In conclusion, MXenes have demonstrated an emerging class of promising two-dimensional adsorbents for the adsorption of various dyes in an aqueous environment. There are various methods for synthesizing MXenes. Presently, the top-down method involving hydrofluoric acid etching is the most commonly used method. Although this approach is less expensive, there is more environmental harm risk. Their high surface areas, active surface terminal groups, hydrophilicity, and distinct combination of layered structures make their adsorption properties excellent. However, its oxidative and aggregative properties make effective adsorption and regeneration difficult. As a result, further modifications are needed. Surface modification, blending, and stripping are some modification methods for MXenes. Blending, in particular,

Published on 04 August 2025. Downloaded by Yunnan University on 8/23/2025 12:46:06 PM.

Nanoscale Accepted Manuscript

can improve the adsorption efficiency, stability, oxidation resistance, hydrophilicity, and other essential features of MXene materials.

This review has highlighted the substantial development in the design and fabrication of MXene-based adsorbents, their adsorption capacity, their physicochemical properties, and adsorption mechanisms of MXenes, including chemical, physical, and electrostatic interactions for the removal of toxic dyes from the aqueous environment. Overall, MXenes are a cutting-edge advance in water treatment, providing an alternative route to more sustainable and effective solutions for dye-contaminated water. Furthermore, with the integration of modern technologies such as IoT, AI, machine learning, and 5G communications, MXene-based nanosorbents have the potential to be next-generation material-based intelligent environmental technologies that form smart and connected societies and cities.

Abbreviation:

2D: Two dimensional

3D: Three dimensional

AA: Acrylic acid

AB93: Methyl blue

AI: Artificial intelligence

BC: Bacterial cellulose

BD: Benzidine

BET: Brunauer–Emmett–Teller

CDCs: carbon-derived carbides

CNT: Carbon nanotubes

COF: Covalent organic framework

CR: Congo Red

CTAB: Cationic surfactant solution

CVD: Chemical Vapor Deposition

DASNP: Dialdehyde starch nanoparticles

DBM: Direct brown M

DBRN: Direct black RN

DMSO: Dimethyl sulphoxide

EDX: Energy-dispersive X-ray

FTIR: Fourier-transform infrared spectroscopy

GPA: Gigapascals

GO: Graphene oxide

HRTEM: High-resolution transmission electron microscopy

IL: Ionic liquid

LCA: Life cycle assessment

LDH: Layered double hydroxides

MB: Methylene Blue

MG: Malachite Green

ML: Machine learning

MO: Methyl Orange

MOF: Metal-organic framework

MPa: Megapascals

NMs: Nanofiber membranes

PA: p-Phenylenediamine

PAN: Polyacrylonitrile

PDA: polydopamine

PEI: Polyethylenimine

PEPLD: Plasma-enhanced pulsed laser deposition

PLA: Polylactic acid

rGO: Reduced graphene oxide

RhB: Rhodamine B

ROS: Reactive oxygen species

SA: Sodium alginate

SAED: Selected area electron diffraction

SEM: Scanning electron microscopy

SSA: Specific surface area

View Article Online
DOI: 10.1039/D5NR02336J

SSbD: Safe and Sustainable by Design

TAPB: 1,3,5- tris(4-aminophenyl) benzene

TMAOH: Tetramethylammonium hydroxide

TP: 1,3,5-triformylphloroglucinol

UN: United Nation

XPS: X-ray photoelectron spectroscopy

XRD: X-ray diffraction

ZIF: Zeolitic imidazolate framework

Acknowledgements

The authors would like to express their gratitude to the institutions and colleagues who provided valuable insights and feedback throughout the preparation of this review article.

Declaration of generative AI in scientific writing

While preparing this work the author(s) used Chatgpt and Claude to improve the readability and language of the manuscript. After using this tool/service, the author(s) reviewed and edited the content as needed and take(s) full responsibility for the content of the published article.

Conflict of Interests

The authors declare no conflicts of interest.

References

- 1 A. Khosla, Sonu, H. T. A. Awan, K. Singh, Gaurav, R. Walvekar, Z. Zhao, A. Kaushik, M. Khalid and V. Chaudhary, 2022, preprint, DOI: 10.1002/adv.202203527.
- 2 D. Pathania, S. Kumar, P. Thakur, V. Chaudhary, A. Kaushik, R. S. Varma, H. Furukawa, M. Sharma and A. Khosla, *Sci Rep*, DOI:10.1038/s41598-022-14984-3.
- 3 Sonu and V. Chaudhary, 2022, preprint, DOI: 10.1149/2754-2726/ac92ed.
- 4 S. Shekhar, A. K. Yadav, A. Khosla and P. R. Solanki, 2022, preprint, DOI: 10.1149/2754-2726/ac9227.
- 5 T. Suzuki, T. Hidaka, Y. Kumagai and M. Yamamoto, 2020, preprint, DOI: 10.1038/s41590-020-0802-6.

- 6 T. T. T. Toan and D. M. Nguyen, *ECS Sensors Plus*, 2022, **1**, 021604.
- 7 C. Valli Nachiyar, A. D. Rakshi, S. Sandhya, N. Britlin Deva Jebasta and J. Nellore, *Case Studies in Chemical and Environmental Engineering*, DOI:10.1016/j.cscee.2023.100339.
- 8 J. Blair, G. Rathee, A. Puertas-Segura, L. M. Pérez and T. Tzanov, *Environ Res*, 2025, **279**, 121783.
- 9 G. Rathee, H. Chugh, S. Kohli, R. K. Gaur and R. Chandra, *Mater Adv*, DOI:10.1039/d2ma01081j.
- 10 Y. Zhou, J. Lu, Y. Zhou and Y. Liu, 2019, preprint, DOI: 10.1016/j.envpol.2019.05.072.
- 11 E. F. D. Januário, T. B. Vidovix, N. de C. L. Beluci, R. M. Paixão, L. H. B. R. da Silva, N. C. Homem, R. Bergamasco and A. M. S. Vieira, 2021, preprint, DOI: 10.1016/j.scitotenv.2021.147957.
- 12 Y. Pan, S. Sanati, R. Abazari, A. Jankowska, J. Goscianska, V. Srivastava, U. Lassi and J. Gao, *Coord Chem Rev*, 2025, **522**, 216231.
- 13 S. X. Chin, K. S. Lau, S. Zakaria, C. H. Chia and C. Wongchoosuk, *Polymers (Basel)*, DOI:10.3390/polym14235165.
- 14 P. V. Nidheesh, M. Zhou and M. A. Oturan, *Chemosphere*, DOI:10.1016/j.chemosphere.2017.12.195.
- 15 L. Bilińska and M. Gmurek, 2021, preprint, DOI: 10.1016/j.wri.2021.100160.
- 16 S. Khamparia and D. K. Jaspal, 2017, preprint, DOI: 10.1007/s11783-017-0899-5.
- 17 A. K. Verma, R. R. Dash and P. Bhunia, 2012, preprint, DOI: 10.1016/j.jenvman.2011.09.012.
- 18 S. Thakur and M. S. Chauhan, 2018.
- 19 M. M. Hassan and C. M. Carr, 2018, preprint, DOI: 10.1016/j.chemosphere.2018.06.043.
- 20 P. Moradihamedani, 2022, preprint, DOI: 10.1007/s00289-021-03603-2.
- 21 S. Sarkar, N. T. Ponce, A. Banerjee, R. Bandopadhyay, S. Rajendran and E. Lichtfouse, 2020, preprint, DOI: 10.1007/s10311-020-01021-w.
- 22 M. Hasanpour and M. Hatami, 2020, preprint, DOI: 10.1016/j.molliq.2020.113094.
- 23 M. Khatami and S. Irvani, *Comments on Inorganic Chemistry*, DOI:10.1080/02603594.2021.1922396.
- 24 K. T. Kubra, M. S. Salman and M. N. Hasan, *J Mol Liq*, DOI:10.1016/j.molliq.2021.115468.
- 25 M. Naushad, A. A. Alqadami, A. A. Al-Kahtani, T. Ahamad, M. R. Awual and T. Tatarchuk, *J Mol Liq*, DOI:10.1016/j.molliq.2019.112075.
- 26 C. Cai, R. Wang, S. Liu, X. Yan, L. Zhang, M. Wang, Q. Tong and T. Jiao, *Colloids Surf A Physicochem Eng Asp*, DOI:10.1016/j.colsurfa.2020.124468.
- 27 R. Xing, W. Wang, T. Jiao, K. Ma, Q. Zhang, W. Hong, H. Qiu, J. Zhou, L. Zhang and Q. Peng, *ACS Sustain Chem Eng*, DOI:10.1021/acssuschemeng.7b00343.

- 28 G. Rathee, A. Puertas-Segura, J. Blair, J. Rathee and T. Tzanov, *Prog Mater Sci*, 2025, **150**, 101403. View Article Online
DOI: 10.1039/D5NR02336J
- 29 G. Rathee, N. Singh and R. Chandra, *ACS Omega*, DOI:10.1021/acsomega.9b03785.
- 30 G. Rathee, S. Kohli, A. Awasthi, N. Singh and R. Chandra, *RSC Adv*, DOI:10.1039/d0ra02766a.
- 31 G. Rathee, A. Awasthi, D. Sood, R. Tomar, V. Tomar and R. Chandra, *Sci Rep*, DOI:10.1038/s41598-019-52849-4.
- 32 M. J. K. Ahmed and M. Ahmaruzzaman, 2016, preprint, DOI: 10.1016/j.jwpe.2016.01.014.
- 33 M. Ahmaruzzaman, 2011, preprint, DOI: 10.1016/j.cis.2011.04.005.
- 34 S. A. Khan, D. Hussain, N. Abbasi and T. A. Khan, *Chemosphere*, DOI:10.1016/j.chemosphere.2021.133232.
- 35 S. A. Khan, N. Abbasi, D. Hussain and T. A. Khan, *Langmuir*, DOI:10.1021/acs.langmuir.2c00702.
- 36 K. S. Novoselov, A. K. Geim, S. V Morozov, D. Jiang, Y. Zhang, S. V Dubonos, I. V Grigorieva and A. A. Firsov, *Electric Field Effect in Atomically Thin Carbon Films*, 2000, vol. 404.
- 37 L. Y. Yuan, Z. Q. Bai, R. Zhao, Y. L. Liu, Z. J. Li, S. Q. Chu, L. R. Zheng, J. Zhang, Y. L. Zhao, Z. F. Chai and W. Q. Shi, *ACS Appl Mater Interfaces*, DOI:10.1021/am405584h.
- 38 R. Ma and T. Sasaki, 2010, preprint, DOI: 10.1002/adma.201001722.
- 39 J. N. Coleman, M. Lotya, A. O'Neill, S. D. Bergin, P. J. King, U. Khan, K. Young, A. Gaucher, S. De, R. J. Smith, I. V. Shvets, S. K. Arora, G. Stanton, H. Y. Kim, K. Lee, G. T. Kim, G. S. Duesberg, T. Hallam, J. J. Boland, J. J. Wang, J. F. Donegan, J. C. Grunlan, G. Moriarty, A. Shmeliov, R. J. Nicholls, J. M. Perkins, E. M. Grieveson, K. Theuvsen, D. W. McComb, P. D. Nellist and V. Nicolosi, *Science (1979)*, DOI:10.1126/science.1194975.
- 40 K. S. Novoselov, A. K. Geim, S. V. Morozov, D. Jiang, M. I. Katsnelson, I. V. Grigorieva, S. V. Dubonos and A. A. Firsov, *Nature*, DOI:10.1038/nature04233.
- 41 K. V. Wong and B. Bachelier, *J Energy Resour Technol*, DOI:10.1115/1.4024917.
- 42 O. P. Chen, Y. J. Lin, W. Z. Cao and C. T. Chang, *Mater Lett*, DOI:10.1016/j.matlet.2017.01.030.
- 43 S. Wang, H. Sun, H. M. Ang and M. O. Tadé, 2013, preprint, DOI: 10.1016/j.cej.2013.04.070.
- 44 F. Perreault, A. Fonseca De Faria and M. Elimelech, *Chem Soc Rev*, DOI:10.1039/c5cs00021a.
- 45 Y. Fan, L. Li, Y. Zhang, X. Zhang, D. Geng and W. Hu, 2022, preprint, DOI: 10.1002/adfm.202111357.
- 46 F. A. Janjhi, I. Ihsanullah, M. Bilal, R. Castro-Muñoz, G. Boczkaj and F. Gallucci, 2023, preprint, DOI: 10.1016/j.wri.2023.100202.
- 47 Y. Ibrahim, M. Meslam, K. Eid, B. Salah, A. M. Abdullah, K. I. Ozoemena, A. Elzatahry, M. A. Sharaf and M. Sillanpää, 2022, preprint, DOI: 10.1016/j.seppur.2021.120083.
- 48 I. Ihsanullah and M. Bilal, 2022, preprint, DOI: 10.1016/j.apmt.2022.101674.
- 49 I. Ihsanullah and M. Bilal, *Chemosphere*, DOI:10.1016/j.chemosphere.2022.135234.

- 50 S. Yu, H. Tang, D. Zhang, S. Wang, M. Qiu, G. Song, D. Fu, B. Hu and X. Wang, 2022, preprint, DOI: 10.1016/j.scitotenv.2021.152280. View Article Online
DOI: 10.1039/D5NR02336J
- 51 X. Jiang, A. V. Kuklin, A. Baev, Y. Ge, H. Ågren, H. Zhang and P. N. Prasad, 2020, preprint, DOI: 10.1016/j.physrep.2019.12.006.
- 52 M. Naguib, V. N. Mochalin, M. W. Barsoum and Y. Gogotsi, *Advanced Materials*, DOI:10.1002/adma.201304138.
- 53 Q. Tao, M. Dahlqvist, J. Lu, S. Kota, R. Meshkian, J. Halim, J. Palisaitis, L. Hultman, M. W. Barsoum, P. O. Å. Persson and J. Rosen, *Nat Commun*, DOI:10.1038/ncomms14949.
- 54 Y. C. Zhou, X. H. Wang, Z. M. Sun and S. Q. Chen, *J Mater Chem*, DOI:10.1039/b101520f.
- 55 K. Huang, Z. Li, J. Lin, G. Han and P. Huang, *Chem Soc Rev*, DOI:10.1039/c7cs00838d.
- 56 I. Persson, A. el Ghazaly, Q. Tao, J. Halim, S. Kota, V. Darakchieva, J. Palisaitis, M. W. Barsoum, J. Rosen and P. O. Å. Persson, *Small*, DOI:10.1002/smll.201703676.
- 57 X. Wang, L. Wu, H. Gao and X. Zhang, *SCIENTIA SINICA Chimica*.
- 58 F. Kong, X. He, Q. Liu, X. Qi, Y. Zheng, R. Wang and Y. Bai, *Electrochim Acta*, DOI:10.1016/j.electacta.2018.01.196.
- 59 J. Halim, J. Palisaitis, J. Lu, J. Thörnberg, E. J. Moon, M. Precner, P. Eklund, P. O. A. Persson, M. W. Barsoum and J. Rosen, *ACS Appl Nano Mater*, DOI:10.1021/acsanm.8b00332.
- 60 B. Anasori, M. R. Lukatskaya and Y. Gogotsi, 2017, preprint, DOI: 10.1038/natrevmats.2016.98.
- 61 A. Lipatov, H. Lu, M. Alhabeb, B. Anasori, A. Gruverman, Y. Gogotsi and A. Sinitskii, *Sci Adv*, DOI:10.1126/sciadv.aat0491.
- 62 J. Zhang, N. Kong, S. Uzun, A. Levitt, S. Seyedin, P. A. Lynch, S. Qin, M. Han, W. Yang, J. Liu, X. Wang, Y. Gogotsi and J. M. Razal, *Advanced Materials*, DOI:10.1002/adma.202070180.
- 63 V. N. Borysiuk, V. N. Mochalin and Y. Gogotsi, *Nanotechnology*, DOI:10.1088/0957-4484/26/26/265705.
- 64 S. Luo, S. Patole, S. Anwer, B. Li, T. Delclos, O. Gogotsi, V. Zahorodna, V. Balitskyi and K. Liao, *Nanotechnology*, DOI:10.1088/1361-6528/ab94dd.
- 65 Y. Gogotsi, *Matter*, DOI:10.1016/j.matt.2021.12.006.
- 66 B. Liang, X. Liao, Q. Zhu, M. Yu, J. Li, B. Geng, K. Liu, D. Jia, Z. Yang and Y. Zhou, *Ceram Int*, DOI:10.1016/j.ceramint.2021.06.198.
- 67 J. Yin, N. Liu and Y. Gao, 2024, preprint, DOI: 10.15541/jim20230397.
- 68 R. Li, L. Zhang, L. Shi and P. Wang, *ACS Nano*, DOI:10.1021/acsnano.6b08415.
- 69 K. Wang, Y. Zhou, W. Xu, D. Huang, Z. Wang and M. Hong, *Ceram Int*, DOI:10.1016/j.ceramint.2016.02.059.
- 70 O. Mashtalir, M. Naguib, V. N. Mochalin, Y. Dall'Agnese, M. Heon, M. W. Barsoum and Y. Gogotsi, *Nat Commun*, DOI:10.1038/ncomms2664.

- 71 X. H. Zha, J. Yin, Y. Zhou, Q. Huang, K. Luo, J. Lang, J. S. Francisco, J. He and S. Du, *Journal of Physical Chemistry C*, DOI:10.1021/acs.jpcc.6b04192. View Article Online
DOI: 10.1039/D5NR02336J
- 72 H. Wang, Y. Wu, J. Zhang, G. Li, H. Huang, X. Zhang and Q. Jiang, *Mater Lett*, DOI:10.1016/j.matlet.2015.08.046.
- 73 C. J. Zhang, B. Anasori, A. Seral-Ascaso, S. H. Park, N. McEvoy, A. Shmeliov, G. S. Duesberg, J. N. Coleman, Y. Gogotsi and V. Nicolosi, *Advanced Materials*, DOI:10.1002/adma.201702678.
- 74 X. Tang, X. Guo, W. Wu and G. Wang, 2018, preprint, DOI: 10.1002/aenm.201801897.
- 75 M. Ghidui, S. Kota, V. Drozd and M. W. Barsoum, *Sci Adv*, DOI:10.1126/sciadv.aao6850.
- 76 E. S. Muckley, M. Naguib, H. W. Wang, L. Vlcek, N. C. Osti, R. L. Sacci, X. Sang, R. R. Unocic, Y. Xie, M. Tyagi, E. Mamontov, K. L. Page, P. R. C. Kent, J. Nanda and I. N. Ivanov, *ACS Nano*, DOI:10.1021/acsnano.7b05264.
- 77 E. S. Muckley, M. Naguib and I. N. Ivanov, *Nanoscale*, DOI:10.1039/c8nr05170d.
- 78 J. Halim, S. Kota, M. R. Lukatskaya, M. Naguib, M. Q. Zhao, E. J. Moon, J. Pitock, J. Nanda, S. J. May, Y. Gogotsi and M. W. Barsoum, *Adv Funct Mater*, DOI:10.1002/adfm.201505328.
- 79 G. Ying, S. Kota, A. D. Dillon, A. T. Fafarman and M. W. Barsoum, *FlatChem*, DOI:10.1016/j.flatc.2018.03.001.
- 80 M. Lu, H. Li, W. Han, J. Chen, W. Shi, J. Wang, X. M. Meng, J. Qi, H. Li, B. Zhang, W. Zhang and W. Zheng, *Journal of Energy Chemistry*, DOI:10.1016/j.jechem.2018.05.017.
- 81 T. Voisin, M. D. Grapes, T. T. Li, M. K. Santala, Y. Zhang, J. P. Ligda, N. J. Lorenzo, B. E. Schuster, G. H. Campbell and T. P. Weihs, *Materials Today*, 2020, **33**, 10–16.
- 82 Y. Ying, Y. Liu, X. Wang, Y. Mao, W. Cao, P. Hu and X. Peng, *ACS Appl Mater Interfaces*, DOI:10.1021/am5074722.
- 83 A. Shahzad, K. Rasool, W. Miran, M. Nawaz, J. Jang, K. A. Mahmoud and D. S. Lee, *ACS Sustain Chem Eng*, DOI:10.1021/acssuschemeng.7b02695.
- 84 M. Bilal, I. Ihsanullah, M. Younas and M. Ul Hassan Shah, 2022, preprint, DOI: 10.1016/j.seppur.2021.119510.
- 85 M. Sajid, 2021, preprint, DOI: 10.1016/j.aca.2020.08.063.
- 86 L. P. Yu, L. Lu, X. H. Zhou and L. Xu, 2023, preprint, DOI: 10.1002/admi.202201818.
- 87 A. Maleki, M. Ghomi, N. Nikfarjam, M. Akbari, E. Sharifi, M. A. Shahbazi, M. Kermanian, M. Seyedhamzeh, E. Nazarzadeh Zare, M. Mehrali, O. Moradi, F. Sefat, V. Mattoli, P. Makvandi and Y. Chen, 2022, preprint, DOI: 10.1002/adfm.202203430.
- 88 Z. Othman, H. R. Mackey and K. A. Mahmoud, *Chemosphere*, DOI:10.1016/j.chemosphere.2022.133849.
- 89 C. J. Zhang, S. Pinilla, N. McEvoy, C. P. Cullen, B. Anasori, E. Long, S. H. Park, A. Seral-Ascaso, A. Shmeliov, D. Krishnan, C. Morant, X. Liu, G. S. Duesberg, Y. Gogotsi and V. Nicolosi, *Chemistry of Materials*, DOI:10.1021/acs.chemmater.7b00745.

- 90 K. Rasool, R. P. Pandey, P. A. Rasheed, S. Buczek, Y. Gogotsi and K. A. Mahmoud, 2019, preprint, DOI: 10.1016/j.mattod.2019.05.017. View Article Online
DOI: 10.1039/D5NR02336J
- 91 S. P. Sreenilayam, I. Ul Ahad, V. Nicolosi and D. Brabazon, 2021, preprint, DOI: 10.1016/j.mattod.2020.10.025.
- 92 M. Soleymaniha, M. A. Shahbazi, A. R. Rafieerad, A. Maleki and A. Amiri, 2019, preprint, DOI: 10.1002/adhm.201801137.
- 93 A. M. Jastrzębska, A. Szuplewska, T. Wojciechowski, M. Chudy, W. Ziemkowska, L. Chlubny, A. Rozmysłowska and A. Olszyna, *J Hazard Mater*, DOI:10.1016/j.jhazmat.2017.06.004.
- 94 A. M. Jastrzębska, A. Szuplewska, A. Rozmysłowska-Wojciechowska, M. Chudy, A. Olszyna, M. Birowska, M. Popielski, J. A. Majewski, B. Scheibe, V. Natsu and M. W. Barsoum, *2d Mater*, DOI:10.1088/2053-1583/ab6a60.
- 95 W. Wu, H. Ge, L. Zhang, X. Lei, Y. Yang, Y. Fu and H. Feng, *Chem Res Toxicol*, 2020, **33**, 2953–2962.
- 96 J. Wu, Y. Yu and G. Su, *Nanomaterials*, DOI:10.3390/nano12050828.
- 97 J. Yoon, S. Kim, K. H. Park, S. Lee, S. J. Kim, H. Lee, T. Oh and C. M. Koo, *Small Methods*, DOI:10.1002/smtd.202201579.
- 98 X. Wu, J. Gong, H. Zhang, Y. Wang and F. Tan, *Science of the Total Environment*, DOI:10.1016/j.scitotenv.2023.169227.
- 99 S. F. Hansen, M. B. Nielsen, L. M. Skjolding, J. Kaur, N. Desivayana, F. Hermansson, J. Bird, S. Barg, A. Khort, I. Odneval, B. Fadeel and R. Arvidsson, *Sci Rep*, 2024, **14**, 31030.
- 100 G. K. Nasrallah, M. Al-Asmakh, K. Rasool and K. A. Mahmoud, *Environ Sci Nano*, DOI:10.1039/c7en01239j.
- 101 Q. Xiang, Z. Wang, J. Yan, M. Niu, W. Long, Z. Ju and X. Chang, *Aquatic Toxicology*, DOI:10.1016/j.aquatox.2024.106904.
- 102 M. Dadashi Firouzjaei, S. K. Nemani, M. Sadrzadeh, E. K. Wujcik, M. Elliott and B. Anasori, *Advanced Materials*, DOI:10.1002/adma.202300422.
- 103 K. S. Novoselov, D. Jiang, F. Schedin, T. J. Booth, V. V. Khotkevich, S. V. Morozov and A. K. Geim, *Proc Natl Acad Sci U S A*, DOI:10.1073/pnas.0502848102.
- 104 M. S. Cao, Y. Z. Cai, P. He, J. C. Shu, W. Q. Cao and J. Yuan, 2019, preprint, DOI: 10.1016/j.cej.2018.11.051.
- 105 M. Naguib, M. Kurtoglu, V. Presser, J. Lu, J. Niu, M. Heon, L. Hultman, Y. Gogotsi and M. W. Barsoum, in *MXenes: From Discovery to Applications of Two-Dimensional Metal Carbides and Nitrides*, 2023.
- 106 J. Liang, C. Ding, J. Liu, T. Chen, W. Peng, Y. Li, F. Zhang and X. Fan, *Nanoscale*, DOI:10.1039/c9nr02085c.
- 107 M. Naguib, J. Halim, J. Lu, K. M. Cook, L. Hultman, Y. Gogotsi and M. W. Barsoum, *J Am Chem Soc*, DOI:10.1021/ja405735d.

- 108 R. B. Rakhi, B. Ahmed, M. N. Hedhili, D. H. Anjum and H. N. Alshareef, *Chemistry of Materials*, DOI:10.1021/acs.chemmater.5b01623. View Article Online
DOI: 10.1039/D5NR02336J
- 109 Z. Sun, S. Li, R. Ahuja and J. M. Schneider, *Solid State Commun*, DOI:10.1016/j.ssc.2003.12.008.
- 110 X. Sang, Y. Xie, M. W. Lin, M. Alhabeib, K. L. Van Aken, Y. Gogotsi, P. R. C. Kent, K. Xiao and R. R. Unocic, *ACS Nano*, DOI:10.1021/acsnano.6b05240.
- 111 M. Ghidui, M. R. Lukatskaya, M. Q. Zhao, Y. Gogotsi and M. W. Barsoum, *Nature*, DOI:10.1038/nature13970.
- 112 A. Lipatov and A. Sinitskii, in *2D Metal Carbides and Nitrides (MXenes): Structure, Properties and Applications*, 2019.
- 113 J. Zhao, L. Zhang, X. Y. Xie, X. Li, Y. Ma, Q. Liu, W. H. Fang, X. Shi, G. Cui and X. Sun, *J Mater Chem A Mater*, DOI:10.1039/c8ta09840a.
- 114 M. Naguib, R. R. Unocic, B. L. Armstrong and J. Nanda, *Dalton Transactions*, DOI:10.1039/c5dt01247c.
- 115 I. R. Shein and A. L. Ivanovskii, *Comput Mater Sci*, DOI:10.1016/j.commatsci.2012.07.011.
- 116 P. Urbankowski, B. Anasori, T. Makaryan, D. Er, S. Kota, P. L. Walsh, M. Zhao, V. B. Shenoy, M. W. Barsoum and Y. Gogotsi, *Nanoscale*, DOI:10.1039/c6nr02253g.
- 117 T. Li, L. Yao, Q. Liu, J. Gu, R. Luo, J. Li, X. Yan, W. Wang, P. Liu, B. Chen, W. Zhang, W. Abbas, R. Naz and D. Zhang, *Angewandte Chemie - International Edition*, DOI:10.1002/anie.201800887.
- 118 T. Li, X. Yan, L. Huang, J. Li, L. Yao, Q. Zhu, W. Wang, W. Abbas, R. Naz, J. Gu, Q. Liu, W. Zhang and D. Zhang, *J Mater Chem A Mater*, 2019, **7**, 14462–14465.
- 119 S. Yang, P. Zhang, F. Wang, A. G. Ricciardulli, M. R. Lohe, P. W. M. Blom and X. Feng, *Angewandte Chemie - International Edition*, DOI:10.1002/anie.201809662.
- 120 M. R. Lukatskaya, J. Halim, B. Dyatkin, M. Naguib, Y. S. Buranova, M. W. Barsoum and Y. Gogotsi, *Angewandte Chemie International Edition*, DOI:10.1002/anie.201403559.
- 121 W. Sun, S. A. Shah, Y. Chen, Z. Tan, H. Gao, T. Habib, M. Radovic and M. J. Green, *J Mater Chem A Mater*, DOI:10.1039/c7ta05574a.
- 122 Z. Zhang, F. Zhang, H. Wang, C. Ho Chan, W. Lu and J. Y. Dai, *J Mater Chem C Mater*, DOI:10.1039/c7tc03652c.
- 123 X. Xiao, H. Yu, H. Jin, M. Wu, Y. Fang, J. Sun, Z. Hu, T. Li, J. Wu, L. Huang, Y. Gogotsi and J. Zhou, *ACS Nano*, DOI:10.1021/acsnano.6b08534.
- 124 J. Jia, T. Xiong, L. Zhao, F. Wang, H. Liu, R. Hu, J. Zhou, W. Zhou and S. Chen, *ACS Nano*, DOI:10.1021/acsnano.7b06607.
- 125 C. Xu, L. Wang, Z. Liu, L. Chen, J. Guo, N. Kang, X. L. Ma, H. M. Cheng and W. Ren, *Nat Mater*, DOI:10.1038/nmat4374.
- 126 Y. Gogotsi, *Nat Mater*, DOI:10.1038/nmat4386.

- 127 Y. Yan, H. Han, Y. Dai, H. Zhu, W. Liu, X. Tang, W. Gan and H. Li, *ACS Appl Nano Mater*, DOI:10.1021/acsanm.1c02339. View Article Online
DOI: 10.1039/D5NR02336J
- 128 C. Hao, G. Li, G. Wang, W. Chen and S. Wang, *Colloids Surf A Physicochem Eng Asp*, DOI:10.1016/j.colsurfa.2021.127730.
- 129 Y. Lei, Y. Cui, Q. Huang, J. Dou, D. Gan, F. Deng, M. Liu, X. Li, X. Zhang and Y. Wei, *Ceram Int*, DOI:10.1016/j.ceramint.2019.05.331.
- 130 P. Najibikhah and A. Rahbar-Kelishami, *Chemosphere*, DOI:10.1016/j.chemosphere.2023.141058.
- 131 O. Mashtalir, K. M. Cook, V. N. Mochalin, M. Crowe, M. W. Barsoum and Y. Gogotsi, *J Mater Chem A Mater*, DOI:10.1039/c4ta02638a.
- 132 Z. Wei, Z. Peigen, T. Wubian, Q. Xia, Z. Yamei and S. ZhengMing, *Mater Chem Phys*, DOI:10.1016/j.matchemphys.2017.12.034.
- 133 C. Peng, P. Wei, X. Chen, Y. Zhang, F. Zhu, Y. Cao, H. Wang, H. Yu and F. Peng, *Ceram Int*, DOI:10.1016/j.ceramint.2018.07.124.
- 134 M. Vakili, G. Cagnetta, J. Huang, G. Yu and J. Yuan, *Molecules*, DOI:10.3390/molecules24132478.
- 135 L. Zhang, D. Huang, P. Zhao, G. Yue, L. Yang and W. Dan, *Sep Purif Technol*, DOI:10.1016/j.seppur.2022.120718.
- 136 W. Li, J. Tong and G. Li, *Chemosphere*, 2024, **360**, 142376.
- 137 K. Li, G. Zou, T. Jiao, R. Xing, L. Zhang, J. Zhou, Q. Zhang and Q. Peng, *Colloids Surf A Physicochem Eng Asp*, DOI:10.1016/j.colsurfa.2018.05.044.
- 138 Y. Li, G. Qu, H. Zhang, L. Xie and Y.-F. Zhang, *Chem Eng Sci*, 2024, **300**, 120648.
- 139 Y. Xu, Z. Zhang, Z. Cui, L. Luo, P. Lin, M. Xie, Q. Zhang, B. Sa and C. Wen, *Chemical Engineering Journal*, 2024, **488**, 151078.
- 140 L. Li, X. Y. Shi, T. Huang, N. Zhang and Y. Wang, *J Mater Chem A Mater*, DOI:10.1039/d3ta04869a.
- 141 R. Wang, H. Cao, C. Yao, C. Peng, J. Qiu, K. Dou, N. Tsidaeva and W. Wang, *Appl Surf Sci*, DOI:10.1016/j.apsusc.2023.157091.
- 142 Z. Zhu, M. Xiang, L. Shan, T. He and P. Zhang, *J Solid State Chem*, DOI:10.1016/j.jssc.2019.120989.
- 143 G. S. Elgarhy, G. M. El-Subruiti, A. M. Omer and A. S. Eltaweil, *J Mol Liq*, DOI:10.1016/j.molliq.2023.123889.
- 144 Y. Zheng, H. Zhang, S. Yu, H. Zhou, W. Chen and J. Yang, *Sep Purif Technol*, 2024, **349**, 127908.
- 145 R. Wang, C. Yao, C. Peng, J. Qiu, Q. Wang, X. Liu, J. Meng and W. Wang, *Chemical Engineering Journal*, DOI:10.1016/j.cej.2024.149916.
- 146 X. Wang, A. Zhang, M. Chen, M. K. Seliem, M. Mobarak, Z. Diao and Z. Li, *Chemical Engineering Journal*, DOI:10.1016/j.cej.2023.145385.

- 147 H. Yang, J. Lin, Z. Wen, Z. Li, J. Zeng, L. Wang, Y. Tao, D. Gao and D. Wang, *Chemosphere*, DOI:10.1016/j.chemosphere.2023.139797. View Article Online
DOI: 10.1039/D5NR02336J
- 148 A. Bukhari, I. Ijaz, A. Nazir, S. Hussain, H. Zain, E. Gilani, A. A. Ifseisi and H. Ahmad, *RSC Adv*, 2024, **14**, 3732–3747.
- 149 I. Ijaz, A. Bukhari, E. Gilani, A. Nazir, H. Zain, A. Bukhari, A. Shaheen, S. Hussain and A. Imtiaz, *Process Biochemistry*, DOI:10.1016/j.procbio.2023.03.029.
- 150 R. Imsong and D. Dhar Purkayastha, *Sep Purif Technol*, DOI:10.1016/j.seppur.2022.122636.
- 151 M. Li, P. Zhang, Q. Wang, N. Yu, X. Zhang and S. Su, *Polymers (Basel)*, DOI:10.3390/polym15092110.
- 152 Y. Feng, H. Wang, J. Xu, X. Du, X. Cheng, Z. Du and H. Wang, *J Hazard Mater*, DOI:10.1016/j.jhazmat.2021.125777.
- 153 Q. Wang, J. Qiao, Y. Xiong, F. Dong and Y. Xiong, *Environ Res*, DOI:10.1016/j.envres.2023.117568.
- 154 G. Song, W. Fan, J. Zhang, T. Xue, Y. Shi, Y. Sun and G. Ding, *Appl Surf Sci*, 2024, **661**, 160036.
- 155 S. yu Chen, Y. fan Deng, T. Huang, N. Zhang and Y. Wang, *Sep Purif Technol*, DOI:10.1016/j.seppur.2023.125040.
- 156 T. Lv, F. Wu, Z. Zhang, Z. Liu, Y. Zhao, L. Yu, J. Zhang, C. Yu, C. Zhao and G. Xing, *ACS Appl Nano Mater*, DOI:10.1021/acsanm.4c00038.
- 157 X. Wang, Q. Xu, L. Zhang, L. Pei, H. Xue and Z. Li, *J Environ Chem Eng*, DOI:10.1016/j.jece.2022.109206.
- 158 H. Xue, X. Gao, M. K. Seliem, M. Mobarak, R. Dong, X. Wang, K. Fu, Q. Li and Z. Li, *Chemical Engineering Journal*, DOI:10.1016/j.cej.2022.138735.
- 159 W. Zhao, H. Chi, S. Zhang, X. Zhang and T. Li, *Molecules*, DOI:10.3390/molecules27134243.
- 160 M. Khazaei, M. Arai, T. Sasaki, C. Y. Chung, N. S. Venkataramanan, M. Estili, Y. Sakka and Y. Kawazoe, *Adv Funct Mater*, DOI:10.1002/adfm.201202502.
- 161 M. A. Hope, A. C. Forse, K. J. Griffith, M. R. Lukatskaya, M. Ghidui, Y. Gogotsi and C. P. Grey, *Physical Chemistry Chemical Physics*, 2016, **18**, 5099–5102.
- 162 M. R. Lukatskaya, O. Mashtalir, C. E. Ren, Y. Dall'Agnese, P. Rozier, P. L. Taberna, M. Naguib, P. Simon, M. W. Barsoum and Y. Gogotsi, *Science (1979)*, DOI:10.1126/science.1241488.
- 163 I. Persson, L. Å. Näslund, J. Halim, M. W. Barsoum, V. Darakchieva, J. Palisaitis, J. Rosen and P. O. Å. Persson, *2d Mater*, DOI:10.1088/2053-1583/aa89cd.
- 164 A. Abdul Ghani, B. Kim, M. Nawaz, K. C. Devarayapalli, Y. Lim, G. Kim and D. S. Lee, *Chemical Engineering Journal*, DOI:10.1016/j.cej.2023.143473.
- 165 A. A. Ghani, A. Shahzad, M. Moztahida, K. Tahir, H. Jeon, B. Kim and D. S. Lee, *Chemical Engineering Journal*, DOI:10.1016/j.cej.2020.127780.
- 166 M. Xu, C. Huang, J. Lu, Z. Wu, X. Zhu, H. Li, L. Xiao and Z. Luo, *Molecules*, DOI:10.3390/molecules26113150.

- 167 M. Szlachta and P. Wójtowicz, *Water Science and Technology*, DOI:10.2166/wst.2013.487, [View Article Online](#)
DOI: 10.1039/D5NR02336J
- 168 T. Lv, J. Zhang, L. Yu, Y. Zhao, T. Zhao, Y. Yang, C. Yu, C. Zhao and G. Xing, *Journal of Industrial and Engineering Chemistry*, 2025, **144**, 454–462.
- 169 R. Li, X. Tang, J. Wu, K. Zhang, Q. Zhang, J. Wang, J. Zheng, S. Zheng, J. Fan, W. Zhang, X. Li and S. Cai, *Chemical Engineering Journal*, DOI:10.1016/j.cej.2023.142706.
- 170 Y. Hu, H. Wang, X. Ren, F. Wu, G. Liu, S. Zhang, H. Luo and L. Fang, *Nanomaterials*, 2024, **14**, 1925.
- 171 J. J. Gao, Y. B. Qin, T. Zhou, D. D. Cao, P. Xu, D. Hochstetter and Y. F. Wang, *J Zhejiang Univ Sci B*, DOI:10.1631/jzus.B12a0225.
- 172 H. M. El-Bery, M. Saleh, R. A. El-Gendy, M. R. Saleh and S. M. Thabet, *Sci Rep*, DOI:10.1038/s41598-022-09475-4.
- 173 K. A. Mohamad Said, M. A. M. Amin, I. Yakub, M. R. Rahman, A. B. H. Kueh, S. Hamdan and M. M. Rahman, *Bioresources*, DOI:10.15376/biores.18.3.5120-5132.
- 174 Z. Li, H. Hanafy, L. Zhang, L. Sellaoui, M. Schadeck Netto, M. L. S. Oliveira, M. K. Seliem, G. Luiz Dotto, A. Bonilla-Petriciolet and Q. Li, *Chemical Engineering Journal*, DOI:10.1016/j.cej.2020.124263.
- 175 N. N. Marnani, F. H. Tezel and O. D. Basu, *Applied Sciences*, 2024, **14**, 9811.
- 176 N. A. Travlou, G. Z. Kyzas, N. K. Lazaridis and E. A. Deliyanni, *Langmuir*, DOI:10.1021/la304696y.
- 177 T. Madrakian, A. Afkhami, M. Ahmadi and H. Bagheri, *J Hazard Mater*, DOI:10.1016/j.jhazmat.2011.08.078.
- 178 T. Aysu and M. M. Küçük, *International Journal of Environmental Science and Technology*, DOI:10.1007/s13762-014-0623-y.
- 179 B. M. Jun, J. Heo, N. Taheri-Qazvini, C. M. Park and Y. Yoon, *Ceram Int*, DOI:10.1016/j.ceramint.2019.09.293.
- 180 E. Ahmed, A. Deep, E. E. Kwon, R. J. C. Brown and K. H. Kim, *Sci Rep*, DOI:10.1038/srep31283.
- 181 X. Liu, H. Pang, X. Liu, Q. Li, N. Zhang, L. Mao, M. Qiu, B. Hu, H. Yang and X. Wang, 2021, preprint, DOI: 10.1016/j.xinn.2021.100076.
- 182 I. Ihsanullah, 2020, preprint, DOI: 10.1016/j.cej.2020.124340.
- 183 M. Alhabeb, K. Maleski, B. Anasori, P. Lelyukh, L. Clark, S. Sin and Y. Gogotsi, *Chemistry of Materials*, DOI:10.1021/acs.chemmater.7b02847.
- 184 N. Bhalla, *Advanced Physics Research*, DOI:10.1002/apxr.202400205.
- 185 K. T. Butler, D. W. Davies, H. Cartwright, O. Isayev and A. Walsh, 2018, preprint, DOI: 10.1038/s41586-018-0337-2.
- 186 G. R. Schleder, A. C. M. Padilha, C. M. Acosta, M. Costa and A. Fazzio, *JPhys Materials*, DOI:10.1088/2515-7639/ab084b.

- 187 M. Zhong, K. Tran, Y. Min, C. Wang, Z. Wang, C. T. Dinh, P. De Luna, Z. Yu, A. S. Rasouli, P. Brodersen, S. Sun, O. Voznyy, C. S. Tan, M. Askerka, F. Che, M. Liu, A. Seifitokaldani, Y. Pang, S. C. Lo, A. Ip, Z. Ulissi and E. H. Sargent, *Nature*, DOI:10.1038/s41586-020-2242-8. View Article Online
DOI: 10.1039/D5NR02336J
- 188 B. Sanchez-Lengeling and A. Aspuru-Guzik, 2018, preprint, DOI: 10.1126/science.aat2663.
- 189 G. Pilania, A. Mannodi-Kanakkithodi, B. P. Uberuaga, R. Ramprasad, J. E. Gubernatis and T. Lookman, *Sci Rep*, DOI:10.1038/srep19375.
- 190 C. T. Chen and G. X. Gu, *MRS Commun*, DOI:10.1557/mrc.2019.32.
- 191 M. Hamadache, J. H. Jung, J. Park and B. D. Youn, *JMST Advances*, DOI:10.1007/s42791-019-0016-y.
- 192 M. Grieves, *White Paper*.
- 193 B. L. Decost and E. A. Holm, *Comput Mater Sci*, DOI:10.1016/j.commatsci.2015.08.011.
- 194 S. Hochreiter and J. Schmidhuber, *Neural Comput*, DOI:10.1162/neco.1997.9.8.1735.
- 195 S. Li, L. Da Xu and S. Zhao, 2018, preprint, DOI: 10.1016/j.jii.2018.01.005.
- 196 L. Da Xu, W. He and S. Li, 2014, preprint, DOI: 10.1109/TII.2014.2300753.
- 197 K. Deb, A. Pratap, S. Agarwal and T. Meyarivan, *IEEE Transactions on Evolutionary Computation*, DOI:10.1109/4235.996017.
- 198 J. M. Granda, L. Donina, V. Dragone, D. L. Long and L. Cronin, *Nature*, DOI:10.1038/s41586-018-0307-8.
- 199 A. Dey, M. Billinghamurst, R. W. Lindeman and J. E. Swan, *Frontiers Robotics AI*, DOI:10.3389/frobt.2018.00037.

Data Availability Statement

[View Article Online](#)
DOI: 10.1039/D5NR02336J

No new data were created in this study